

FUNDAMENTAL INTERACTIONS AND PHYSICAL PROPERTIES OF STARCH, POLY
VINYL ALCOHOL AND MONTMORILLONITE CLAY BASED NANOCOMPOSITES
PREPARED USING SOLUTION MIXING AND MELT EXTRUSION

by

SAMER SHAUR ALI

B.Sc.(Hons.), University of Agriculture Faisalabad, Pakistan, 1999
M.Sc., University of Agriculture Faisalabad, Pakistan, 2002

A THESIS

submitted in partial fulfillment of the requirements for the degree

MASTER OF SCIENCE

Department of Grain Science and Industry
College of Agriculture

KANSAS STATE UNIVERSITY
Manhattan, Kansas

2010

Approved by:

Major Professor
Dr. Sajid Alavi

Copyright

SAMER SHAUR ALI

2010

Abstract

Plastics from petroleum sources are the main raw materials used for producing food packaging films. But these plastic films cause a great environmental concern due to their non-degradable nature and non-renewable source. Biodegradable polymers like starch can be used as a base material which can replace petroleum based plastics packaging. In this study, starch (0-80%) and polyvinyl alcohol (PVOH) (20-100%) were used as base polymers to produce nanocomposites. Glycerol (30%) and sodium montmorillonite (0-20%) were used as a plasticizer and nano-filler, respectively. Nanocomposites were produced through two methods: solution and melt extrusion method. Extrusion method resulted in greater exfoliation of nanocomposites than solution method because it provided more shear stress to disrupt the layered silicate structure. In extrusion method, a lab scale extruder was used to produce these nanocomposites and films were made by casting. Process parameters, including screw speed (200-400 RPM) and barrel temperature (145-165°C), were varied systematically.

X-ray diffraction (XRD) and transmission electron microscopy (TEM) were conducted to characterize the nanostructure of these nanocomposites. Thermal characterization of these films was carried out through differential scanning calorimetric (DSC) studies. Results from XRD and TEM explained the phenomenon of intercalation and exfoliation in these nanocomposites. Structural and thermal data indicated important role for Na⁺MMT along with process parameters in controlling exfoliation and glass transition temperature of the nanocomposites. These results also helped in understanding the fundamental interactions among all the components. The tensile strength and elongation at break of films ranged from 4.72 to 23.01MPa and 63.40 to 330.15% respectively, while water vapor permeability ranged from 1.68 to 0.79g.mm/kPa.h.m². These results provide a great understanding for further improvements in order to bring these films close to commercial plastic films which have superior tensile strength (10-80MPa), elongation at break (200-800%) and water vapor permeability (0.002- 0.05g.mm/kPa.h.m²). The cost for polyethylene is approximately \$0.70/lb while the raw material cost for this starch based films is approximately \$0.85/lb.

Table of Contents

List of Figures	vii
List of Tables	xii
Acknowledgements.....	xiv
CHAPTER 1 - Introduction	1
Plastic Packaging	1
Biodegradable Packaging	1
Starch based packaging.....	2
Nanocomposites preparation.....	3
Solution casting method.....	3
Melt Intercalation method.....	3
In situ polymerization	4
Experimental techniques for nanocomposite characterization	4
Figures and Tables	5
CHAPTER 2 - . Structure and physical properties of starch/polyvinyl alcohol/Na ⁺ MMT nanocomposites films prepared by solution method	8
Abstract.....	8
Introduction.....	8
Materials and Methods.....	11
Materials	11
Preparation of nanocomposites and film casting	12
X-Ray diffraction analysis	12
Transmission electron microscopy	12
Thermal analysis	12
Moisture content measurement	13
Tensile properties.....	13
Water vapor permeability.....	13
Experimental design and statistical analysis.....	14
Results and Discussion	14

Effect of Na ⁺ MMT level	14
Different molecular weights of PVOH	17
Nanocomposite films at different starch contents	20
Conclusion	22
Figures and Tables	24
CHAPTER 3 - Structure and physical properties of starch/polyvinyl alcohol/ Na⁺MMT	
nanocomposites prepared using melt extrusion processing	41
Abstract	41
Introduction	41
Materials and methods	44
Materials	44
Preparation of nanocomposites	44
Specific mechanical energy (SME)	45
Film casting	45
X-Ray diffraction analysis	45
Transmission electron microscopy	46
Thermal analysis	46
Moisture content	46
Rapid visco analysis	46
Tensile properties	46
Water vapor permeability	47
Experimental design and statistical analysis	48
Results and discussion	48
Different levels of Na ⁺ MMT	48
Extrusion processing parameters	51
Effect of screw speed	51
Different temperature profiles	53
Solution versus melt extrusion processing	54
Conclusion	55
Figures and Tables	56
References	72

Appendix A - Replicated figures and raw data tables for Chapter 2	76
Appendix B - Replicated figures and raw data tables for Chapter 3	83

List of Figures

Figure 1-1 Schematic representation of polymer-clay composites a) Phase separated (Microcomposites) b) Intercalated (Nanocomposites) c) Exfoliated (Nanocomposites).....	5
Figure 2-1 Molecular structures for a) Starch poly- α -1,4-D-glucopyranoside chain (present in both amylose and amylopectin) b) PVOH and c) schematic for molecular structure of Na ⁺ MMT.....	24
Figure 2-2 XRD patterns for nanocomposites with different Na ⁺ MMT levels	25
Figure 2-3 TEM scans for (a) 5% (b) 10% and (c) 20 % Na ⁺ MMT levels.....	26
Figure 2-4 Glass transition temperature (T_g) for nanocomposite films with different Na ⁺ MMT levels. Results with same letters are not significantly different. Values at bottom of the bars show moisture content of films. Error bars indicate the standard deviation.	27
Figure 2-5 ΔC_p at T_g for nanocomposites with different levels of Na ⁺ MMT. Results with same letters are not significantly different. Error bars indicate the standard deviation.	27
Figure 2-6 Tensile strength and elongation at break for nanocomposite films with different levels of Na ⁺ MMT. Results with same letters are not significantly different. Error bars indicate the standard deviation.	28
Figure 2-7 Water vapor permeability (WVP) for nanocomposite films with different levels of Na ⁺ MMT. Results with same letters are not significantly different. Error bars indicate the standard deviation.	28
Figure 2-8 XRD patterns of nanocomposites containing PVOH with different molecular weight ranges	29
Figure 2-9 Glass Transition Temperature (T_g) at different molecular weights of PVOH. Results with same letters are statistically non-significant. Values at the bottom of the bars show moisture content of films.	30
Figure 2-10 ΔC_p at T_g for nanocomposites with different molecular weight ranges of PVOH. Results with same letters are statistically non-significant. Error bars indicate the standard deviation.....	30
Figure 2-11 DSC Curves showing melting range peaks for different molecular weights of PVOH.	31

Figure 2-12 Melting Temperature (T_m) at different molecular weights of PVOH. Results with same letters are statistically non-significant. Values at the bottom of the bars show moisture content of films. Error bars indicate the standard deviation.	31
Figure 2-13 Tensile Strength for nanocomposite films with different molecular weight ranges of PVOH. Results with same letters are statistically non-significant. Error bars indicate the standard deviation.	32
Figure 2-14 Elongation at break for nanocomposite films with different molecular weight ranges of PVOH. Results with same letters are statistically non-significant. Error bars indicate the standard deviation.	32
Figure 2-15 Water Vapor Permeability (WVP) of films with different molecular weight ranges. Results with same letters are statistically non-significant. Error bars indicate the standard deviation.....	33
Figure 2-16 Schematics for possible molecular interaction between (a) Starch and PVOH (b) PVOH and Na^+MMT (c) Starch and Na^+MMT	34
Figure 2-17 XRD patterns of nanocomposites with different levels of starch	35
Figure 2-18 Glass Transition Temperature (T_g) at different starch levels. Results with same letters are not significantly different. Superscript values show moisture content of films. Error bars indicate the standard deviation.....	36
Figure 2-19 ΔC_p at T_g for different levels of starch. Error bars indicate the standard deviation..	36
Figure 2-20 Melting temperature (T_m) at different starch levels. Results with same letters are not significantly different. Superscript values show moisture content of films. Error bars indicate the standard deviation.....	37
Figure 2-21 DSC curves indicating broadening of melting range peaks with different levels of starch	37
Figure 2-22 Schematic presentation of preferred interactions between different components	38
Figure 2-23 Schematic diagram for PVOH/ Na^+MMT and starch/ Na^+MMT interactions at different starch levels	38
Figure 2-24 Mechanical properties of nanocomposites films with different levels of starch. Results with same letters are not significantly different. Error bars indicate the standard deviation.....	39

Figure 2-25 WVP for nanocomposite films with different levels of starch. Results with same letters are not significantly different. Error bars indicate the standard deviation.	39
Figure 3-1 Temperature profile, screw configuration and die design for laboratory-scale extruder used in the experiment.	56
Figure 3-2 XRD patterns for nanocomposites with different Na ⁺ MMT levels	57
Figure 3-3 TEM scans for (a) 5% (b) 10% and (c) 15 % Na ⁺ MMT levels.....	58
Figure 3-4 Glass Transition Temperature (T _g) at different Na ⁺ MMT levels. Results with same letters are statistically non-significant. Values at the bottom of the bars show moisture content of films. Error bars indicate standard deviation.	59
Figure 3-5 ΔC _p at T _g for nanocomposites with different levels of Na ⁺ MMT. Results with same letters are statistically non-significant. Error bars indicate standard deviation.	59
Figure 3-6 Melting Temperature (T _m) with different Na ⁺ MMT levels. Results with same letters are statistically non-significant. Values at bottom of the bars show moisture content (% wet basis) of films. Error bars indicate standard deviation.	60
Figure 3-7 Tensile strength and elongation at break with different levels of Na ⁺ MMT. Results with similar letters are not significantly different. Error bars indicate standard deviation...	60
Figure 3-8 WVP for nanocomposite films with different levels of Na ⁺ MMT. Results with same letters are statistically non-significant. Error bars indicate standard deviation.	61
Figure 3-9 XRD patterns for nanocomposites with different screw speeds.	62
Figure 3-10 Glass transition temperature of nanocomposites at different screw speeds. Results with same letters are statistically non-significant. Values at the bottom of the bars show moisture content (% wet basis) of films. Error bars indicate standard deviation.	63
Figure 3-11 Melting temperature of nanocomposites at different screw speeds. Results with same letters are statistically non-significant. Values at the bottom of the bars show moisture content (% wet basis) of films. Error bars indicate standard deviation.	63
Figure 3-12 Tensile Strength of nanocomposites at different screw speeds. Results with same letters are statistically non-significant. Error bars indicate standard deviation.	64
Figure 3-13 Elongation at break of nanocomposite films at different screw speeds. Results with same letters are statistically non-significant. Error bars indicate standard deviation.	64
Figure 3-14 WVP for nanocomposite films at different screw speeds. Results with same letters are statistically non-significant. Error bars indicate standard deviation.	65

Figure 3-15 XRD patterns for nanocomposites with different barrel temperature profiles.....	65
Figure 3-16 Tg for nanocomposite films with different temperature profiles. Results with same letters are statistically non-significant. Values at the bottom of the bars show moisture content (% wet basis) of films. Error bars indicate standard deviation.	66
Figure 3-17 Melting temperature of nanocomposite films with different temperature profiles. Results with same letters are statistically non-significant. Values at the bottom of bars show moisture content (% wet basis) of films. Error bars indicate standard deviation.	67
Figure 3-18 Tensile Strength for nanocomposite films with different temperature profiles of extruder. Results with same letters are statistically non-significant. Error bars indicate standard deviation.	67
Figure 3-19 Elongation at break for nanocomposite films with different temperature profiles of extruder. Results with same letters are statistically non-significant. Error bars indicate standard deviation.	68
Figure 3-20 Water Vapor Permeability (WVP) for nanocomposite films at temperature profiles of extruder. Results with same letters are statistically non-significant. Error bars indicate standard deviation.	68
Figure 3-21 RVA profiles for nanocomposites through extrusion and solution method.....	69
Figure A-1 DSC Curves of first replicate for nanocomposites with different molecular weights of PVOH.....	76
Figure A-2 DSC Curves of second replicate for nanocomposites with different molecular weights of PVOH	76
Figure A-3 DSC Curves of third replicate for nanocomposites with different molecular weights of PVOH	77
Figure A-4 DSC Curves of first replicate for nanocomposites with different starch levels	77
Figure A-5 DSC Curves of second replicate for nanocomposites with different starch levels	78
Figure A-6 DSC Curves of third replicate for nanocomposites with different starch levels	78
Figure A-7 DSC Curves of first replicate for nanocomposites with different Na ⁺ MMT content	79
Figure A-8 DSC Curves of second replicate for nanocomposites with different Na ⁺ MMT content	79
Figure A-9 DSC Curves of third replicate for nanocomposites with different Na ⁺ MMT content	80
Figure B-1 DSC Curves of first replicate for nanocomposites with different Na ⁺ MMT content.	83

Figure B-2 DSC Curves of second replicate for nanocomposites with different Na ⁺ MMT content	84
Figure B-3 DSC Curves of third replicate for nanocomposites with different Na ⁺ MMT content	84
Figure B-4 DSC Curves of first replicate for nanocomposites produced with different screw speeds	84
Figure B-5 DSC Curves of second replicate for nanocomposites produced with different screw speeds	85
Figure B-6 DSC Curves of third replicate for nanocomposites produced with different screw speeds	85
Figure B-7 DSC Curves of first replicate for nanocomposites produced at different temperature profiles of extruder	86
Figure B-8 DSC Curves of second replicate for nanocomposites produced at different temperature profiles of extruder.....	86
Figure B-9 DSC Curves of third replicate for nanocomposites produced at different temperature profiles of extruder.....	87

List of Tables

Table 1-1 Water Vapor Permeability of biopolymer, bio-nanocomposite and plastic films (Kumar, 2009).....	6
Table 1-2 Tensile Strength and Elongation at break of biopolymer, bio-nanocomposite and plastic films (Kumar, 2009)	7
Table 2-1 PVOH types used for studying molecular weight effect. Molecular weights were estimated from viscosity ranges given by the manufacturer.	40
Table 2-2 Moisture content of nanocomposite films with different molecular weights.....	40
Table 2-3 Moisture content of nanocomposite films with different starch levels.	40
Table 2-4 Moisture content of nanocomposite films with different Na ⁺ MMT content.....	40
Table 3-1 Moisture content of nanocomposite films at different levels of Na ⁺ MMT	70
Table 3-2 Specific mechanical energy (SME) for different treatments.	70
Table 3-3 Comparison of nanocomposit films through solution casting melt extrusion	71
Table A-1 Tensile strength for nanocomposite films with different molecular weight ranges of PVOH.....	80
Table A-2 Elongation at break for nanocomposite films with different molecular weight ranges of PVOH	80
Table A-3 Tensile strength for nanocomposite films with different starch levels.....	81
Table A-4 Elongation at break for nanocomposite films with different starch levels	81
Table A-5 Tensile strength for nanocomposite films with different Na ⁺ MMT content	81
Table A-6 Elongation at break for nanocomposite films with different Na ⁺ MMT content	81
Table A-7 WVP for nanocomposite films with different molecular weight ranges of PVOH.....	82
Table A-8 WVP for nanocomposite films with different starch levels	82
Table A-9 WVP for nanocomposite films with different Na ⁺ MMT content.....	82
Table B-1 Tensile Strength for nanocomposite films with different Na ⁺ MMT content.....	87
Table B-2 Elongation at break for nanocomposite films with different Na ⁺ MMT content.....	87
Table B-3 WVP for nanocomposite films with different Na ⁺ MMT content	88
Table B-4 Tensile Strength for nanocomposite films produced with different screw speeds	88
Table B-5 Elongation at break for nanocomposite films produced with different screw speeds .	88

Table B-6 WVP for nanocomposite films produced with different screw speeds.....	88
Table B-7 Tensile Strength for nanocomposite films produced with different temperature profiles of extruder	89
Table B-8 Elongation at break for nanocomposite films produced with different temperature profiles of extruder.....	89
Table B-9 WVP for nanocomposite films produced with different temperature profiles of extruder	89

Acknowledgements

This thesis is a great milestone in my quest of knowledge. There are a number of important people who were there to make this possible. It is my pleasure to thank all those who supported me during my two years at Kansas State University.

First of all, I owe deepest gratitude to my major advisor Dr. Sajid Alavi, for his continuous support and guidance during my graduate studies. His knowledge along with critical approach in finding answers to challenging questions was always inspirational for me. I found a mentor in him who was always available with a positive and friendly attitude.

I would like to thank my committee members Dr. Jon Faubion and Dr. Fadi Aramouni for their valuable suggestions and insightful comments. I am so grateful for their encouragement which helped me in achieving my research goals.

I would also like to thank Dr. Xiaozhi Tang and Mr. Eric Michael for being a great resource and support in completing my experiments. I am grateful to my lab mates Elisa Karkle, Yuhyun Yoo and Jhoe de Mesa for their positive attitude and friendship. I also want to thank my colleagues at Jardine Apartments Complex and all the friends at K-State for their continuous support and encouragement.

My family deserves special thanks as this thesis was not possible without their support and love. I feel indebted to my wife Javaria, my daughter Ayeza and my son Ahmad for their love, patience and understanding. I was also blessed with the prayers of my mother and support of my brother who were always a source of everlasting love.

CHAPTER 1 - Introduction

Plastic Packaging

Plastics are the most common materials used for food packaging due to their excellent barrier and mechanical properties. Their strength, light-weight, inexpensiveness, durability and ease in processing make them popular for food packaging (Narayan, 1993). However, durability and strength are the attributes which create problems after they are disposed off. They are not easily broken down by natural environmental elements or through waste management processes like composting to become a part of biological system (Mohee & Unmar, 2007). This results in building up the landfill and increasing danger for marine life, littering up beaches and destroying the overall landscape. Plastics are mainly composed of carbon, hydrogen, nitrogen, oxygen, chlorine, and bromine and are produced mainly from non-renewable petroleum sources (Leja & Lewandowicz, 2010). This is another environmental effect which results in eating up of these non renewable energy sources. Increased use of plastic materials over the last two decades has raised great environmental concerns. This has lead scientists to explore two main areas for finding solution to save the environment. One is recycling of plastic materials and second is using biodegradable plastics. Recycling does not provide a complete and permanent solution for petroleum based plastics but use of biodegradable plastics is an alternative method to replace plastic packaging.

Biodegradable Packaging

A polymer which is degradable and primary mechanism of degradation is through microorganisms like bacteria, fungi and algae is biodegradable polymer (Mohee & Unmar, 2007). Most of the biodegradable plastics are produced from natural biopolymers or synthetic biodegradable polymers. They provide a solution in replacing the petroleum based plastics but main constraint in their utilization is their inferior physical properties and raw material costs. Biopolymers or even synthetic degradable polymers have very limited applications in packaging due to these constraints. Therefore it is very important to take both of these factors into consideration before developing biodegradable plastics. The best solution to overcome these constraints can be to find an inexpensive biodegradable raw material with desired properties. Synthetic degradable polymers have advantages to be used in biodegradable plastics due to their

predictable properties, batch-to-batch uniformity and easily tailored nature (Nair & Laurencin, 2007). But these polymers are quite expensive to replace petroleum based plastics. Natural biopolymers on the other hand are inexpensive but they lack the required physical properties. So the main focus in producing biodegradable plastics is to improve their physical properties through the most inexpensive methods. Water vapor permeability and mechanical properties of biopolymer based films and plastic films are enlisted in Table 1-1 and Table 1-2.

Starch based packaging

Starch is a completely biodegradable (Alberta Araújo, Cunha & Mota, 2004), low cost, renewable and easily available (Zhang & Sun, 2004) material which make it a promising candidate for developing plastic packaging. Starch can be used to make biodegradable packaging films but these films are very brittle in nature with poor water barrier properties (Mao, Imam, Gordon, Cinelli & Chiellini, 2000). These properties can be improved through blending starch with other biodegradable polymers having better mechanical properties. Starch blends with polyvinyl alcohol (PVOH) are one such option. PVOH is a synthetic water soluble polymer which is produced by hydrolysis of polyvinyl acetate (Roohani, Habibi, Belgacem, Ebrahim, Karimi & Dufresne, 2008). It is well recognized as biodegradable polymer as it goes through biodegradation by enzymes and microorganism in natural environment (Spiridon, Popescu, Bodarlau & Vasile, 2008). PVOH films show good mechanical and oxygen barrier properties and can be used to replace the plastic food packaging. But poor moisture barrier properties and cost are the major constraints in using PVOH only films. Starch and PVOH has shown good compatibility by making hydrogen bonds and films made from these composites show improved mechanical properties (Mao, Imam, Gordon, Cinelli & Chiellini, 2000). Though blending of starch with PVOH does improve the mechanical and barrier properties of these films but they are still inferior to commercial films, especially at high starch levels. Nanocomposites from these blends are another option which can improve the mechanical and barrier properties.

Application of nanotechnology in food packaging has not only improved the properties but also the cost-price-efficiency (Sorrentino, Tortora & Vittoria, 2006). Layered silicates like Na⁺MMT have shown good compatibility with both starch and PVOH with improvement in mechanical and barrier properties of these polymers (Avella, De Vlieger, Errico, Fischer, Vacca & Volpe, 2005; Chivrac, Pollett, Schmutz & Averous, 2008; Dean, Yu & Wu, 2007;

Strawhecker & Manias, 2000; Tang, Alavi & Herald, 2008a, b). The materials based on layered silicates and polymers are of three types (Figure 1-1) 1) microcomposites in which the polymer is not miscible with clay and stays in a separate phase with no structural change occurring to the platelets, 2) intercalated nanocomposites in which the polymer can enter clay interlayer regions without disrupting the layered structure and 3) exfoliated nanocomposites in which the layered structure is completely disrupted (Alexandre & Dubois, 2000; Paul & Robeson, 2008). Glycerol is the conventional plasticizer used in starch and PVOH blends as it forms hydrogen bonds with these biopolymers (Zhou, Cui, Jia & Xie, 2009). Glycerol helps starch and PVOH molecules entering the Na⁺MMT interlayer galleries and creates well intercalated nanocomposite structures. Glycerol also hydrogen bond with PVOH molecules and thereby, hinder the formation of crystallites in these plasticized films (Lim & Wan, 1994). Starch/PVOH based nanocomposites are an emerging research area which can provide biodegradable films with improved barrier and mechanical properties.

Different

Nanocomposites preparation

There are three main methods which are commonly used to prepare nanocomposites: 1) Solution casting method, 2) Melt Intercalation method, and 3) In situ polymerization (Chen et al., 2008)

Solution casting method

In solution casting method, polymer solution is heated with layered silicates to form nanocomposites. This technique is mostly used in water soluble polymers to produce intercalated nanocomposites (Oriakhi, 1998). Main factors which help in the formation of nanocomposites are temperature and swelling of silicate clay. Temperature increases the movement of polymer chains which results in the intercalated nano-structures.

Melt Intercalation method

In melt Intercalation method polymer in its molten state enters the silicate layered structures and forms either intercalated or exfoliated nanocomposites (Alexandre & Dubois, 2000). Extrusion process is one of the techniques used to produce nanocomposites through melt intercalation method. It is a high temperature and pressure process which provides high shear stress through

mechanical energy input. The high shear stress helps in disruption of silicate layered structures and polymer in its molten state forms exfoliated nanocomposites

In situ polymerization

In situ polymerization technique is used to create nanocomposites by allowing liquid monomers to polymerize between swollen layered silicates (Alexandre & Dubois, 2000). Polymerization is initiated with heat, radiation or diffusion of some initiator where appropriate (Okada & Usuki, 2006).

Experimental techniques for nanocomposite characterization

X-ray diffraction (XRD) analysis is technique is widely used to measure the d-spacing of layered silicates which indicates degree of intercalation and exfoliation in nanocomposite structures. It has been used to study the nano-structure of starch based nanocomposites (Dimonie, Constantin, Vasilievici, Popescu & Garea, 2008; Tang, Alavi & Herald, 2008a). In XRD analysis d-spacing is calculated by using Bragg's Law

$$D = \frac{\lambda}{2\sin\theta} \quad (1)$$

where λ = wavelength of X-ray beam, θ = the angle of incidence.

Transmission electron microscopy (TEM) is used for further evidence of intercalation and exfoliation in nanocomposites. TEM provides an understanding of the internal structure, spatial distribution, and dispersion of the layered silicates in nanocomposites that are thin (< 100 nm) enough to transmit electrons. TEM has been used to understand the nano-structures of starch based nanocomposites (Tang, Alavi & Herald, 2008a).

Differential scanning calorimetry (DSC) analysis is very useful in providing information about the structural changes in polymer during the formation of nanocomposites. Parameters like glass transition temperature (T_g) and ΔC_p at T_g are very important in this regard. They provide information about structural conformations and also the interactions of polymer chains with clay. Zhang & Loo (2009) used DSC to understand the dynamic behaviors of polymer chains in polymer/layered silicate nanocomposites.

Figures and Tables

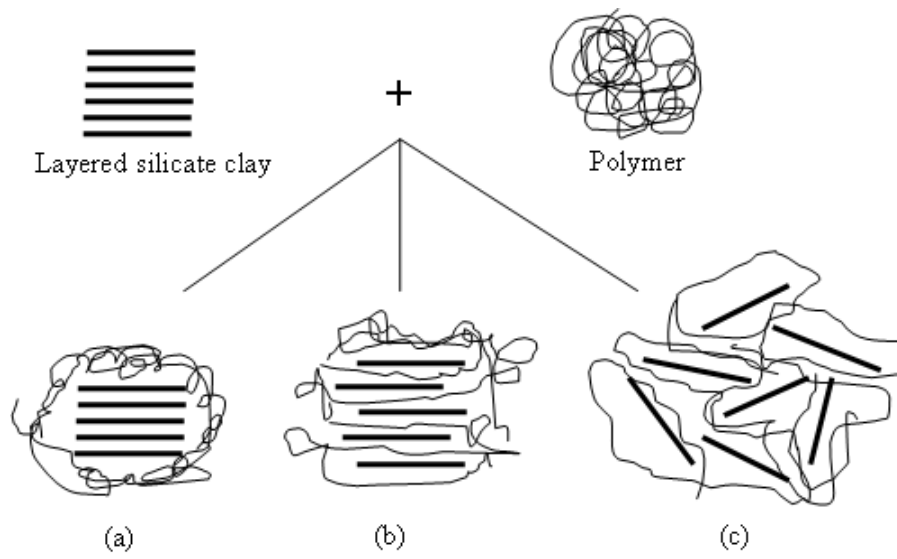


Figure 1-1 Schematic representation of polymer-clay composites a) Phase separated (Microcomposites) b) Intercalated (Nanocomposites) c) Exfoliated (Nanocomposites)

**Table 1-1 Water Vapor Permeability of biopolymer, bio-nanocomposite and plastic films
(Kumar, 2009)**

Films	WVP (g.mm/kPa.h.m²)
SPI	3.80 ± 0.11
SPI-5% MMT	2.96 ± 0.10
Soy protein	1.62-6.42
Whey protein	1.58-12.12
Chitosan	4.72
Chitosan-5% MMT	3.52
Starch	1.61
Starch-6% MMT	1.06
Cellophane	0.05-0.25
Poly lactic acid (PLA)	0.06
Polyvinyl alcohol (PVOH)	3.15
Low density polyethylene (LDPE)	0.001
Polypropylene (PP)	0.02-0.04
Polyvinylidene chloride (PVDC)	0.01

Table 1-2 Tensile Strength and Elongation at break of biopolymer, bio-nanocomposite and plastic films (Kumar, 2009)

Films	TS (MPa)	%E
SPI	2.26 ± 0.48	11.85 ± 0.39
SPI-5% MMT	6.28 ± 0.88	64.60 ± 4.69
Soy protein	3-14	10-172
Whey protein	1-29	4-41
Chitosan	32.9	54.6
Chitosan-5% MMT	35.1	50.3
Starch	14.22	5.26
Starch-6% MMT	18.60	4.44
Cellophane	55-124	16-604
Poly lactic acid (PLA)	50.5	3
Polyvinyl alcohol (PVOH)	44-64	150-400
Low density polyethylene (LDPE)	8.2-31.4	100-965
Polypropylene (PP)	31-41.3	100-600
Polyvinylidene chloride (PVDC)	19.3-34.5	160-400

CHAPTER 2 - . Structure and physical properties of starch/polyvinyl alcohol/Na⁺MMT nanocomposites films prepared by solution method

Abstract

Nanocomposites of starch, poly (vinyl alcohol) (PVOH) and sodium montmorillonite (Na⁺MMT) were produced using a solution method and films were prepared by casting. The tensile strength (TS) and elongation at break (E %) of films ranged from 11.87 to 23.01MPa and 63.4 to 130.5% respectively, while water vapor permeability (WVP) ranged from 0.718 to 1.68 g.mm/kPa.h.m². Increasing molecular weight of PVOH increased the TS and E% of nanocomposites films, while the WVP was negatively affected. TS, E% and WVP decreased with increasing starch level. Na⁺MMT content increased the TS while decreasing the E% and WVP of nanocomposite films. X-ray diffraction (XRD) and transmission electron microscopy (TEM) analyses were utilized to study the structure of these nanocomposites. Differential scanning calorimetric (DSC) studies were conducted to understand the structural changes and molecular interactions in these nanocomposites. Three types of interactions were observed in these nanocomposites; 1) Starch/ Na⁺MMT, 2) PVOH/Na⁺MMT and 3) starch/PVOH. A conceptual model was developed for preference of these interactions and the phenomena of intercalation and exfoliation were explained on the basis of this model.

Introduction

Packaging plays a variety of important roles in the food industry. The major role of packaging is to protect food from spoilage (through microbial contamination, physical damage or biochemical reactions) (Marsh & Bugusu, 2007; Robertson, 2006). Packaging also provides ease in handling, storage efficiency, attractiveness and product information for food (Marsh & Bugusu, 2007). The ideal food packaging material serves all of these purposes and is cost efficient. Many different packaging materials are used for food depending on the specific needs. Plastics can be used for different types of packaging including packaging films. The use of plastic packaging for food is increasing because of low material cost and functional advantages over other materials (Marsh & Bugusu, 2007).

According to the Municipal Solid Waste report issued by the U.S. Environmental Protection Agency (EPA) for the year 2008, 76.76 million tons of waste was generated from different types of packaging materials. This included 13.01 million tons from plastics with 4.89 million tons of plastic packaging in the form of films. Only 13.2% of this plastic packaging waste was recycled while only 9.8% of plastic films were recovered; the rest was added to landfills. Recycling plastics is challenging because of their diverse nature. Plastics are commonly produced from petroleum-based sources that are nonrenewable and non-degradable. According to US energy information administration, in 2006, 331 million barrels of liquid petroleum gases (LPG) and natural gas liquids (NGL) were used to make plastic materials and in the resin industry which is 4.6% of total oil consumption in U.S. According to an online report from Resource Conservation Manitoba, every year 100-billion plastic bags are used in U.S. which takes 12-million barrels of oil, an amount which can produce 240-million gallons of gasoline. Plastics that are not recycled become a permanent part of our environment. Though plastics are one of the cheapest sources available for food packaging, their long term impact on environment is unrecoverable.

In recent years, research has focused on exploring biodegradable and renewable sources to replace petroleum-based packaging materials. Starch is one such inexpensive, abundantly available and renewable material which can be used for making biodegradable packaging films. Starch is composed of linear amylose (poly- α -1,4-D-glucopyranoside) and branched amylopectin (poly- α -1,4-D-glucopyranoside and poly- α -1,6-D-glucopyranoside) (Dean, Do, Petinakis & Yu, 2008) (Figure 2-1a). Starch films are very brittle in nature (elongation ranging from 4 to 8%) with poor water barrier properties (1.61 to 0.77 g.mm/kpa.hr.m²) (Dean, Yu & Wu, 2007; Tang, Alavi & Herald, 2008a, b). In comparison, plastic films have better tensile strength (10-80MPa), elongation at break (200-800%) (Krevelen & Nijenhuis, 2009) and water vapor permeability (0.002- 0.05g.mm/kPa.h.m²)(Massey, 2003). To improve the properties of starch-based films, researchers have blended starch with other polymers such as polyhydroxyalkonates (Parulekar & Mohanty, 2007), poly lactic acid (PLA)(Jang, Shin, Lee & Narayan, 2007; Jun, 2000) and polyvinyl alcohol (PVOH) (Mao, Imam, Gordon, Cinelli & Chiellini, 2000; Yang & Huang, 2008; Zou, Ping-Qu & Liang-Zou, 2008).

PVOH is produced by the hydrolysis of polyvinyl acetate and contains secondary hydroxyl groups in every alternate carbon (Finch, 1992) (Figure 2-1b). PVOH can be used to

make blends with starch because it is highly compatible with it and forms hydrogen bonds easily (Russo, O'Sullivan, Rounsefell, Halley, Truss & Clarke, 2009; Zhou, Cui, Jia & Xie, 2009). Films from starch and PVOH blends show improved mechanical properties over starch alone films (Mao, Imam, Gordon, Cinelli & Chiellini, 2000), and are biodegradable (Russo, O'Sullivan, Rounsefell, Halley, Truss & Clarke, 2009). However, PVOH is a poor barrier for moisture just like starch and also expensive. Although higher starch content in starch/ PVOH composite films would minimize the cost, but at the same time lead to deterioration in mechanical properties (Ramaraj, 2007; Yang & Huang, 2008). Therefore there is a clear need to further improve such composite films.

An innovative approach to improve the mechanical and barrier properties of polymer films is to produce nanocomposites by adding nanoparticles such as layered silicates. Clay minerals are a diverse class of layered silicates that have been used for producing nanocomposites with biopolymers (Paul & Robeson, 2008). Smectite clays are the type mostly used in polymer clay nanocomposites due to their swelling properties and capacity to host water and organic molecules between their layers. These clays have high cation exchange capacity, large surface area and high aspect ratio (Chen et al., 2008). Montmorillonite (MMT) is smectite clay that exists as platelets of two tetrahedral silicate layers with an inner (sandwiched) octahedral aluminum oxide sheet. Some of the aluminum atoms are replaced with magnesium creating a difference in valences and a negative charge distribution within the platelets. These charges are balanced by positively charged ions such as Na^+ (Figure 2-1c). Hydration of these sodium ions causes the clay to swell and provides the ability to host polymer chains between the layers, which are facilitated by attractive forces such as hydrogen bonds (Paul & Robeson, 2008). When Na^+ MMT is mixed with a polymer three distinct composite structures can form. If the polymer is not miscible with clay, it will stay in a separate phase and no structural change will occur to the platelets. These types of composites are called microcomposites. If the polymer can enter clay interlayer regions without disrupting the layered structure the resulting composites are called intercalated nanocomposites. Thirdly, nanocomposites with a disrupted layered structure are called exfoliated nanocomposites (Alexandre & Dubois, 2000; Paul & Robeson, 2008). Starch is compatible with Na^+ MMT due to interaction between its polar hydroxyl groups and inorganic Na^+ ions of nanoclay. This results in well intercalated or exfoliated nanocomposites, which help in improving the mechanical and barrier properties of the starch

films (Avella, De Vlieger, Errico, Fischer, Vacca & Volpe, 2005; Dean, Yu & Wu, 2007; Dean, Do, Petinakis & Yu, 2008; Tang, Alavi & Herald, 2008a, b). PVOH is also highly compatible with Na⁺MMT and films made from these nanocomposites have exhibited better mechanical and barrier properties than do PVOH films (Strawhecker & Manias, 2000).

It is always desirable to get well-intercalated and well-exfoliated system by increasing the movement of PVOH and starch biopolymers into the interlayer galleries of Na⁺MMT. A plasticizer can be used to improve the movement to these molecules. Glycerol is the conventional plasticizer used in these blends as it forms hydrogen bonds with both PVOH and starch, which replace the strong bonds between and within starch and PVOH (Zhou, Cui, Jia & Xie, 2009). This helps starch and PVOH molecules in entering the Na⁺MMT interlayer galleries and provides better exfoliation and intercalation. Hydrogen bonding between glycerol and PVOH molecules also hinders the formation of crystallites in the plasticized films (Lim & Wan, 1994).

Nanocomposites based on starch/PVOH/ Na⁺MMT have been studied recently (Dean, Do, Petinakis & Yu, 2008; Dimonie, Constantin, Vasilievici, Popescu & Garea, 2008; Spiridon, Popescu, Bodarlan & Vasile, 2008; Vasile, Stoleriu, Popescu, Duncianu, Kelnar & Dimonie, 2008a). However little is still known about the various interactions that take place in such a multi-component system and their impact on physical properties of films produced from these nanocomposites. Thus, the aim of this study is to understand the molecular interactions in starch/PVOH/ Na⁺MMT nanocomposites and their impact on mechanical and barrier properties of films, produced from these nanocomposites.

Materials and Methods

Materials

Regular corn starch was obtained from CornProducts Internationals (Westchester, IL). Four fully hydrolyzed brands of polyvinyl alcohol having different molecular weights (Table 2-1) were obtained from Celanese Corporation, Dallas, Texas. Na⁺MMT was obtained from Nanocor Inc. (Arlington Heights, IL). Glycerol was sourced from ChemistryStore.com (Cayce, SC)

Preparation of nanocomposites and film casting

A solution was prepared by mixing 4% by wt of starch/PVOH/Na⁺MMT/glycerol to 96% of water and then heating this mixture at 95°C for 30 minutes. The heated solution was cooled to 55°C and equal amounts (60 g) were poured in 150 x 15 mm Petri dishes. The water was allowed to evaporate while drying for 24 to 36 hours at room temperature and the resulting films were peeled off and stored at room temperature in air tight bags for further tests.

X-Ray diffraction analysis

X-ray diffraction studies were carried using a XRG 3100 X-ray diffractometer (Philips Electronics, Netherlands) operating at 35kv and 20 mA. Scans were carried out at diffraction angles (2θ) of 1.5-10° and a scan speed of 1°/minute with step size of 0.04. The x-ray radiation was generated from Cu-Kα source with a wavelength (λ) of 0.154 nm. D-spacing was estimated from the XRD scans by using Bragg's Law

$$D = \frac{\lambda}{2\sin\theta} \quad (1)$$

where λ = wavelength of X-ray beam, θ = the angle of incidence.

Transmission electron microscopy

Transmission electron microscopy (TEM) was performed using a Philips CM100 electron microscope (Mahwah, NJ), operating at 100kV. Solution prepared for film casting was put on a carbon-coated copper grid and was dried for one minute to make a film. These samples were then analyzed for clay dispersion in the system.

Thermal analysis

Glass transition temperature (T_g), heat capacity change at T_g (ΔC_p) and melting temperature (T_m) were measured using differential scanning calorimetry (DSC) (Model: Q100, TA Instruments, New Castle, DE). Samples were conditioned at 23°C and 50% RH for 3 days prior to testing. Samples (8-10 mg) were hermetically sealed in aluminum pans then heated from 10°C to 250°C at a heating rate of 10°C/ min. An empty aluminum pan was used as a reference.

Moisture content measurement

Sample moisture content was measured using AACC 44-19 air-oven standard method.

Tensile properties

Tensile properties of films were measured with a texture analyzer (TA-XT2, Stable Micro Systems Ltd., UK) using ASTM D882-02 (ASTM 2002) method. A detailed description of this method was also provided by Tang et al. (2008a, b). Films were cut into 2cm × 8cm strips and were conditioned at 23°C and 50% RH. These strips were then mounted on the stretching arms of the machine which were 40cm apart. A crosshead speed of 1 mm/sec was used. Tensile strength (TS) and elongation at break (%E) were calculated using the following equations.

$$TS(MPa) = \frac{Lp}{a} \times 10^{-6} \quad (2)$$

where Lp = peak load (N), and a = cross-sectional area of samples (m^2)

$$E\% = \frac{\Delta L}{L} \times 100 \quad (3)$$

where ΔL = increase in length at breaking point (mm), and L = original length (mm) (40×10 mm).

Water vapor permeability

Water vapor permeability (WVP) was determined according to the standard method ASTM E96-00 (ASTM 2000). This was also described in detail by Tang et al. (2008a, b). Films were tightly fixed with screws on top of the desiccant (silica gel) containing aluminum test cells (area = 30 cm^2). These test cells were placed in a relative humidity chamber at 25°C and 75% relative humidity (RH) and were allowed to equilibrate for 2 hours. Then weight of test cells was measured at 0 hour and after every 12 hours over three days. The change in the weight of these cells was used to calculate the slope for each sample after plotting as a function of time. The water vapor transmission rate (WVTR) was calculated from the slope of the straight line ($\frac{\Delta G}{\Delta t}$) divided by the transfer area (A):

$$WVTR = \frac{\Delta G}{\Delta t A} \text{ g/h}\cdot\text{m}^2 \quad (4)$$

Where G = weight change (g), t = time (h) and A = test area (m²),

WVP was then calculated using WVTR as follow:

$$WVP = \frac{WVTR \times L}{\Delta P} \text{ g}\cdot\text{mm}/\text{kPa}\cdot\text{h}\cdot\text{m}^2 \quad (5)$$

Where

L = film thickness (mm) and ΔP = partial pressure difference across the films (kPa).

Film thickness was measured from five different locations of the films using electronic digital micrometer (Marathon Watch Company Ltd. Ontario, Canada) and average thickness was used for further calculations.

Experimental design and statistical analysis

To assess the effect of PVOH molecular weight, four different molecular weights of PVOH were used to prepare nanocomposites with starch (1:1 ratio) and Na⁺MMT (10% polymer basis). Starch content effects were assessed by varying starch (0, 20,33,50,67 and 80%) and PVOH, while keeping Na⁺MMT level at 10% (polymer basis). In the third experiment, Na⁺MMT contents of 0,5,10, 15 and 20% were used with starch and PVOH (2:1 ratio). Glycerol was used in all experiments as a plasticizer at a concentration of 30% (polymer basis). All treatments were replicated three times.

Data were analyzed using statistical analysis software (SAS, Version 9 SAS Institute Inc. Cary, NC). Analysis of variance (ANOVA) was carried out to determine the effect of treatment and statistical significance of differences in means was determined using the Tukey HSD multiple-comparison method at p<0.05.

Results and Discussion

Effect of Na⁺MMT level

X-ray diffraction analysis for natural Na⁺MMT showed a peak angle of 7.11° with a corresponding d-spacing of 1.24 nm (Figure 2-2). Ahmad et al.(2009) and Tang et al.(2008a,b) also reported similar 2θ and d-spacing values. XRD patterns of starch/PVOH (67:33) composite films with 0 to 20% MMT are shown in Figure 2-2. Films with 0 and 5% Na⁺MMT did not exhibit any XRD peaks, while those with 15 and 20% Na⁺MMT possessed intensity peaks at 2θ

of 4.30° and 6.58° , respectively, corresponding to d-spacing of 2.06 and 1.34 nm.

Nanocomposites with 10% Na^+MMT had a low intensity broadened peak between 2θ of 3.5° and 5.0° . XRD peaks were observed at a lower 2θ than pure Na^+MMT ($2\theta = 7.11^\circ$ and d-spacing = 1.24 nm). These results suggest that the degree of exfoliation decreased with increase in Na^+MMT content from 5-20%. The nanocomposite with 5% Na^+MMT was highly exfoliated while that with 10% Na^+MMT was partially exfoliated. On the other hand, nanocomposites with 15 and 20% Na^+MMT exhibited only an intercalated structure with the former having a higher d-spacing. TEM scans for nanocomposites with Na^+MMT levels of 5 and 10% confirmed exfoliation and intercalation, respectively, while Na^+MMT structure was more intact at 20% levels (Figure 2-3). This corresponded to the nanostructures inferred from XRD analysis.

Dimonie et al. (2008) observed exfoliated structures in starch/PVOH/ Na^+MMT nanocomposites at 3% MMT level, although these nanocomposites were produced through melt processing. Decreasing intercalation and exfoliation with increasing clay level has been reported for other polymer nanocomposites. Tang et al. (2008a) studied starch/ Na^+MMT nanocomposites with different levels of Na^+MMT and observed good intercalation at all levels of clay (3, 6, 9, 15 and 21%) and also partial exfoliation that decreased with increasing Na^+MMT level. Wilhelm et al. (2003) prepared nanocomposite films with glycerol plasticized Cara starch and Ca^{2+} hectorite clay by solution casting method. They found that the degree of intercalation depended on the proportion of available clay and that less intercalation occurred with higher levels of clay.

DSC analysis of nanocomposite films provided information about glass transition temperature (T_g) and change in heat capacity (ΔC_p) at T_g , from which useful insight into structural conformations and interactions between polymers and clay could be inferred. T_g of starch/PVOH composite with 0% Na^+MMT was 70.28°C , while that of starch/PVOH/ Na^+MMT nanocomposites with 5-20% MMT ranged from 71.75 to 61.22°C (Figure 2-4). In general, increase in Na^+MMT level led to a steady decrease in T_g , although these results were not statistically different. ANOVA results showed that Na^+MMT content had no effect on T_g ($p=0.845$). Conflicting effects of clay on polymer relaxation behavior, and thus the T_g , has been reported in nanocomposite films in previous studies depending on the interplay between confinement of polymer chains, surface interactions and disruption of intermolecular structure (Chen et al., 2008; Lu & Nutt, 2003; Tran, Said & Grohens, 2005; Vaia, Sauer, Tse & Giannelis, 1997; Zax, Yang, Santos, Hegemann, Giannelis & Manias, 2000; Zhang & Sun, 2004). With

increase in Na⁺MMT content, more polymer chains are likely to be confined between clay galleries of the intercalated nanostructures. This could lead to disruption of bonding between starch and PVOH, and a more unstable intermolecular structure, thus causing faster relaxation of chain segments and depressed T_g in these nanocomposites. A similar reasoning was offered by Zhang & Loo (2009) for T_g depression with increased 20AMMT clay level (2-10%) in amorphous polyamide (aPA) nanocomposites.

Decreases in heat capacity (ΔC_p) from 0.0587 J/g^oC to 0.0175 J/g^oC was observed with increase in Na⁺MMT content from 0 to 20% (Figure 2-5). Significant effect of Na⁺MMT content on ΔC_p (p =0.0012) was shown by ANOVA. The decrease in ΔC_p can also attributed to increased polymer chain confinement at higher clay levels, which results in decreased degrees of freedom for polymer chain segments (Vyazovkin & Dranca, 2004; Zhang & Loo, 2009).

Tensile strength (TS) increased (Figure 2-6) from 8.39 to 18.84MPa with increasing Na⁺MMT content (0 to 20%). Elongation at break (E %) decreased (Figure 2-6) from 136.82 to 41.57% with increasing Na⁺MMT levels (0 to 20%). Na⁺MMT content had a significant effect on TS (p= 0.0001) and E% (p= 0.001), as determined by ANOVA. This is consistent with several studies involving polymer-clay nanocomposite systems (Chivrac, Pollett, Schmutz & Averous, 2008; Dean, Yu & Wu, 2007; Dean, Do, Petinakis & Yu, 2008; Follain, Joly, Dole & Bliard, 2005; Ray & Okamoto, 2003; Tang, Alavi & Herald, 2008a). In an intercalated or exfoliated system, higher clay content leads to greater interaction with polymer as substantiated by DSC results described earlier. This leads to strengthening of the nanocomposites, while on the other hand it prevents easy 'sliding' of polymer chain against each other thus lowering elongation properties.

Water vapor permeability (WVP) decreased from 1.68 to 0.718g.mm/kPa.h.m² (Figure 2-7) with increasing Na⁺MMT levels (0 to 20%). ANOVA results showed a significant effect (p= 0.001) of Na⁺MMT content on WVP. The diffusion rate of water in nanocomposite films is controlled by a tortuous pathway of silicate layers (Sorrentino, Tortora & Vittoria, 2006; Tang, Alavi & Herald, 2008a). As intercalation and exfoliation increases, these pathways are increased and as a consequence WVP decreases. Tang et al. (2008a) observed a similar trend in starch/Na⁺MMT nanocomposites with different levels of Na⁺MMT.

Different molecular weights of PVOH

XRD analysis for starch/PVOH (50:50) composites, with varying PVOH molecular weight and 10% Na⁺MMT, identified new peaks at lower 2θ angles than natural Na⁺MMT ($2\theta = 7.11^\circ$, d-spacing= 1.24nm) (Figure 2-8). Such a reduction in 2θ angle and increase in d-spacing indicated that MMT platelets were pushed apart by starch and PVOH polymers. The polymers entered the inter-layer galleries and increased the gallery spacing, thus forming intercalated nanocomposites. The new peaks varied with the molecular weights of PVOH. The peak corresponding to Celvol107 had an intensity of 145, which was much lower than that for other PVOH types (279-318). The d-spacing corresponding to Celvol107 was 2.39 nm, as compared to 2.13 to 2.50 nm for other PVOH types. The low intensity for Celvol107 indicated that some silicate layers are disrupted resulting in a partially exfoliated system. In solution casting method hydration of Na⁺ ions causes MMT to swell which results in increased d-spacing. This phenomenon greatly helps the polymer to enter silicate galleries to form intercalated nanocomposites (Paul & Robeson, 2008). Temperature plays an important role in intercalation and exfoliation in such systems by increasing mobility of polymer molecules. Temperature also causes degradation of starch that further assists in mobility. Glycerol makes hydrogen bonds with polymers and creates a plasticization effect, which also increase polymer mobility. However, increased polymer molecular weight reduces mobility and makes it difficult for molecules to penetrate the interlayer galleries of layered silicates resulting in lower exfoliation (Lee, Mielewski & Baird, 2004; Shen, Simon & Cheng, 2002; Vaia, Jandt, Kramer & Giannelis, 1995; Zhong & De Kee, 2005).

Glass transition temperatures (T_g) was determined as the midpoint of the glass transition region on the DSC curve. Nanocomposites containing Celvol107, Celvol310, Celvol325, and Celvol350 had T_g values of 65.14, 71.0, 74.94 and 72.60°C, respectively (Figure 2-9). PVOH molecular weight showed a significant effect on T_g ($p=0.0104$), as determined by ANOVA. It is well known that T_g for polymers increases with increasing molecular weight (Zhang & Loo, 2009). The smaller polymers have a greater number of chain end segments in a given weight of polymer and therefore, increased segmental movement. Glass transition temperature (T_g) of polymers increases with restricted segmental movement in molecular chains of polymers with higher molecular weight (Gowariker, Viswanathan & Sreedhar, 2003). This increase in T_g continues till the molecular weight reaches its critical level at which level it becomes constant

(Mark, 2004). An increase in PVOH molecular weight resulted in increase in T_g of nanocomposite films. These results are in accordance with general trend for T_g in polymers with change in molecular weight.

Change in heat capacity (ΔC_p) at the glass transition temperature (T_g) gives information about polymer chain mobility in nanocomposite systems as it depends on internal degrees of freedom of molecular motion (Vyazovkin & Dranca, 2004). An increase in ΔC_p from 0.0454 to 0.0676 J/g/ $^{\circ}$ C (Figure 2-10) was observed with increasing molecular weight of PVOH, although this was not statistically significant. ANOVA results also showed that there was no significant impact of molecular weight ($P=0.482$) on ΔC_p at T_g . Increased ΔC_p indicates a greater number of degrees of freedom due to lower interactions between PVOH and Na^+MMT .

DSC curves showed that the melting range peak broadened with increasing molecular weight of PVOH (Figure 2-11). The broadening of melting range with increasing molecular weight can be due to increased interactions between starch and PVOH molecules. As the PVOH chain length increases with increasing molecular weight, it is hard for these chains to enter silicate galleries. This reduces interactions between PVOH and Na^+MMT resulting in increased interactions between starch and PVOH. Results from XRD and DSC analysis also provided evidence for reduced interactions between PVOH and Na^+MMT . PVOH types used in this experiment are fully hydrolyzed with same melting temperature range. This was confirmed by DSC analysis of nanocomposite films showing small and non-significant differences in peak melting temperatures (T_m), ranging from 162.49 $^{\circ}$ C to 159.04 $^{\circ}$ C (Figure 2-12). PVOH molecular weight had no significant effect on T_m ($P= 0.744$), as determined by ANOVA.

Tensile strength (TS) for Celvol107, Clevol310 and Celvol325 was 11.87, 13.84 and 16.44MPa, respectively, but this increasing trend was discontinued with a decrease to 14.38MPa for Celvol350. (Figure 2-13). ANOVA results showed a significant effect of PVOH molecular weight on TS ($P= 0.0006$). Tensile strength of polymers increases with increased molecular weight because longer chains are more entangled physically at higher molecular weights (Nielsen & Landel, 1994). Sekisui Chemical Co. (2009) has reported that TS increases with increased molecular weight of PVOH which can be due to physical entanglement of polymer chains. Elizondo et al. (2009) studied blends of amaranthus cruentus flour with Celvol107, Celvol325 and Celvol350. They observed that tensile strength increased significantly with increasing molecular weight to celvol325. They also observed a non significant decrease in

tensile strength for Celvol350. These trends are similar to the results observed in this experiment. El-Kader et al. (2002) studied optical and mechanical properties of PVOH films with different molecular weights. They reported a decrease in tensile strength with increasing molecular weight of PVOH. They attributed this decrease to the decrease in crystallinity of the polymer with increasing molecular weight. Results from this particular experiment are not in accordance with their results except celvol350.

Elongation at break (E %) results also showed an increase ranging from 66.73% for Celvol107 to 162.20% for Celvol350 with increased molecular weight (Figure 2-14). PVOH molecular weight had a significant effect on E% ($P= 0.0001$), as determined by ANOVA. Polymer chain length and flexibility are important factors in determining the elongation at break of a polymer. Longer chains result in increasing elongation at break (Nielsen & Landel, 1994) and PVOH polymer chains increase in length with increasing molecular weight. Increase in molecular weight increases PVOH chain lengths and these flexible chains can easily slide past each other. This leads to increased elongation at break with increased molecular weight. Another reason for increased elongation at break can be the lower polymer/ Na^+ MMT interactions with increased molecular weight. As confirmed by DSC analysis of these films. Elizondo et al (2009) also reported similar trends in elongation at break with increased molecular weight of PVOH. Fornes et al. (2001) also observed increase in elongation at break and tensile strength with increasing molecular weight of nylon-6 matrices in nanocomposites. While their results are not from PVOH nanocomposites they provide insight into polymer behavior in nanocomposite systems as a function of molecular weights.

As the molecular weight of PVOH in the films increased, water vapor permeability (WVP) decreased from 1.41 to 1.16 g.mm/kPa.h.m² (Figure 2-15). This was the case up to the molecular weight of Celvol325 after which a non-significant increase to 1.29g.mm/kPa.h.m² was observed. AVONA results showed that PVOH molecular weight had a significant effect on WVP ($P= 0.0273$) of these nanocomposite films. Permeability coefficient depends on the solubility and diffusion coefficients through following relationship;

$$P=DS \quad (6)$$

where P = permeability coefficient, D = diffusion coefficient and S = solubility coefficient.

This relationship shows that decreased solubility will have a decreasing effect on permeability.

PVOH water resistance and solvent resistance increases with increased molecular weight

(Sekisui Chemical Co.). This decreased solubility with increasing molecular weight lead to decrease in WVP through the relationship stated above.

While the mechanical and barrier properties of nanocomposite films are affected by the degree of intercalation and exfoliation in the system, it was clear that polymer physical properties as determined by PVOH molecular weight were the predominant factors.

Nanocomposite films at different starch contents

In multi-component starch/PVOH/Na⁺MMT nanocomposites, three types of interactions take place at the molecular level as shown in Figure 2-16 1) hydrogen bonding between hydroxyl groups of starch and PVOH, 2) interactions between PVOH hydroxyl groups and Na⁺ ions of Na⁺MMT and 3) interactions between hydroxyl groups of starch and Na⁺ ions of Na⁺MMT. XRD and DSC results, discussed below, provide a good understanding of the relative intensity of these interactions as starch level is varied.

X-ray diffraction results of Celvol325/starch composite films containing different levels of starch and 10% MMT are presented in Figure 2-17. Nanocomposites with starch levels of 20, 33 and 50% have intensity peaks at 2 θ angles of 3.41 $^{\circ}$, 2.98 $^{\circ}$ and 3.91 $^{\circ}$, respectively, with corresponding d-spacing of 2.60, 2.97 and 2.29 nm. These peaks have lower 2 θ and higher d-spacing than the peak corresponding to natural Na⁺MMT (2 θ of 7.11 $^{\circ}$ and d-spacing of 1.24 nm, as reported earlier). This indicated that starch and PVOH (Celvol325) created well intercalated nanocomposites with Na⁺MMT. The XRD peaks from these nanocomposites are also broader than pure MMT peak which provides evidence for partial exfoliation. The lack of a detectable peak from nanocomposites at starch levels of 0, 67 and 80% is attributed to their fully exfoliated structure.

DSC analysis did not show any statistically significant change in T_g with increased starch content. Starch content had no significant effect on T_g (p= 0.209), as determined by ANOVA. Though an increase in T_g from 71.49 $^{\circ}$ C to 76.95 $^{\circ}$ C (Figure 2-18) with increasing starch levels from 0 to 33% level was observed. This can be attributed to strong interaction between both starch and PVOH resulting in restricted segmental movement of polymer chains and also lower affinity for moisture. The latter is confirmed by the observed decrease in moisture content from 16.42 to 10.43% as starch content increased from 0 to 50% (Table 2-3). Moisture has an important role in determining T_g as water is a plasticizer for both starch and PVOH. Further

increase in starch levels to 50, 67 and 80% resulted in a decreased T_g of 73.60, 68.34 and 67.03°C, respectively (Fig 2-18). This can also be partially attributed to higher affinity for moisture as lesser hydroxyl groups are involved in starch-PVOH interactions. The observed increase in moisture content to 14.88% with increase in starch content to 80% (Table 2-3) confirms this reasoning. Change in content of PVOH, which has higher T_g than starch in this moisture range, and also extent of intercalation/ exfoliation might be other factors that affected the T_g of these nanocomposites. DSC analysis also showed higher ΔC_p for nanocomposites with 20-50% starch (Figure 2-19) as compared to other starch levels, indicating lower degrees of freedom due to decreased interaction between polymers and Na⁺MMT. Starch levels showed a significant effect on ΔC_p ($p=0.0008$), as determined by ANOVA. These results corresponded well with trends found in XRD analysis of these nanocomposites.

There was a gradual decrease in melting temperature (T_m) with increasing starch content, although the differences were not significant (Figure 2-20). ANOVA results also did not show any effect ($p= 0.411$) of starch content on T_m . DSC thermograms also showed broadening in melting temperature peaks with increased starch levels (Figure 2-21). The broadening of melting peak can be attributed to increased hydrogen bonding between starch and PVOH. Zou et al. (2008) also observed slight decrease in T_m and broadening of melting peak of starch/PVOH extruded blends with increasing starch content, and attributed it to decrease in PVOH crystallinity and high miscibility of starch and PVOH.

Based on the XRD and DSC studies of starch/PVOH/Na⁺MMT systems, it can be surmised that starch/PVOH interactions were the strongest, followed by PVOH/Na⁺MMT and starch/Na⁺MMT (Figure 2-22). At starch level of 0%, interaction of PVOH with Na⁺MMT through hydrogen bonding results in rupturing the layered structure to form exfoliated nanocomposites. With the addition of starch, stronger hydrogen bonds are formed between the two polymers which compete with the PVOH-Na⁺MMT bonds and also increase the effective polymer chain lengths. This reduces exfoliation and results in intercalated nanocomposites. While on the other hand when starch level is increased to 67 and 80%, there are sufficient numbers of hydroxyl groups in the system available to interact with Na⁺MMT which might be a reason for formation of exfoliated nanostructures. A conceptual model for changes in intensity of PVOH/Na⁺MMT and starch/Na⁺MMT interactions at different starch levels is shown in Figure 2-23.

Tensile strength (TS) and elongation at break (%E) of films are shown in Figure 2-24. Starch level had a significant effect on both TS ($p=0.0004$) and %E ($p=0.0001$), as determined by ANOVA. TS decreased from 23.01 to 16.44MPa with an increase in starch content from 0 to 50%, while there was a gradual increase in TS up to 18.08MPa as starch level was increased from 50 to 80%. E% continuously decreased from 291.28 to 28.93% with increase in starch level from 0 to 80%. Yang & Huang (2008), Ramaraj (2007) and Mao et al. (2000) also reported a decrease in tensile strength and elongation at break with the increase of starch content in PVOH/starch blends. In the current study, increase in TS at 67 and 80% starch levels could be due to formation of exfoliated nanocomposites as discussed above.

Water vapor permeability (WVP) decreased from 1.483 to 1.048 g.mm/kPa.h.m² with increase in starch level from 0 to 80% (Figure 2-25). ANOVA results showed a significant effect on WVP ($p =0.0001$) of these nanocomposite films. WVP of these nanocomposite films was lower than that reported for starch films by Tang et al. (2008a) (1.61 g.mm/kPa.h.m²) and PVOH films by Strawhecker & Manias (2000) (2.0g.mm/kPa.h.m²). The intercalated and exfoliated nanocomposites structures in the current study probably played an important role in reducing WVP. Decreased WVP of the nanocomposite films with increasing starch content can be attributed to lower WVP of starch as compared to PVOH.

Conclusion

Starch/ PVOH/ Na⁺MMT nanocomposites were created in this study and it was confirmed that all the components are highly compatible with each other. Both intercalated and exfoliated structures were observed under different treatments which provided an evidence of strong molecular interactions between each component. These interactions greatly affected the physical properties of films produced from these nanocomposites. Increase in PVOH molecular weight resulted in increased TS and E% of nanocomposites films while WVP was decreased. According to the general polymer trends, longer polymer chains at high molecular weight improve mechanical and barrier properties and same was observed in these nanocomposites. Starch has poor mechanical properties and PVOH while it has better WVP. This was reflected in physical properties on nanocomposite films by decreasing TS, %E and WVP when starch level was increased. Increased Na⁺MMT levels showed an improvement in TS and WVP with reduction in %E.

XRD and TEM were used to study the nano-structure of starch/PVOH/Na⁺MMT nanocomposites and provided evidence of well intercalated and exfoliated nanostructures with different treatments. DSC results provided further insight into the structural conformations in these nanocomposites.

Figures and Tables

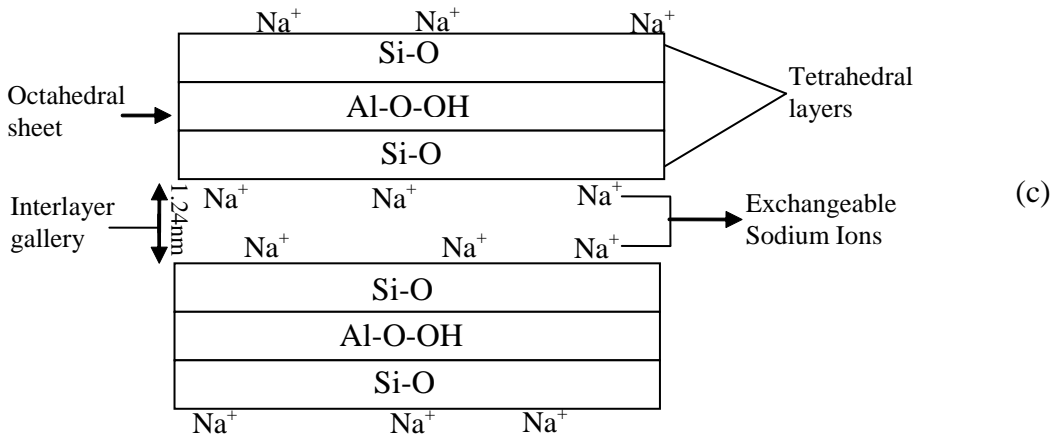
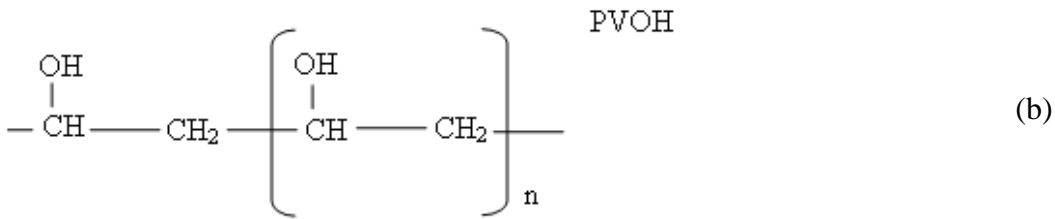
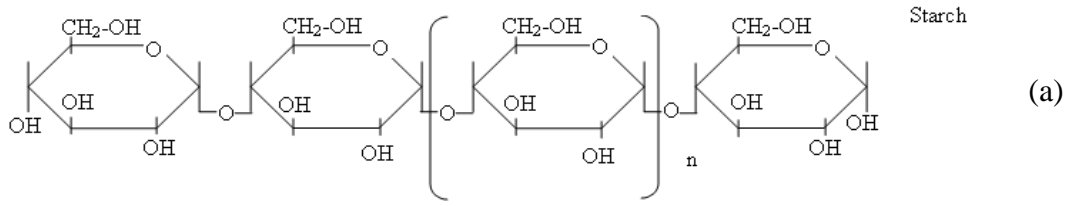


Figure 2-1 Molecular structures for a) Starch poly- α -1,4-D-glucopyranoside chain (present in both amylose and amylopectin) b) PVOH and c) schematic for molecular structure of Na^+MMT

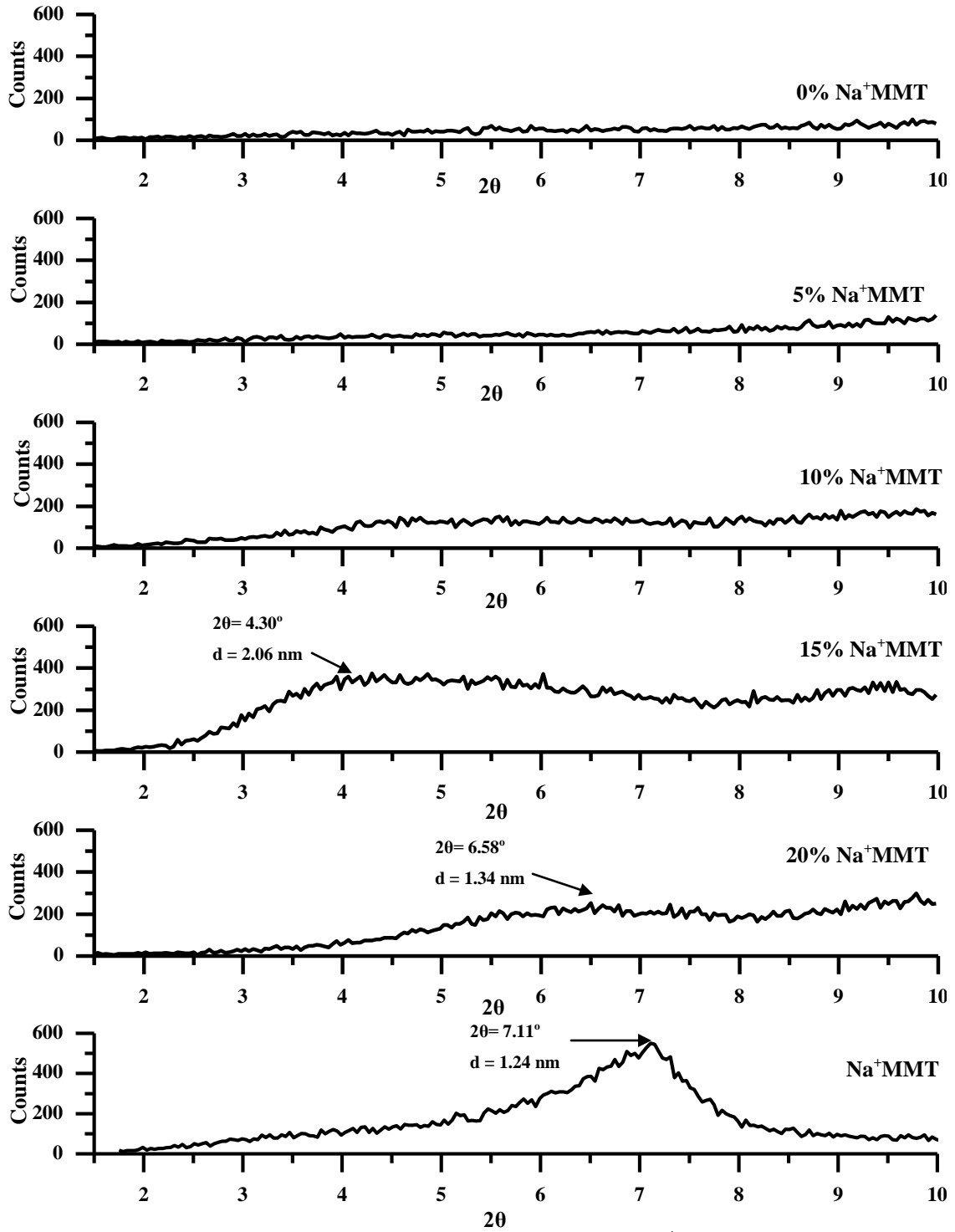
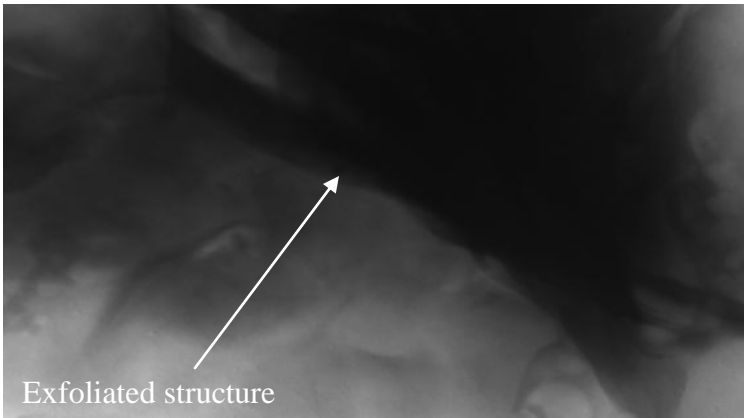
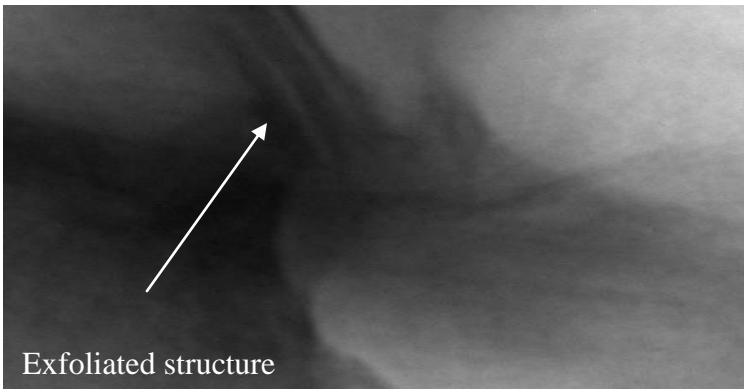
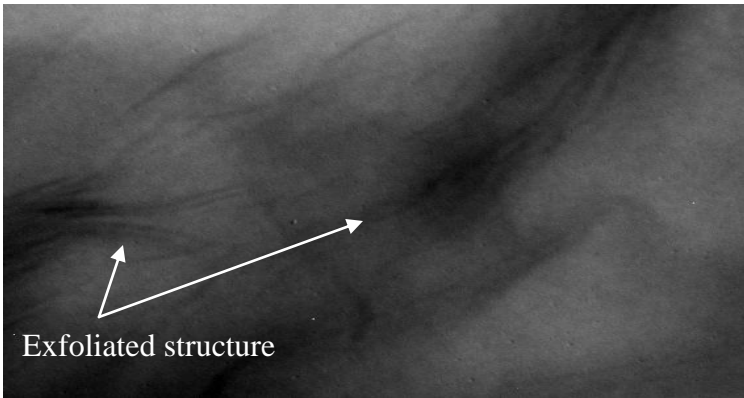


Figure 2-2 XRD patterns for nanocomposites with different Na⁺MMT levels



100 nm
HV=100kV
Direct Mag: 130000x

Figure 2-3 TEM scans for (a) 5% (b) 10% and (c) 20 % Na⁺MMT levels

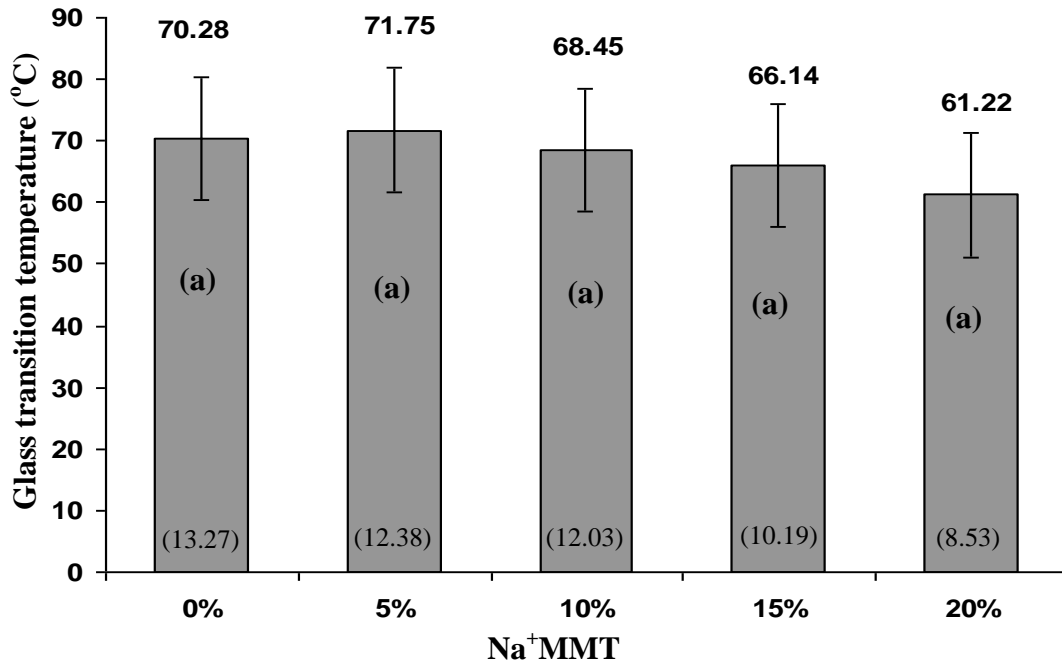


Figure 2-4 Glass transition temperature (T_g) for nanocomposite films with different Na^+ MMT levels. Results with same letters are not significantly different. Values at bottom of the bars show moisture content of films. Error bars indicate the standard deviation.

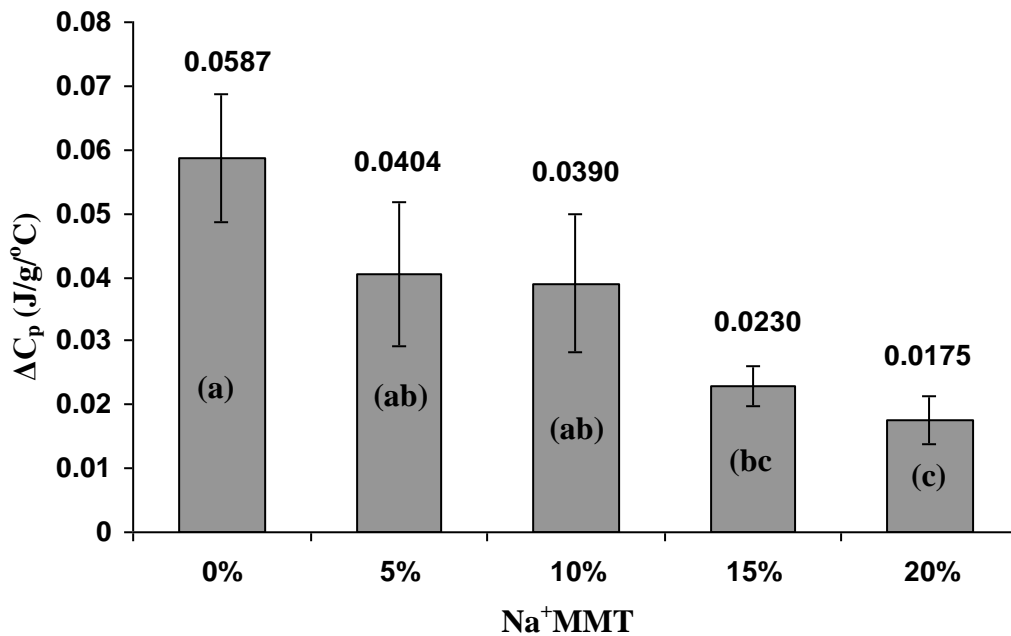


Figure 2-5 ΔC_p at T_g for nanocomposites with different levels of Na^+ MMT. Results with same letters are not significantly different. Error bars indicate the standard deviation.

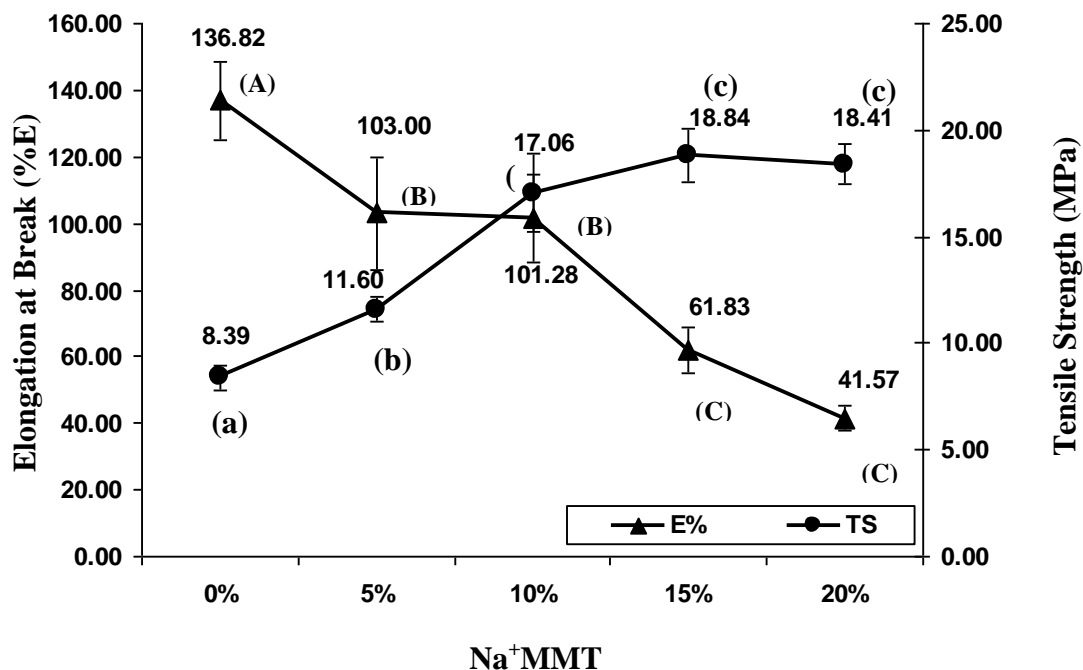


Figure 2-6 Tensile strength and elongation at break for nanocomposite films with different levels of Na⁺MMT. Results with same letters are not significantly different. Error bars indicate the standard deviation.

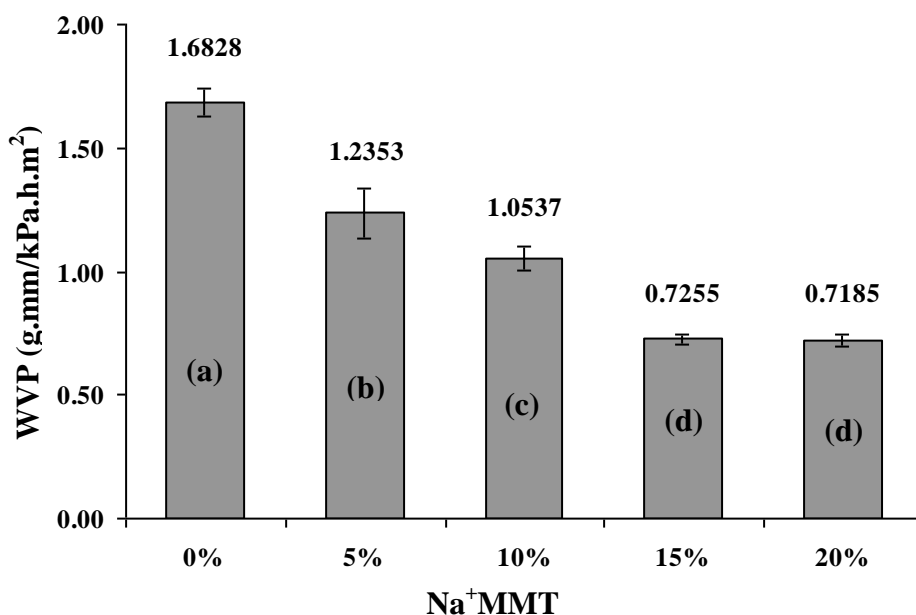


Figure 2-7 Water vapor permeability (WVP) for nanocomposite films with different levels of Na⁺MMT. Results with same letters are not significantly different. Error bars indicate the standard deviation.

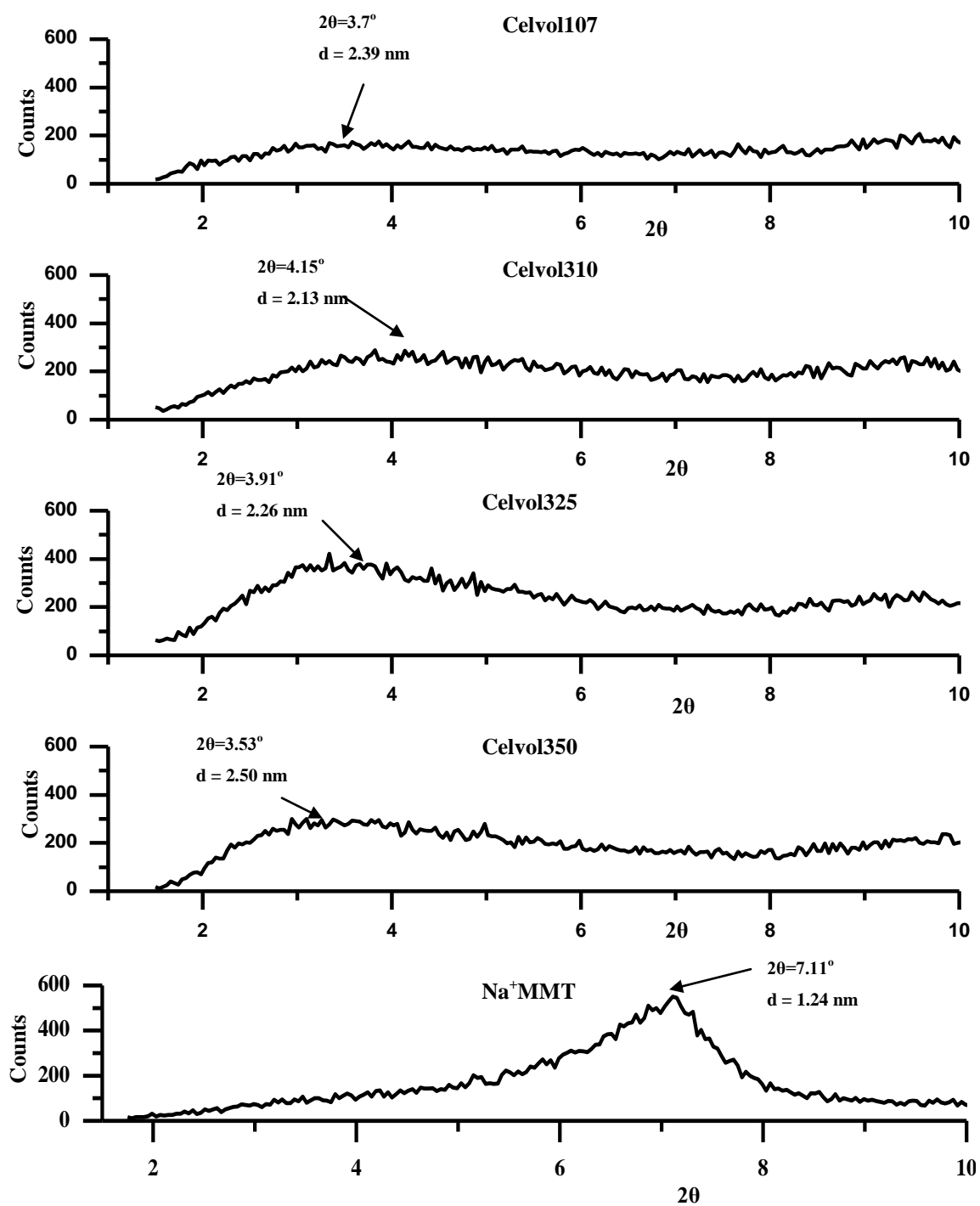


Figure 2-8 XRD patterns of nanocomposites containing PVOH with different molecular weight ranges

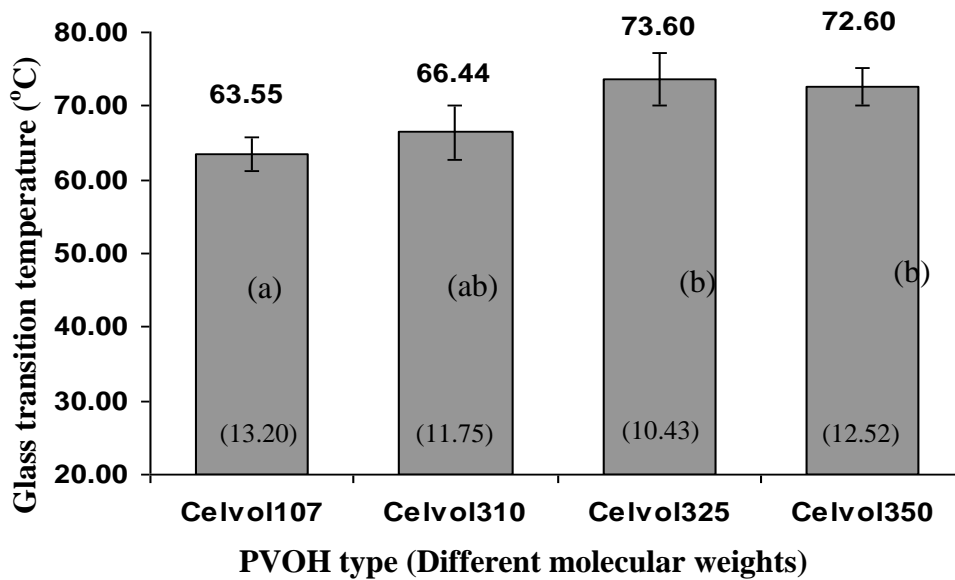


Figure 2-9 Glass Transition Temperature (T_g) at different molecular weights of PVOH. Results with same letters are statistically non-significant. Values at the bottom of the bars show moisture content of films.

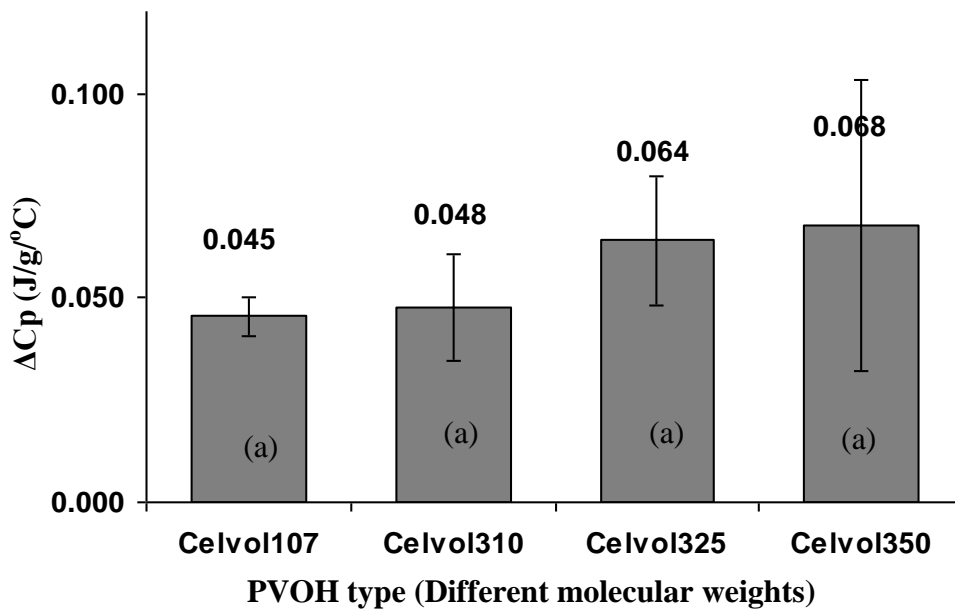


Figure 2-10 ΔC_p at T_g for nanocomposites with different molecular weight ranges of PVOH. Results with same letters are statistically non-significant. Error bars indicate the standard deviation.

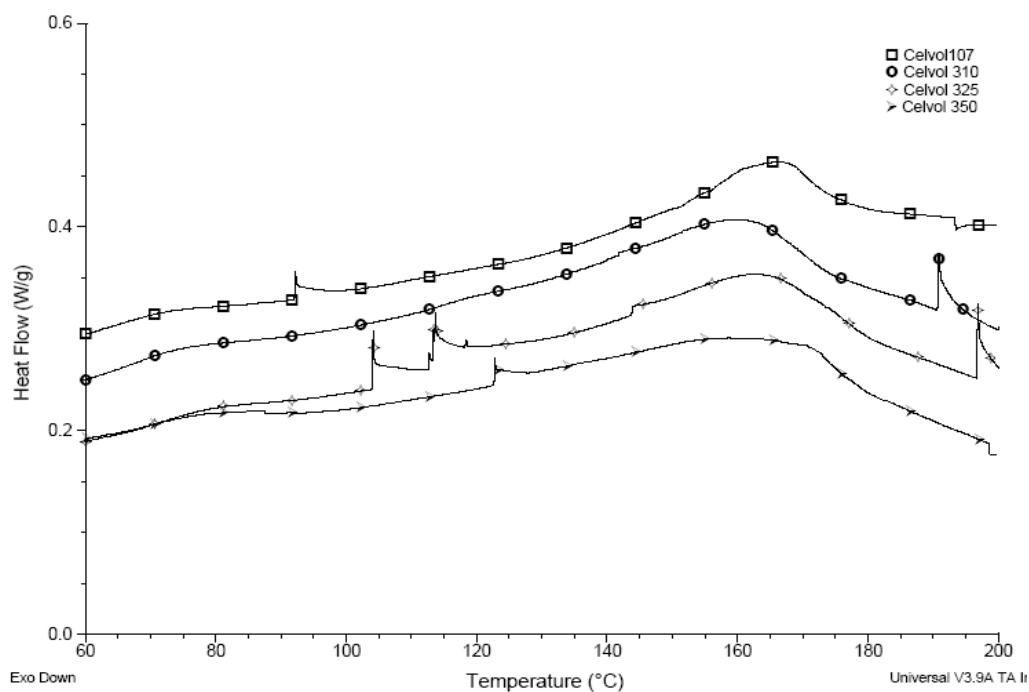


Figure 2-11 DSC Curves showing melting range peaks for different molecular weights of PVOH.

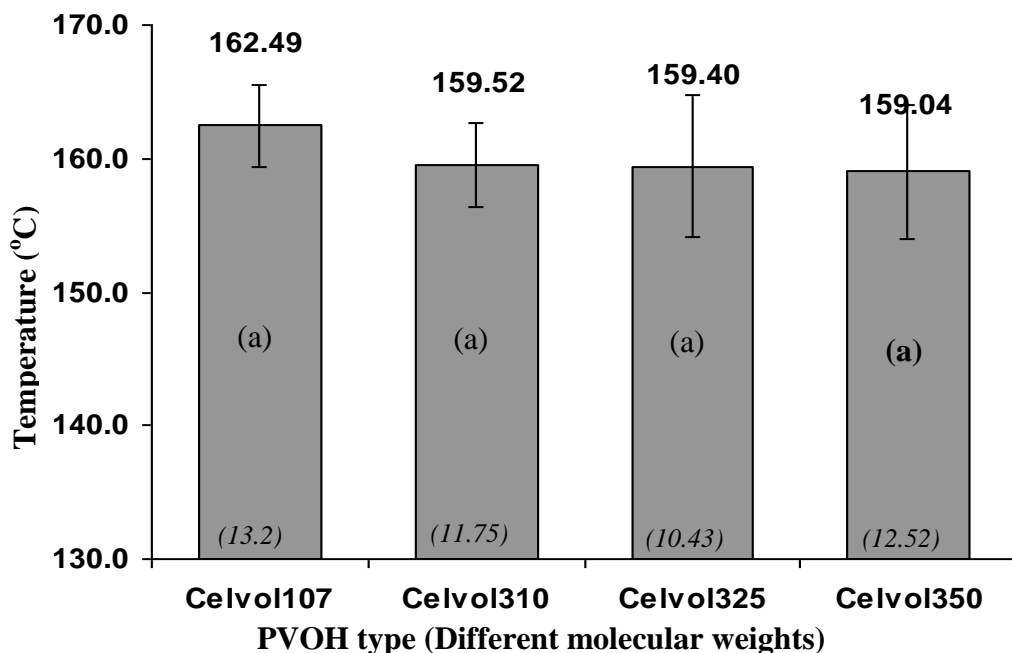


Figure 2-12 Melting Temperature (T_m) at different molecular weights of PVOH. Results with same letters are statistically non-significant. Values at the bottom of the bars show moisture content of films. Error bars indicate the standard deviation.

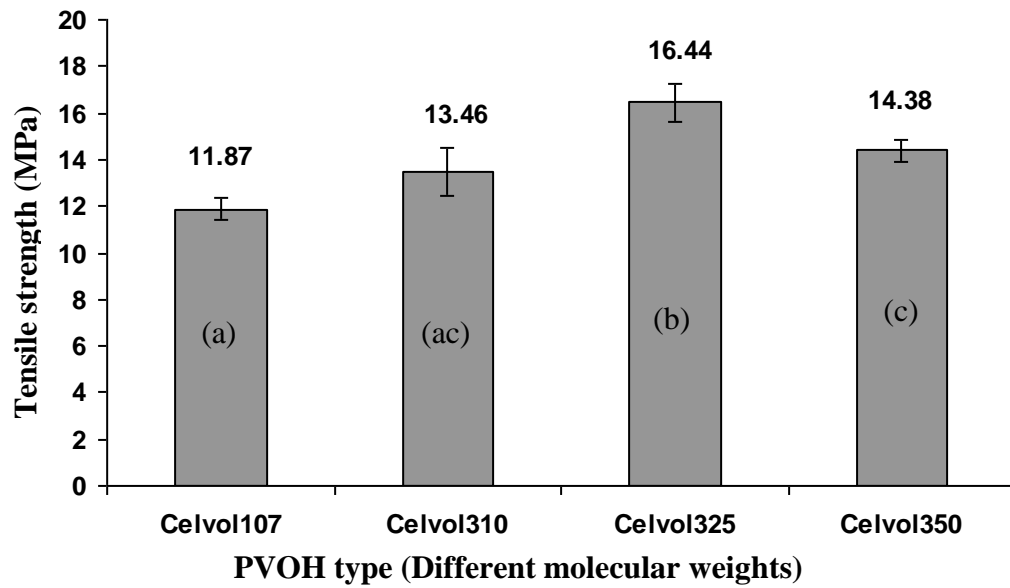


Figure 2-13 Tensile Strength for nanocomposite films with different molecular weight ranges of PVOH. Results with same letters are statistically non-significant. Error bars indicate the standard deviation.

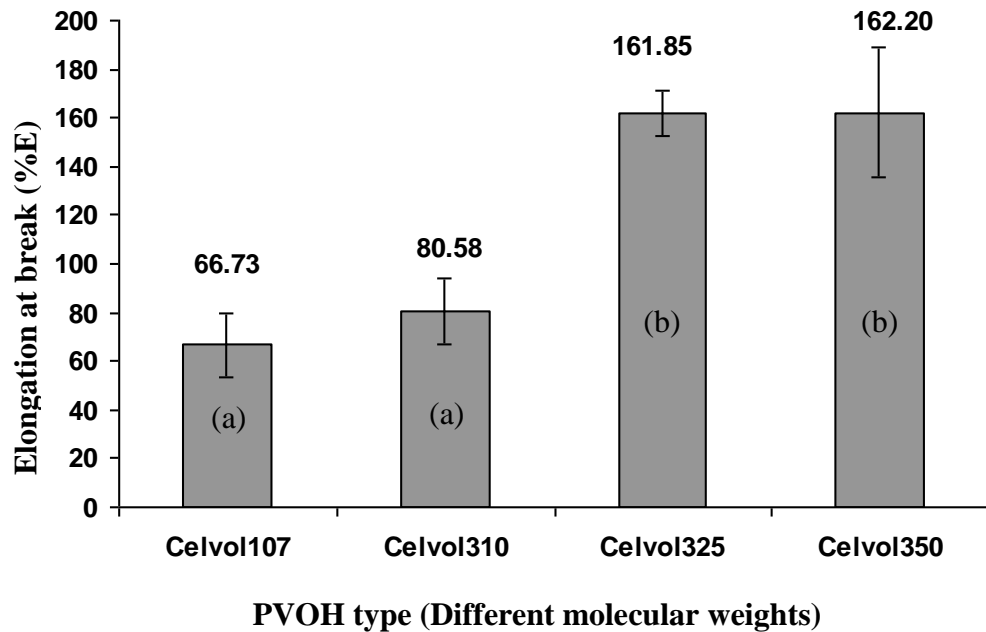


Figure 2-14 Elongation at break for nanocomposite films with different molecular weight ranges of PVOH. Results with same letters are statistically non-significant. Error bars indicate the standard deviation.

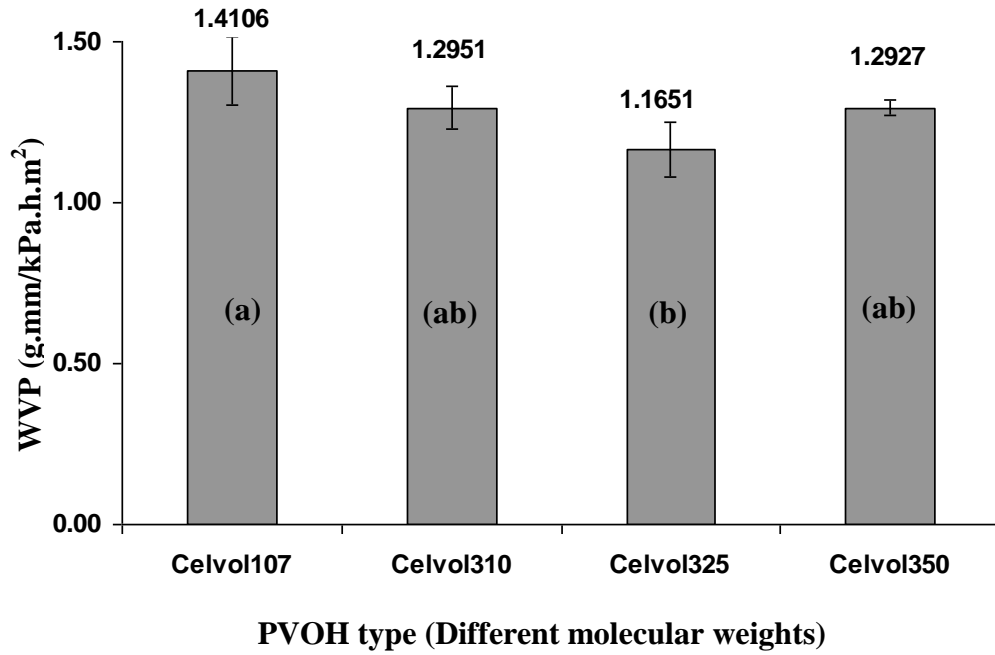


Figure 2-15 Water Vapor Permeability (WVP) of films with different molecular weight ranges. Results with same letters are statistically non-significant. Error bars indicate the standard deviation.

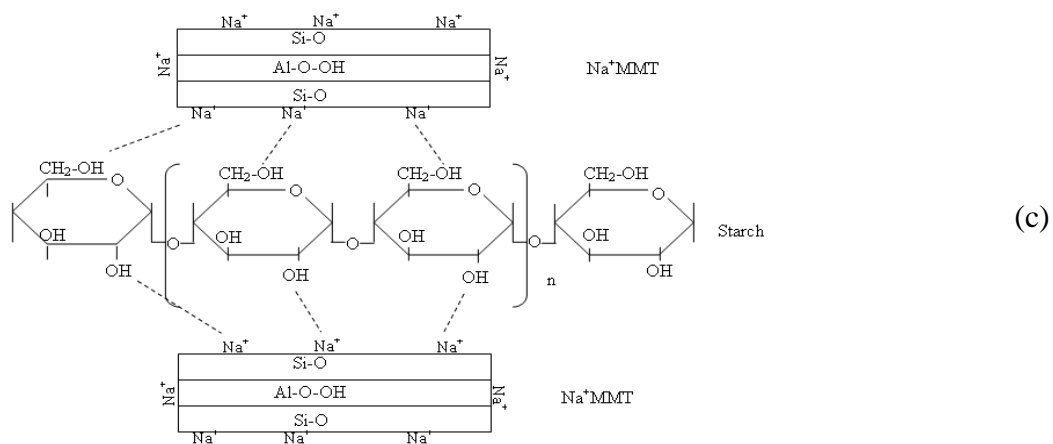
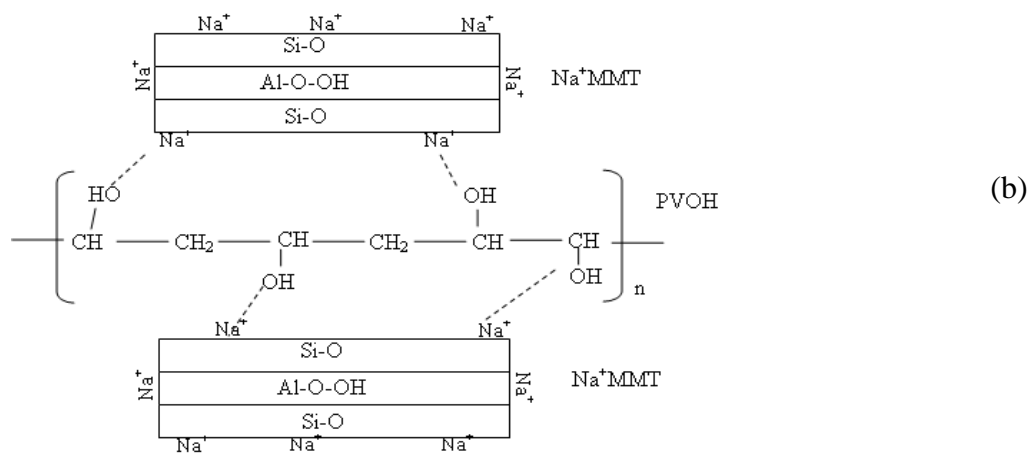
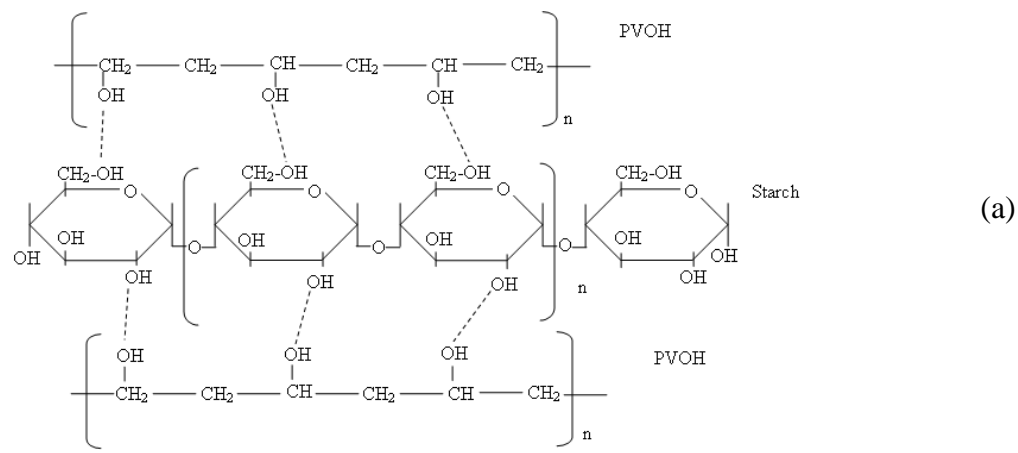


Figure 2-16 Schematics for possible molecular interaction between (a) Starch and PVOH (b) PVOH and Na⁺MMT (c) Starch and Na⁺MMT

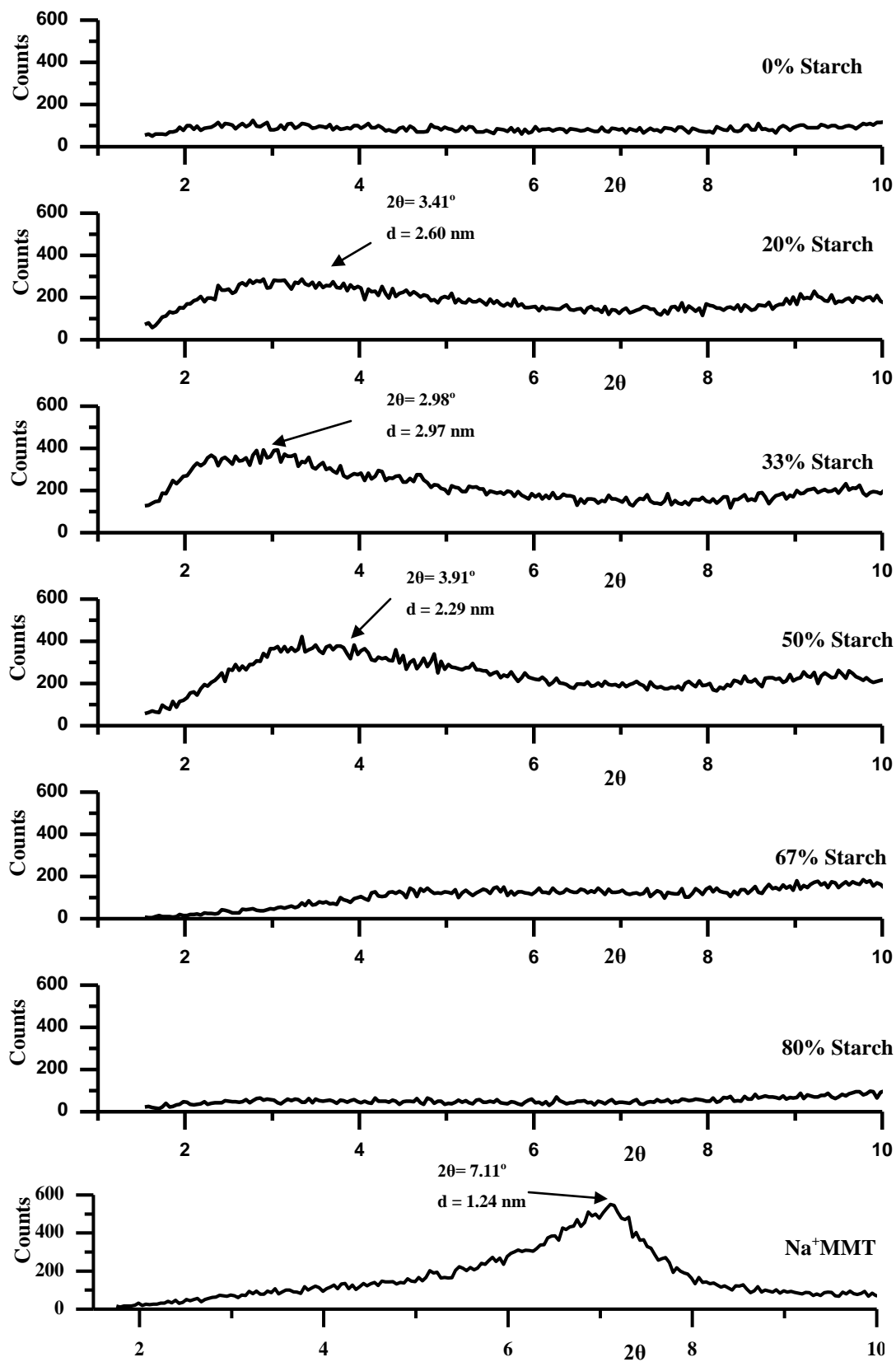


Figure 2-17 XRD patterns of nanocomposites with different levels of starch

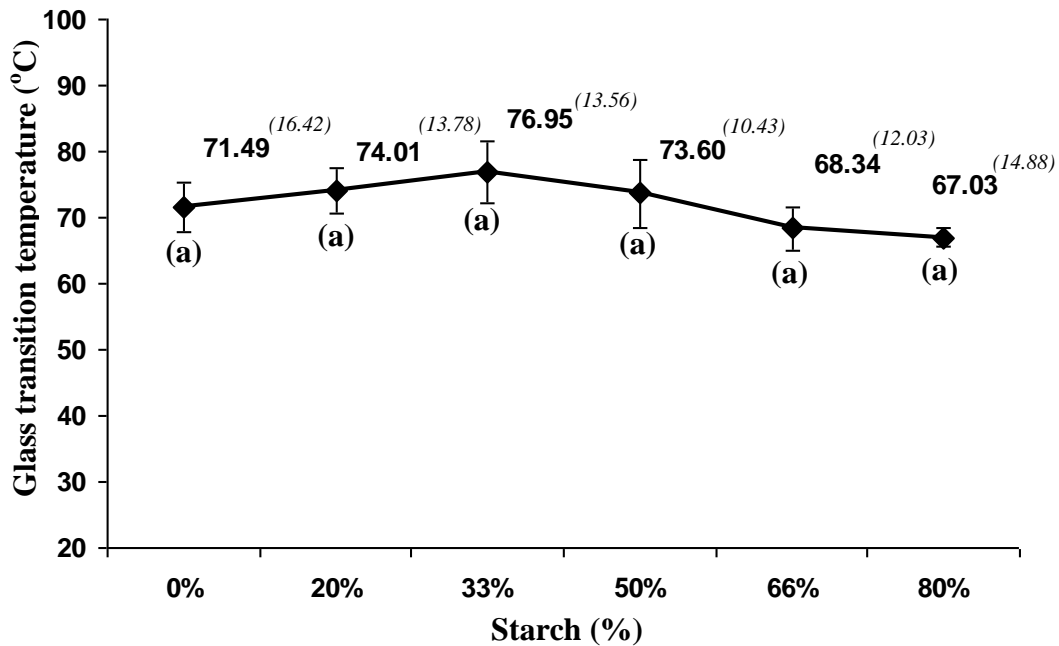


Figure 2-18 Glass Transition Temperature (T_g) at different starch levels. Results with same letters are not significantly different. Superscript values show moisture content of films. Error bars indicate the standard deviation.

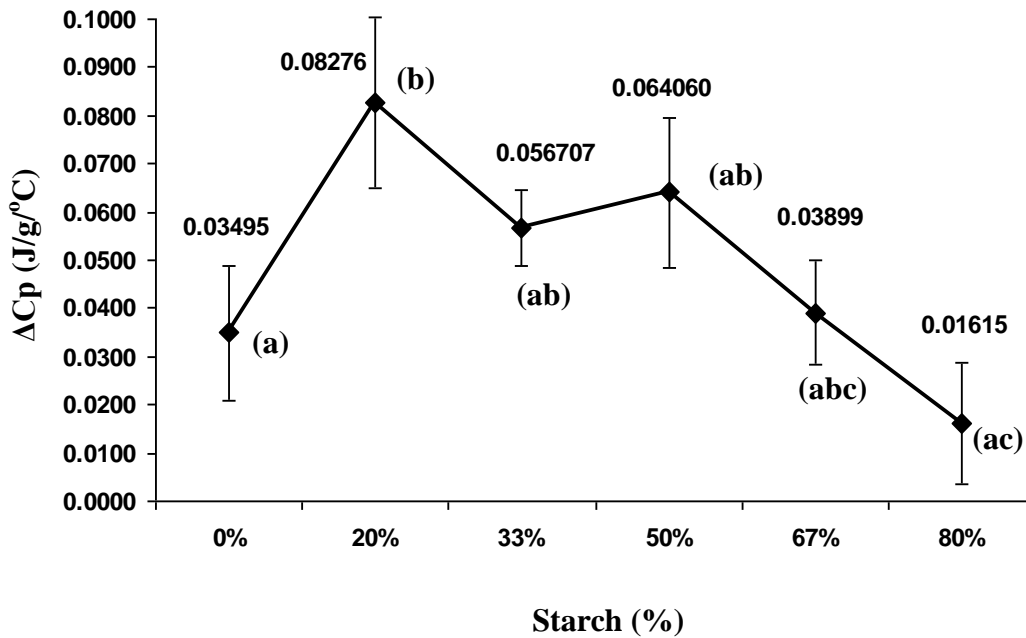


Figure 2-19 ΔC_p at T_g for different levels of starch. Error bars indicate the standard deviation.

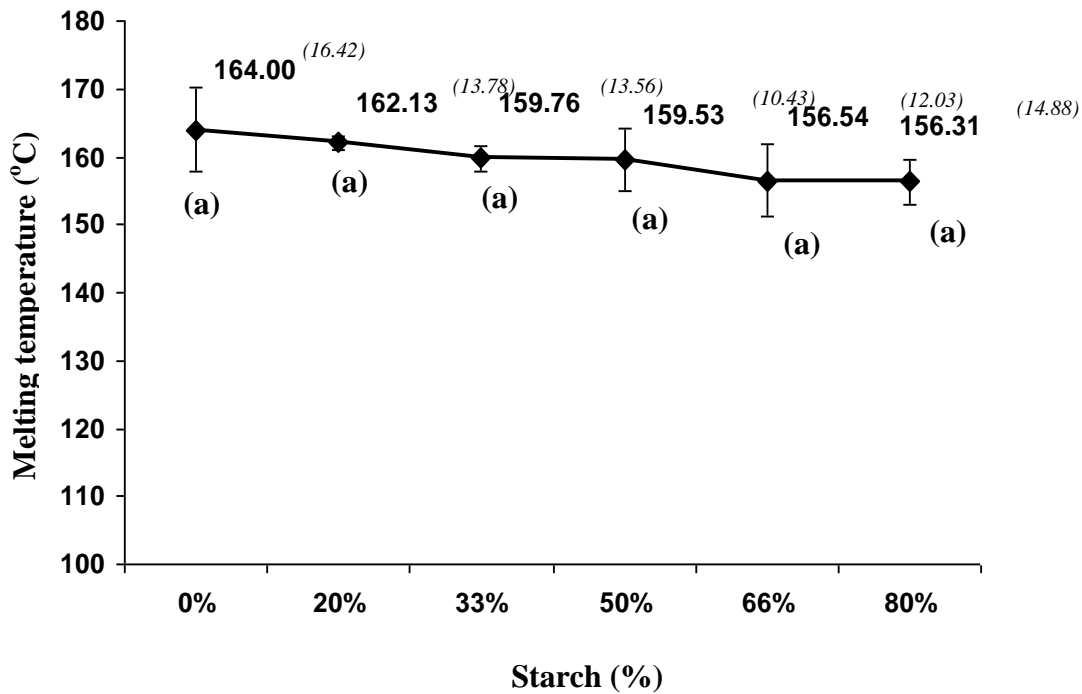


Figure 2-20 Melting temperature (T_m) at different starch levels. Results with same letters are not significantly different. Superscript values show moisture content of films. Error bars indicate the standard deviation.

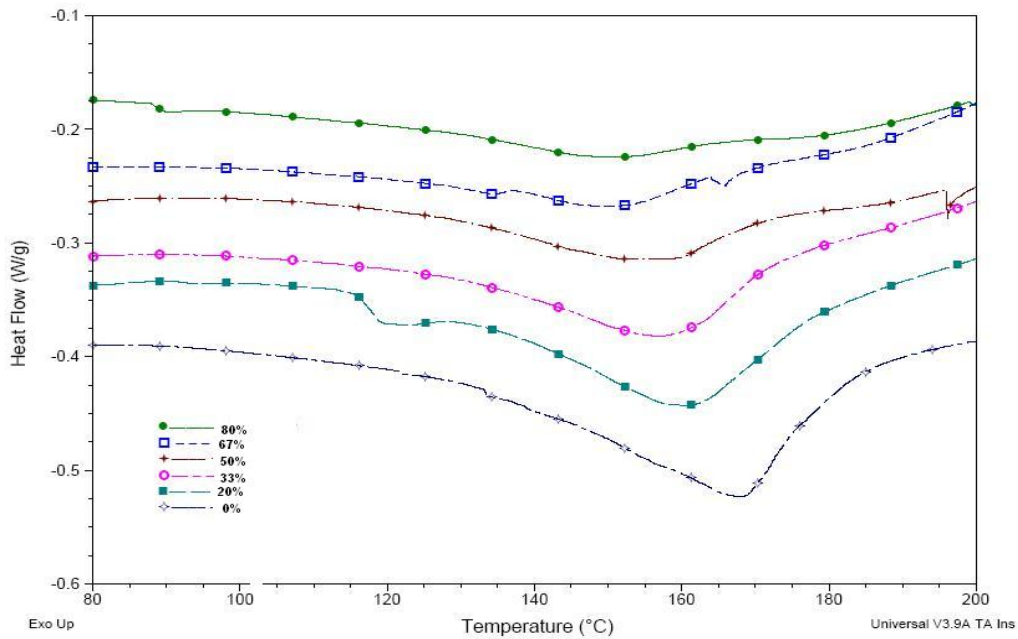


Figure 2-21 DSC curves indicating broadening of melting range peaks with different levels of starch

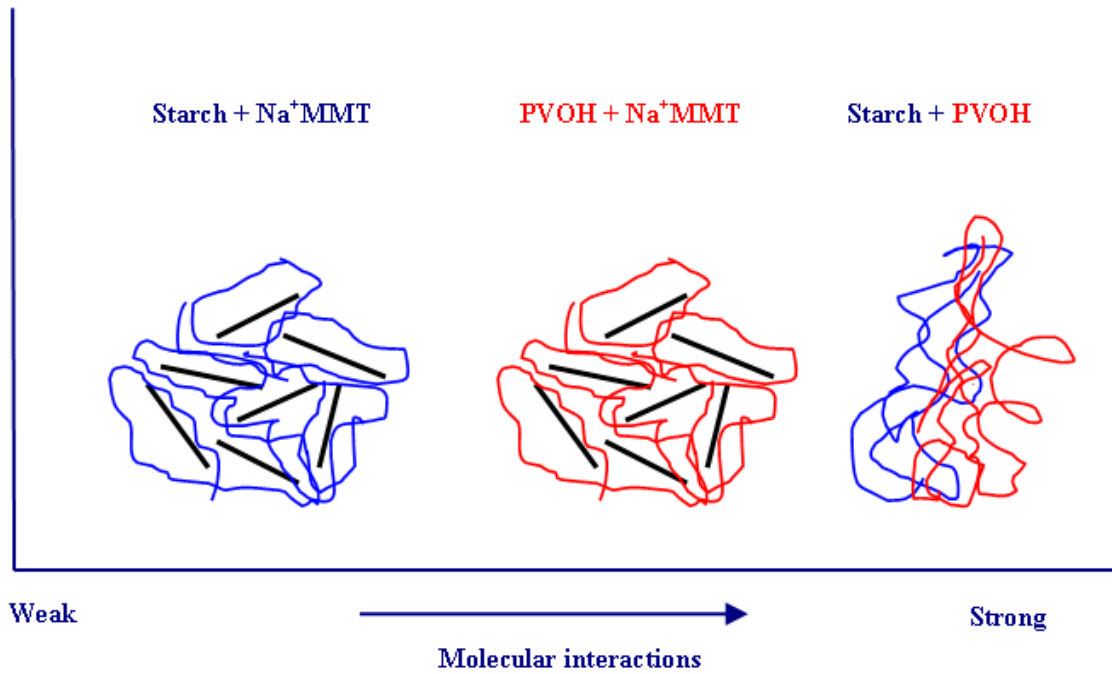


Figure 2-22 Schematic presentation of preferred interactions between different components

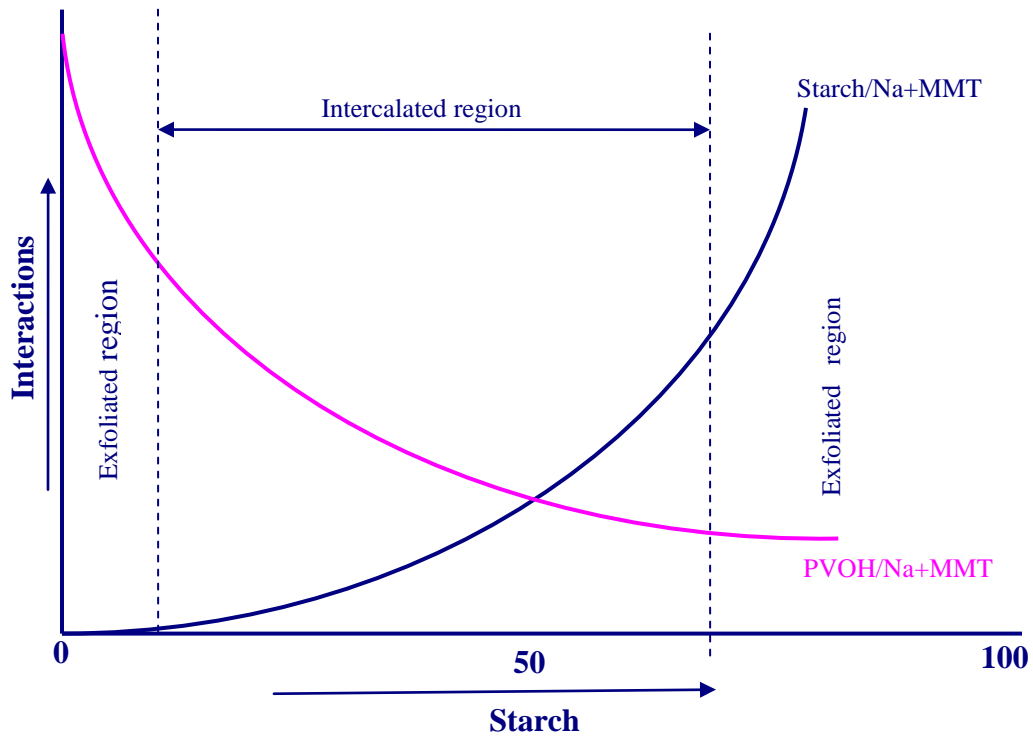


Figure 2-23 Schematic diagram for PVOH/Na⁺MMT and starch/Na⁺MMT interactions at different starch levels

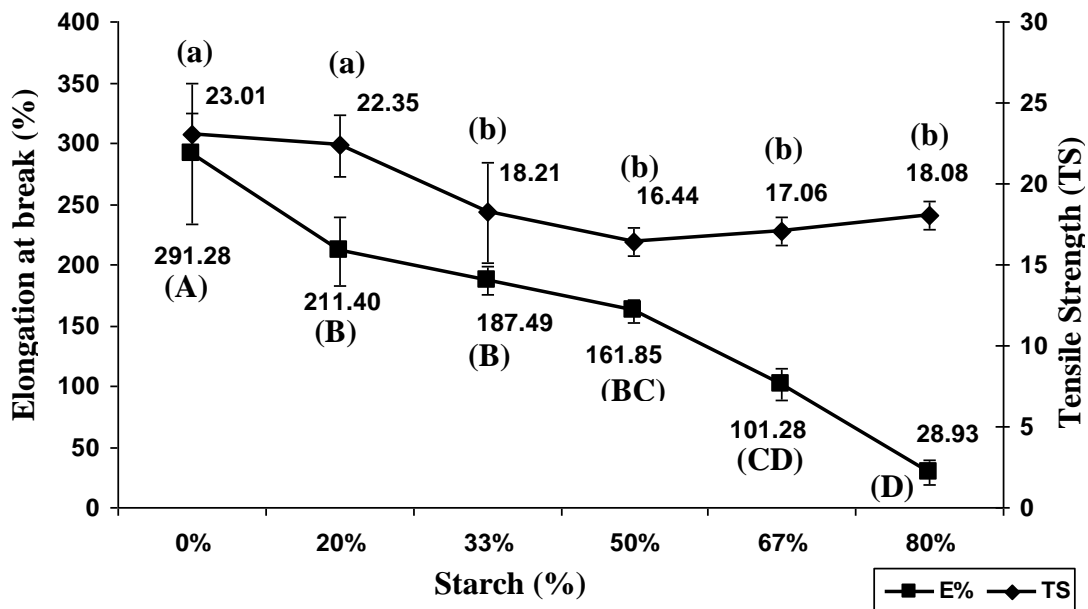


Figure 2-24 Mechanical properties of nanocomposites films with different levels of starch. Results with same letters are not significantly different. Error bars indicate the standard deviation.

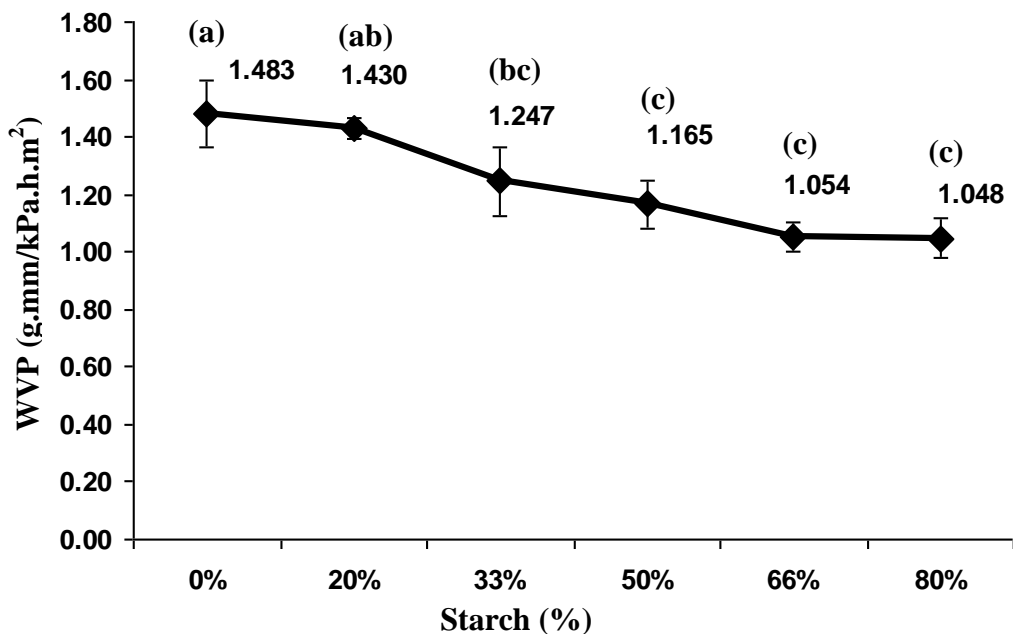


Figure 2-25 WVP for nanocomposite films with different levels of starch. Results with same letters are not significantly different. Error bars indicate the standard deviation.

Table 2-1 PVOH types used for studying molecular weight effect. Molecular weights were estimated from viscosity ranges given by the manufacturer.

Polyvinyl Alcohol Type	Molecular Weight	Viscosity (cps)
Celvol107	31,000 - 50,000	5.5 -6.6
Celvol310	60,000 – 70,000	9-11
Celvol325	100,000-130,000	28-32
Celvol350	150,000-186,000	62-72

Table 2-2 Moisture content of nanocomposite films with different molecular weights.

PVOH Type	Celvol107	Celvol310	Celvol325	Celvol350
Moisture Content(%)	13.24±0.86	11.75±1.38	10.43±0.80	12.52±1.26

Table 2-3 Moisture content of nanocomposite films with different starch levels.

Starch Levels	0%	20%	33%	50%	67%	80%
Moisture Content(%)	16.42±0.70	13.78±0.51	13.56±0.55	10.43±0.80	12.03±0.69	14.88±1.50

Table 2-4 Moisture content of nanocomposite films with different Na⁺MMT content.

Na⁺MMT Content	0%	5%	10%	15%	20%
Moisture Content(%)	13.27±1.60	12.38±0.74	12.03±0.69	10.19±0.98	8.53±1.08

CHAPTER 3 - Structure and physical properties of starch/polyvinyl alcohol/ Na⁺MMT nanocomposites prepared using melt extrusion processing

Abstract

Starch is an inexpensive and abundant renewable source which has great potential for use as a base material in the production of biodegradable packaging. This study is a step towards replacing petroleum-based packaging with biodegradable nanocomposite material made from starch (67%) and poly vinyl alcohol (PVOH) (33%) as base polymers. Glycerol (30%) and sodium montmorillonite (0-20%) were used as a plasticizer and nano-filler, respectively. A lab scale melt extrusion process was used to produce these nanocomposites and films were made by casting. Process parameters, including screw speed (200-400 RPM) and barrel temperature (145-165°C), were varied systematically. Film nanostructure was characterized by X-ray diffraction (XRD) and transmission electron microscopy (TEM). Differential scanning calorimetry (DSC) was utilized to characterize the thermal properties of nanocomposites and understand the molecular-level interactions between various components. Tensile strength and elongation at break ranged from 4.72 to 10.86 MPa and 93.66 to 330.15%, respectively, while water vapor permeability ranged from 1.672 to 1.458g.mm/kPa.h.m². Structural and thermal data indicated important role for Na⁺MMT along with process parameters in controlling exfoliation and glass transition temperature of the nanocomposites.

Introduction

Use of biodegradable materials can provide a solution to the environmental deterioration caused by solid waste from petroleum based packaging (Jayasekara, Harding, Bowater, Christie & Lonergan, 2004). Consumer awareness of environmental damage and strain on scarce resources caused by non-degradable and non-renewable conventional plastic packaging is playing an importance role in the increased interest in alternatives (Elizondo, Sobral & Menegalli, 2009). Starch has unique advantage of being an inexpensive, biodegradable and abundant material, with the potential of replacing petroleum based packaging such as films (Averous, 2004). However, starch films are very brittle in nature and have poor water barrier

properties (Dean, Yu & Wu, 2007; Tang, Alavi & Herald, 2008a). This limits their use in packaging applications for various products, especially processed foods. Consequently, different methods to improve barrier and mechanical properties of starch based biodegradable films are being investigated.

One successful option is to produce starch blends with other polymers such as polyhydroxyalkonates (Parulekar & Mohanty, 2007), poly lactic acid (PLA) (Jang, Shin, Lee & Narayan, 2007; Jun, 2000) and polyvinyl alcohol (PVOH) (Mao, Imam, Gordon, Cinelli & Chiellini, 2000; Yang & Huang, 2008; Zou, Ping-Qu & Liang-Zou, 2008). Starch and PVOH blends are of particular interest because they are highly compatible with each other and make hydrogen bonds readily (Russo, O'Sullivan, Rounsefell, Halley, Truss & Clarke, 2009; Zhou, Cui, Jia & Xie, 2009). Films from starch and PVOH blends both show improved mechanical properties over those of starch alone (Mao, Imam, Gordon, Cinelli & Chiellini, 2000) and are biodegradable (Yang & Huang, 2008).

However, films based on starch and/or PVOH have inferior water vapor barrier properties because of the hydrophilic nature of these materials. Creation of nanocomposites of biopolymers with layered silicates or clays is one approach to improve barrier properties of biodegradable films along with other physical properties including mechanical strength. The naturally occurring clay montmorillonite or Na^+MMT is one such layered silicate which can be used with starch and PVOH to produce nanocomposites. Starch is compatible with Na^+MMT due to the interaction between its polar hydroxyl groups and inorganic Na^+ ions of the nano-clay. This results in improved mechanical and barrier properties of the starch films (Avella, De Vlieger, Errico, Fischer, Vacca & Volpe, 2005; Dean, Yu & Wu, 2007; Tang, Alavi & Herald, 2008a). PVOH is also highly compatible with Na^+MMT and films made from these nanocomposites exhibit better mechanical and barrier properties than do films based on PVOH alone (Strawhecker & Manias, 2000).

Not all mixtures of polymers and layered silicates exist as nanocomposites. In fact, such composites can be of three types; microcomposites, in which the polymer is not miscible with clay and stays in a separate phase with no structural change occurring in the clay platelets, intercalated nanocomposites, in which the polymer can enter clay interlayer regions without completely disrupting the layered structure; and exfoliated nanocomposites, in which the layered structure is completely disrupted (Alexandre & Dubois, 2000; Paul & Robeson, 2008).

Different methods are used to prepare polymer-layered silicate nanocomposites including; solution, melt intercalation and *in situ* intercalative polymerization (Alexandre & Dubois, 2000). In solution method, layered silicates such as Na⁺MMT are dispersed in the solvent and the dissolved polymer forms nanocomposites after the solvent is evaporated. In this process, there are two main factors which play an important role in the formation of nanocomposites: 1) hydration of Na⁺ ions which results in swelling of MMT layers providing the ability to host polymer chains between them (Paul & Robeson, 2008), and 2) heat increases mobility of polymer chains and also degrades the polymer in some cases which helps the polymer chains to enter silicate layer galleries. In melt intercalation method, polymer is mixed with layered silicates in molten state and no solvent is required in this case (Alexandre & Dubois, 2000). The extrusion process is one method used to create nanocomposites by melt intercalation. Extrusion provides the high energy required to melt polymers, via thermal and/or mechanical means, and also disrupts layered silicate structure due to shearing action of the screw. In *in situ* intercalative polymerization, layered silicates are swollen in liquid monomers or monomer solution and polymerization occurs between silicate layers. This results in the formation of intercalated nanocomposites. Solution and melt intercalation are the most widely explored methods for preparing starch/ Na⁺MMT or PVOH/ Na⁺MMT nanocomposites (Avella, De Vlieger, Errico, Fischer, Vacca & Volpe, 2005; Chivrac, Pollett, Schmutz & Averous, 2008; Dean, Yu & Wu, 2007; Strawhecker & Manias, 2000; Tang, Alavi & Herald, 2008a, b). The extrusion process however provides better exfoliation in resulting nanocomposites, as compared to solution method.

Glycerol is the conventional plasticizer used in starch and PVOH blends as it forms hydrogen bonds with these biopolymers (Zhou, Cui, Jia & Xie, 2009). Glycerol helps starch and PVOH molecules to enter the Na⁺MMT interlayer galleries and creates well intercalated nanocomposite structures. The hydrogen bonds formed by glycerol with PVOH and starch also hinder the formation of crystallites in these plasticized films (BeMiller & Whistler, 2009; Lim & Wan, 1994)

Starch and PVOH blends have shown good compatibility and researchers have already explored starch/ Na⁺MMT and PVOH/ Na⁺MMT interactions. A series of investigations has also shown good compatibility among starch/PVOH/Na⁺MMT multi-component nanocomposites. These studies are focused on structural and thermal properties of starch/PVOH/Na⁺MMT

nanocomposites. (Dean, Do, Petinakis & Yu, 2008; Dimonie, Constantin, Vasilievici, Popescu & Garea, 2008; Spiridon, Popescu, Bodarlan & Vasile, 2008; Vasile, Stoleriu, Popescu, Duncianu, Kelnar & Dimonie, 2008b). These nanocomposites are also found to be biodegradable. (Spiridon, Popescu, Bodarlan & Vasile, 2008) However, starch/PVOH/ Na⁺MMT nanocomposites are a relatively new research area and little is known about their interactions. Investigations in the preceding chapter provided an evidence for interactions in these nanocomposites.

This study focused on utilization of melt extrusion method for synthesis of starch/PVOH/ Na⁺MMT nanocomposites and developing a fundamental understanding of molecular level interactions between various components and their impact on physical properties of films made from these nanocomposites. The impact of extrusion processing parameters and Na⁺MMT concentration were specifically investigated, and comparison was made with nanocomposites synthesized by solution method as previously described.

Materials and methods

Materials

Corn starch was obtained from Cargill, Incorporated (Minneapolis, MN). Celvol325, a fully hydrolyzed brand of polyvinyl alcohol, was obtained from Celanese Corporation, Dallas, Texas. Na⁺MMT (Cloisite Na⁺) was obtained from Southern Clay Products Inc. (Gonzales, TX, USA). Glycerol was purchased from ChemistryStore.com (Walter Price St. Cayce, SC).

Preparation of nanocomposites

In all experiments, starch (67%) and PVOH (33%) were used as base polymers, to which glycerol was added at a concentration of 30% by wt (polymer basis). The level of Na⁺MMT was adjusted according to the treatment as described later. Starch, PVOH, Na⁺MMT, glycerol and water (800 g) were mixed in a lab scale N-50 Hobart mixer (N-50, Hobart Corporation, Troy, OH). Glycerol and water were added drop by drop while mixing rest of the materials. Moisture addition was calibrated to achieve an in-barrel moisture content of 15%. Extrusion was conducted in a lab scale co-rotating twin screw extruder (Micro-18, American Leistritz, Somerville, NJ) with a six-head configuration, screw diameter of 18 mm, and L/D ratio of 30. The screw configuration, die design and barrel temperature profiles are shown in Figure 3-1. Final zone temperature was lowered to 110°C in order to keep the extrudates unexpanded. Dried

extradites were ground using a Wiley mill (model 4, Thomas-Wiley Co., Philadelphia, PA) and an Ultra mill (Kitchen Resource LLC., North Salt City, UT) to reduce the particle size to 75 micron maximum.

Specific mechanical energy (SME)

The specific mechanical energy (SME) is an important parameter in extrusion. It provides information about the specific work input from motor to material being extruded. SME can be computed as;

$$SME = \frac{(\tau - \tau_0) \times P_{rated} \times \frac{N}{N_{rated}}}{m} \text{ KJ / Kg} \quad (1)$$

where τ is the measured torque, τ_0 is the no-load torque P_{rated} is the rated power for extruder, N is the measured extruder speed in RPM, N_{rated} is the rated screw speed (500RPM); and m is mass flow rate, kg/sec.

Film casting

Solution was prepared by heating to 95°C a mixture of 4% by wt of ground extrudate and 96% water, followed by continuous mixing for 30 minutes while maintaining the temperature. The heated solution was cooled to 55°C and equal amounts (60g) were poured in 150 x 15 mm Petri dishes. The water was allowed to evaporate for 24 to 36 hours at room temperature. The resulting films were peeled off the Petri dishes and stored at room temperature in air tight bags until analyzed.

X-Ray diffraction analysis

Dispersion of Na⁺MMT in the polymer matrix was investigated by X-ray diffraction (XRD) using a Bruker D838Advance X-ray diffractometer (40kV, 40mA) (Karlsruhe, Germany). Film samples were scanned at diffraction angles (2θ) of 1-10° and a scan speed of 1.5 sec/step with step size of 0.01°. D-spacing of Na⁺MMT layers was estimated from the XRD scans by using Bragg's Law as follows:

$$D = \frac{\lambda}{2\text{Sin}\theta} \quad (2)$$

where λ = wavelength of X-ray beam, θ = the angle of incidence corresponding to the observed XRD peak.

Transmission electron microscopy

Nanostructure of the composites was studied by transmission electron microscopy (TEM) using a Philips CM100 electron microscope (Mahwah, NJ), operating at 100kV. Solution prepared from ground extrudate was placed on a carbon-coated copper grid and dried for one minute to create a film, which was then analyzed using TEM.

Thermal analysis

Glass transition temperature (T_g), heat capacity change at T_g (ΔC_p) and melting temperature (T_m) were measured by differential scanning calorimetry (DSC) using Model: Q100 (TA Instruments, New Castle, DE). Film samples were conditioned at 23°C and 50% RH for 3 days prior to testing. Samples (20-25 mg) were hermetically sealed in aluminum pans then heated from 10°C to 250°C at a heating rate of 10°C/ min. An empty aluminum pan was used as a reference.

Moisture content

Moisture content was measured using AACC 44-19 (air-oven method) by placing the samples in oven at 135°C for 2 hours.

Rapid visco analysis

A Rapid Visco Analyzer (model RVA4, Newport Scientific Pty. Ltd, Australia) was used to study polymer degradation during nanocomposite synthesis. Ground extrudate (3g) with a particle size of 75 micron maximum was added to 25 ml of water in an aluminum cannister. The RVA temperature profile was: raising to 95°C in 10 min, holding for 30 min, and lowering to 55°C in 35 minutes. The peak viscosity obtained from the pasting curve was used to infer the degree of polymer degradation.

Tensile properties

Tensile properties of films were measured with a texture analyzer (TA-XT2, Stable Micro Systems Ltd., UK) using ASTM D882-02 method. Detailed testing methodology was

described by Tang et al (2008a, b). Films were cut into 2cm × 8cm strips and conditioned at 23°C and 50% RH. These strips were then mounted on the stretching arms of the machine which were 4cm apart. A crosshead speed of 1 mm/sec was used. Tensile strength (TS) and elongation at break (%E) were calculated using the following equations:

$$TS(MPa) = \frac{L_p}{a} \times 10^{-6} \quad (3)$$

where L_p = peak load (N), and a = cross-sectional area of samples (m^2), and

$$E\% = \frac{\Delta L}{L} \times 100 \quad (4)$$

where ΔL = increase in length at breaking point (mm), and L = original length (mm).

Water vapor permeability

Water vapor permeability (WVP) was determined according to the standard method ASTM E96-00. This method was also discussed in detail by Tang et al. (2008a,b). Films were tightly fixed with screws on top of the desiccant (silica gel) containing aluminum test cells (area = 30cm²). These test cells were placed in a relative humidity chamber at 25°C and 75% relative humidity (RH) and were allowed to equilibrate for 2 hours. Then weight of test cells was measured at 0 hour and after every 12 hours over three days. The change in the weight of these cells was used to calculate the slope for each sample after plotting as a function of time. The water vapor transmission rate (WVTR) was calculated from the slope of the straight line ($\frac{\Delta G}{\Delta t}$) divided by the transfer area (A):

$$WVTR = \frac{\Delta G}{\Delta t A} \text{ g/h}\cdot\text{m}^2 \quad (5)$$

where G = weight change (g), t = time (h) and A = test area (m^2). WVP was calculated using WVTR as follows:

$$WVP = \frac{WVTR \times d}{\Delta P} \text{ g}\cdot\text{mm/kPa}\cdot\text{h}\cdot\text{m}^2 \quad (6)$$

where d = film thickness (mm) and ΔP = partial pressure difference across the films (kPa). Film thickness was measured from five different locations of the films using electronic digital micrometer (Marathon Watch Company Ltd. Ontario, Canada) and average thickness (0.12 to 0.15 mm) was used for further calculations.

Experimental design and statistical analysis

Five levels of Na⁺MMT 0,5,10, 15 and 20% (polymer basis) were investigated under constant processing conditions of 300 RPM screw speed and low barrel temperature profile (Figure 3-1). To study the effect of extrusion processing parameters, the blend with 10% Na⁺MMT was processed at three screw speeds (200RPM, 300RPM and 400RPM) at the low barrel temperature conditions, and two barrel temperature profiles at a screw speed of 300 RPM (Figure 3-1). All other extrusion parameters were kept same as described earlier.

Three replicates were conducted for each analysis described above. Data were analyzed using statistical analysis software (SAS, Version 9 SAS Institute Inc. Cary, NC). One-way analysis of variance (ANOVA) was used to determine the significance of treatment effects ($p < 0.05$), whereas significant differences between treatment means were evaluated using the Tukey multiple-comparison method ($p < 0.05$).

Results and discussion

Different levels of Na⁺MMT

In general, specific mechanical energy (SME) input (407.6 - 911.9 kJ/kg) during the extrusion process increased as clay level was raised. Extrusion being a high energy process provided enough shear stress to disrupt the clay structure resulting in nanocomposites with partial to complete exfoliation. X-ray diffraction scans for starch/PVOH composite films with different Na⁺MMT levels (0-20%) are shown in Figure 3-2. No diffraction peak was noticeable at Na⁺MMT levels of 5 and 10%. This indicated that Na⁺MMT layered structure was completely disrupted resulting in a exfoliated nanocomposite system. These exfoliated structures were also confirmed by TEM scans for nanocomposites with 5 and 10% Na⁺MMT, which showed disrupted silicate layers (Figure 3-3). Dimonie et al. (2008) also observed exfoliated structures in starch/PVOH/ Na⁺MMT nanocomposites produced through melt processing with Na⁺MMT level of 3%. New peaks at lower 2θ angles than natural Na⁺MMT ($2\theta = 7.11^\circ$, d -spacing= 1.24nm)

were identified for 15 and 20% Na⁺MMT (Figure 3-2). Such a reduction in 2θ angle and increase in d-spacing provides evidence of intercalation in the nanocomposites. Peak intensities for these nanocomposites were also lower than that of pure Na⁺MMT which also indicated partial exfoliation in the system. TEM scans for nanocomposites with 15% Na⁺MMT (Figure 3-3) showed that substantial portion of silicate layers were still organized parallel to each other, which confirmed presence of intercalated structures. Different studies on polymer nanocomposites have shown same trend of decreased exfoliation with increasing Na⁺MMT level, including results obtained earlier by our research group for starch/ clay nanocomposites using extrusion (Tang, Alavi & Herald, 2008a). Good intercalation at all levels of Na⁺MMT (3, 6, 9, 15 and 21%) was observed, however degree of exfoliation decreased with increasing clay levels in the nanocomposites.

DSC analysis of nanocomposite films provided information about glass transition temperature (T_g), heat capacity (ΔC_p) at T_g and melting temperature (T_m). T_g for the nanocomposites with different levels of Na⁺MMT is shown in Figure 3-4. Variation in T_g provided useful information for understanding structural conformations and interactions between polymer and clay, although ANOVA results did not indicate significant impact of Na⁺MMT content ($p=0.27$). Starch/PVOH composites with 0% Na⁺MMT had a T_g of 63.09°C which increased to 70.19°C with the addition of 5% Na⁺MMT. Further increases in Na⁺MMT levels to 10, 15 and 20% Na⁺MMT showed a decrease in T_g to 66.77, 61.54 and 59.32°C, respectively. In polymer/clay nanocomposite systems, two types of dynamic behaviors are commonly observed. One is associated with slower relaxation of polymer chain segments and results in increased T_g . This is observed in most exfoliated and some intercalated systems where the slower relaxation behavior is attributed to increased interlayer distance and enhanced surface interactions between polymer and clay (Lu & Nutt, 2003; Tran, Said & Grohens, 2005). The second type of behavior occurs when silicate interlayer distance is smaller and intercalated polymer chain segments relax faster which results in lower T_g or even absence of a T_g in some cases (Tran, Said & Grohens, 2005; Vaia, Sauer, Tse & Giannelis, 1997). These general dynamic behaviors were also observed in the present study. Increase in T_g at 5% can be attributed to complete exfoliation of these nanocomposites as seen from X-ray diffraction (XRD) and TEM results. Such highly exfoliated nanocomposites provide more surface interactions between polymer and clay resulting in slower relaxation of polymer chain segments which leads to increased T_g . X-ray diffraction analysis of

nanocomposites with 10% Na⁺MMT also showed an exfoliated structure which resulted in higher T_g than 0% Na⁺MMT. As Na⁺MMT content increases, more polymer chains are confined between clay galleries resulting in intercalated nanocomposites. This increased confinement could lead to unstable polymer structures by disrupting intermolecular bonds, hence causing faster relaxation by chain segments. This faster relaxation behavior can be a reason for depressed T_g in these nanocomposites. Zhang & Loo (2009) studied amorphous polyamide (aPA) nanocomposites containing different layered silicate fillers and observed a similar trend in T_g for aPA/30BMMT and aPA/10AMMT nanocomposites. T_g increased at lower filler concentration (2-10%) and decreased with further increases in the filler content. They also provided a similar reasoning for depressed T_g in these nanocomposites. T_g of hydrophilic polymer systems is also impacted by water content, In the current study that might have played a role in dampening the effect of above discussed interactions, as equilibrium moisture in the nanocomposites films decreased steadily from 18.4 to 10.6% with increase in clay level from 0 to 20% (Figure 3-4).

Change in heat capacity (ΔC_p) at T_g decreased with increasing Na⁺MMT content (Figure 3-5), although ANOVA results did not indicate significant impact (p=0.27). Decrease in ΔC_p is attributed to increased polymer chain confinement with increasing Na⁺MMT contents which results in decreased degree of freedoms for polymer chain segments (Vyazovkin & Dranca, 2004). Zhang & Loo (2009) also observed a decrease in ΔC_p at T_g with increasing filler content in nanocomposites using aPA/20AMMT. They provided similar reasoning for decreased ΔC_p at higher filler content.

Melting temperatures (T_m), also obtained from DSC analysis, did not have a noticeable trend with respect to Na⁺MMT level (Figure 3-6). ANOVA results also showed that Na⁺MMT did not have a significant effect on T_m (p=0.24).

Tensile strength (TS) increased from 4.39 to 10.86 MPa while elongation at break (E %) decreased from 330.15 to 93.66% with increasing Na⁺MMT content (0 to 20%) (Figure 3-7). ANOVA results indicated that Na⁺MMT content had significant effect both on tensile strength (p<0.0001) and elongation at break (p<0.0001). Increasing Na⁺MMT levels enhanced the confinement of polymer chains and polymer-Na⁺MMT interactions, which results in increased tensile strength and decreased elongation at break. These results are in agreement with the XRD and TEM analyses, which showed good exfoliation at 5 and 10% Na⁺MMT and intercalation at higher levels of Na⁺MMT. Several other studies on polymer-clay nanocomposites have shown

increase in tensile strength and decrease in elongation at break with increase in clay content (Chivrac, Pollett, Schmutz & Averous, 2008; Dean, Yu & Wu, 2007; Dean, Do, Petinakis & Yu, 2008; Follain, Joly, Dole & Bliard, 2005; Ray & Okamoto, 2003; Tang, Alavi & Herald, 2008a).

Water vapor permeability (WVP) significantly decreased from 1.638 to 1.404 g.mm/kPa.h.m² (Figure 3-8) with increasing Na⁺MMT levels (0 to 20%). ANOVA results showed a significant effect of Na⁺MMT on WVP (p=0.013). Tang et al. 2008a also observed a decrease in WVP with increasing Na⁺MMT content, in the case of starch/ Na⁺MMT nanocomposite films. In nanocomposite films, silicate layers lead to torturous pathways that control the diffusion rate of water (Sorrentino, Tortora & Vittoria, 2006; Tang, Alavi & Herald, 2008a). In intercalated and exfoliated systems, the mean length of these pathways is substantially increased, which results in a decrease in WVP. Permeability coefficient depends on the solubility and diffusion coefficients through following relationship:

$$P=D' \times S \quad (7)$$

where, P = permeability coefficient, D' = effective diffusion coefficient and S = solubility coefficient. In these nanocomposite films, diffusion coefficient is decreased due to increased torturous pathways and solubility coefficient is also decreased due to increased starch/PVOH/Na⁺MMT interactions. This results in decrease in permeability coefficient.

Extrusion processing parameters

Effect of screw speed

Screw speed is an important factor in melt extrusion process that can affect shear intensity, mechanical energy and residence time of nanocomposites in the extruder. No XRD peaks were observed for nanocomposite films at screw speeds of 200 and 300 RPM (Figure 3-9). This indicated a highly exfoliated structure for these nanocomposites. Nanocomposites produced with screw speed of 400 RPM showed a new low intensity peak ($2\theta=4.57^\circ$, $d=1.95$ nm) at lower 2θ angle than pure Na⁺MMT ($2\theta=7.11^\circ$, $d=1.24$ nm) (Figure 3-9). This new peak at lower angle and increased d-spacing indicated a partially exfoliated and intercalated structure for these nanocomposites. High screw speed is considered to provide better de-lamination and dispersion of clay platelets due to high shear intensity (Tang, 2008). On the other hand, residence time in the extruder is another important factor. Longer residence time provides greater dispersion of clay in nanocomposites (Paul & Robeson, 2008), but higher extruder screw speed leads to lower

residence time. XRD analysis results showed an increased exfoliation when screw speed was increased from 200 RPM to 300 RPM. This can be attributed to higher shear intensity along with enough residence time to disperse the clay platelets. Further, increase in screw speed (400 RPM) lead to lower exfoliation which can be attributed to lower residence time.

The glass transition temperature (T_g) of nanocomposite films increased from 64.91 to 76.69°C with increasing screw speed from 200 to 400 RPM (Figure 3-10), although ANOVA results did not show a significant effect of screw speed ($p=0.29$). In extrusion process stable polymer structure is disrupted through shear stress which can lead to depressed T_g . But on the other hand increased screw speed reduces residence time which does not provide enough time to disrupt molecular structure of polymers and can lead to higher T_g

Melting temperatures (T_m) were measured as 149.08, 150.12 and 152.85°C for screw speeds of 200, 300 and 400 RPM, respectively, and did not exhibit a specific trend (Fig 3-11). ANOVA results also confirmed the non-significant effect of extruder screw speed ($p=0.63$).

Tensile strength for nanocomposite films was 10.92, 9.01 and 9.27MPa for screw speeds of 200, 300 and 400 RPM respectively (Figure 3-12). Elongation at break (%E) of these films was 198.66, 218.40 and 154.47% for screw speeds of 200, 300 and 400 RPM respectively (Figure 3-13). ANOVA results showed a significant effect of screw speed on tensile strength ($p=0.009$) but did not show any effect on elongation at break ($p=0.15$). However, the trends in tensile strength and elongation at break provided useful information about structural changes in the polymer chains, which probably had a greater impact than any changes polymer/ clay interactions. Extrusion process helps in stretching out the PVOH macromolecules in a linear conformation (Follain, Joly, Dole & Bliard, 2005). Similarly extrusion processing leads to breakage of intra-molecular H-bonds in starch, which increases the number of free hydroxyl groups (Liu, Xie, Yu, Chen & Li, 2009). These increased free hydroxyl groups in the system facilitate more interactions between starch and PVOH molecules, which in turn result in decreased intra-molecular bonding in PVOH. Increase in screw speed from 200 to 300 RPM led to increase in SME from 537.3 to 805.9 kJ/kg, thus enabling these changes in polymer chains and resulting in decreased tensile strength and increased elongation at break. Further increase in screw speed to 400 RPM did not increase the SME (796.0 kJ/kg) and at the same time led to inadequate residence time for the above mentioned changes to take place, which was reflected in

mechanical properties of nanocomposite films. RVA pasting curves at different screw speeds confirmed that the polymers are least degraded at 400 RPM.

ANOVA results indicated a significant effect of screw speed on WVP ($p=0.02$). Water vapor permeability (WVP) decreased from 1.747 to 1.506 g.mm/kPa.h.m² with increase in screw speed from 200 to 300 RPM, followed by almost no change (1.514g.mm/kPa.h.m²) as the screw speed increased to 400 RPM (Figure 3-14). Greater disruption of polymer chains and silicate layers at 300 RPM led to higher dispersion of the latter and thus the decrease in WVP.

Different temperature profiles

X-ray diffraction analysis results did not show any noticeable peak at both temperature profiles (Figure 3-15), thus pointing toward exfoliated nanostructures. The only difference between the two results was the lower intensity of XRD curve in case of higher temperature profile. These results indicated exfoliated nanocomposite structure for both temperature profiles with greater exfoliation at higher temperature profile. Extruder barrel temperature affects the melt viscosity of blends which helps in creating the exfoliated structures for these nanocomposites. Higher extruder barrel temperature lowered the melt viscosity, increasing polymer chain movement and interactions with clay. Lower SME (Table 3-2) at higher temperature was observed which attested to lower melt viscosity of the system. Both of these temperature profiles were good enough to create enough shear stress for disrupting the layered silicate structure. But the high temperature profile showed better exfoliation due to increased melt viscosity of the system.

The glass transition temperature (T_g) (Figure 3-16) and melting temperature (T_m) (Figure 3-17) of nanocomposites processed at the two temperature profiles were similar. ANOVA results also did not show a significant effect of barrel temperature on T_g ($p=0.78$) and T_m ($p= 0.67$).

Tensile strength increased (Figure 3-18) while there were a decrease in elongation at break (Figure 3-19) with increasing barrel temperature, although ANOVA results did not indicate significant effect of temperature profile ($p= 0.26$ and $p= 0.20$, respectively). These changes were consistent with XRD results where greater exfoliation was observed for extrusion at high temperature profile. The increased exfoliation resulted in increased tensile strength and decreased elongation at break.

A decrease in WVP was observed at the higher temperature profile (Fig 3-20), although ANOVA results showed that temperature profile had a non-significant effect on WVP ($p=0.45$).

The decrease in WVP can be attributed to increased exfoliation in case of higher temperature profile. Tang (2008) also studied different temperature profiles for extrusion process while preparing starch/Na⁺ MMT nanocomposites and showed similar trends for WVP results.

Solution versus melt extrusion processing

Films from starch/PVOH/Na⁺MMT nanocomposites were prepared using solution casting method and their physical properties and characterization are discussed in preceding chapter. Comparisons of results from solution casting method with melt extrusion method are summarized in Table 3-3. XRD results indicated more exfoliated and intercalated nanocomposites through extrusion than solution casting method which can be attributed to the high shear stress provided by extrusion process. DSC results did not show much difference in T_g.

Interestingly, elongation at break was more than 100% higher in case of extruded samples at all levels of Na⁺MMT levels. Whereas tensile strength was 60-100% lower than films produced from nanocomposites with solution casting method. RVA profile for extruded nanocomposites was compared with that from solution method (Figure 3-21). Peak viscosity for extruded nanocomposites was lower (79) than the solution method (490) which can be attributed to more degradation in extrusion process. The degradation of starch and structural changes in PVOH during extrusion results in decreased tensile strength and increased elongation at break. Follain et al. (2005) studied starch/PVOH blends and reported an increase in elongation at break with extrusion method as compared to solution method. This increase was attributed to forced linear conformation through extrusion method which results in increased hydrogen bonding with starch molecules. Similarly intermolecular H-bonds in starch will break resulting in increased number of free hydroxyl groups (Liu, Xie, Yu, Chen & Li, 2009). These changes in polymer chain structures are in contrast with solution method where PVOH molecules are favored to develop self associations between PVOH macromolecules (random coil chain) with decreased starch/PVOH interactions (Follain, Joly, Dole & Bliard, 2005). Linear conformation of PVOH chains in extruded samples can a reason for increased elongation at break and decreased tensile strength. WVP was increased in extruded nanocomposites due to polymer degradation which can provide more water affinity due to increased number of hydroxyl groups.

Conclusion

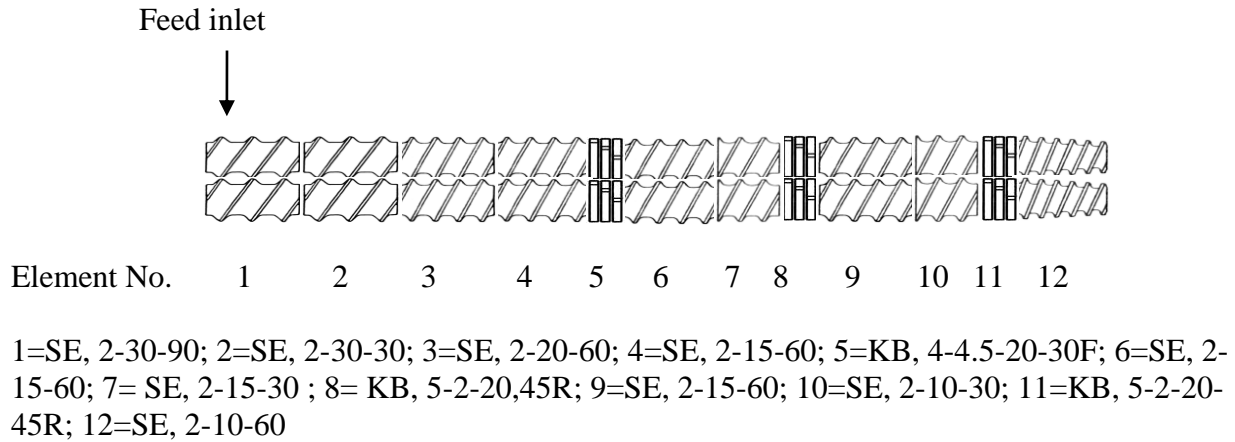
Melt extrusion process was used to produce starch/PVOH/Na⁺MMT nanocomposites. Study showed that increased Na⁺MMT levels had a positive effect on tensile and barrier properties while elongation at break was decreased. These properties were dependent on the structure of these nanocomposites which showed less exfoliation at higher levels of Na⁺MMT.

Highly exfoliated nanocomposites were created with melt extrusion process due to higher shear stress. Extrusion process also lead to degradation of starch and there were structural changes in PVOH. These changes in polymers resulted in improvement in elongation at break, but deterioration in tensile strength and WVP properties relative to nanocomposite films synthesized by solution method. XRD analysis revealed the importance of melt extrusion processing conditions for proper dispersion of silicate layers of clay which was also confirmed through TEM scans. DSC analysis provided information structural confirmations and interactions in these nanocomposites

In order to improve these properties, future work in this area can be focused on minimizing the polymer degradation. Some of the approaches can include use of a lower shear screw configuration and higher levels and/or different types of plasticizers..

Figures and Tables

Head no.	1	2	3	4	5	6
Low Temp Profile	40°C	110°C	145°C	145°C	130°C	110°C
High Temp Profile	40°C	120°C	165°C	165°C	140°C	110°C



SE=screw element

Numbers:

1st – number of flight

2nd – length of flight (mm)

3rd – total element length (mm)

KB=kneading blocks

Letters: F – forward, R – reverse

Numbers:

1st – number of block

2nd – length of block (mm)

3rd – total element length (mm)

4th – angle of block

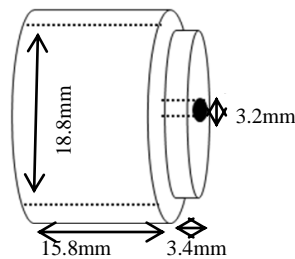


Figure 3-1 Temperature profile, screw configuration and die design for laboratory-scale extruder used in the experiment.

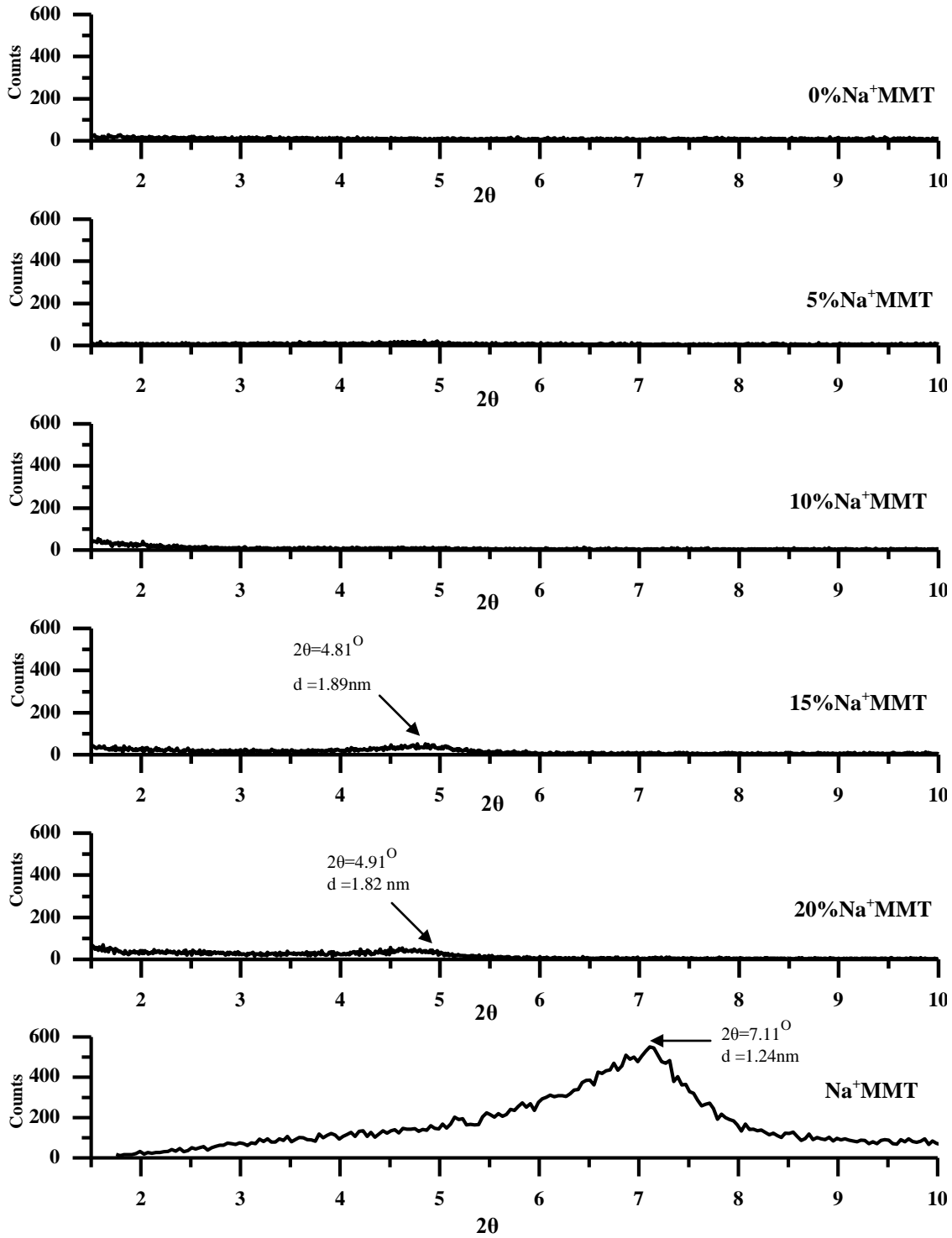
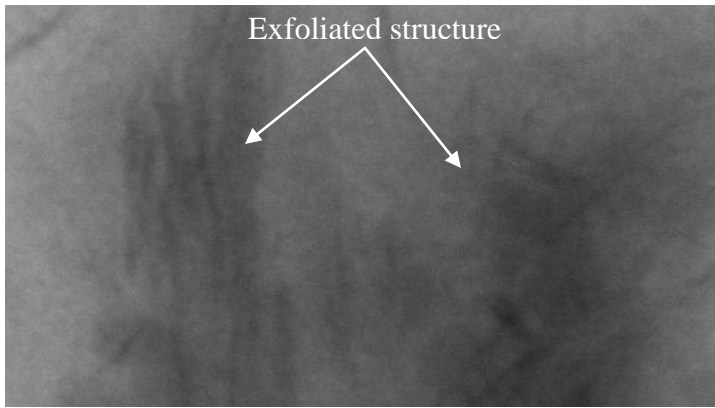
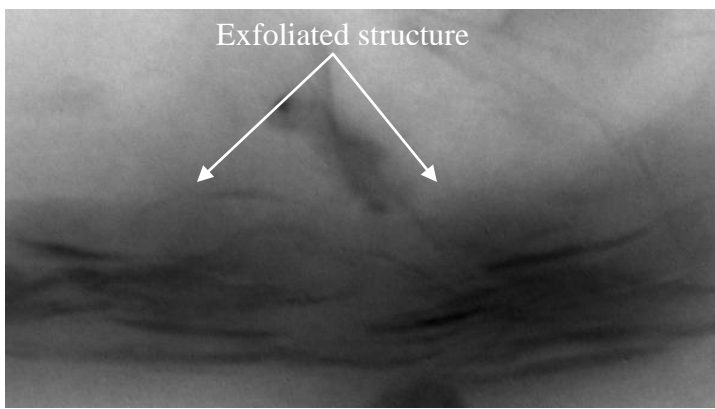


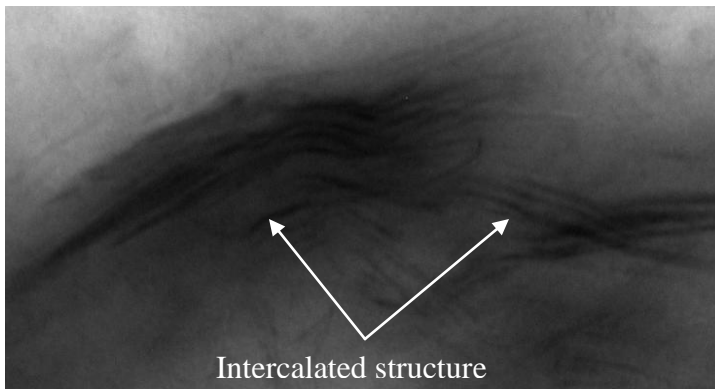
Figure 3-2 XRD patterns for nanocomposites with different Na⁺MMT levels



(a)



(b)



(c)

100 nm
HV=100kV
Direct Mag: 130000x

Figure 3-3 TEM scans for (a) 5% (b) 10% and (c) 15 % Na⁺MMT levels.

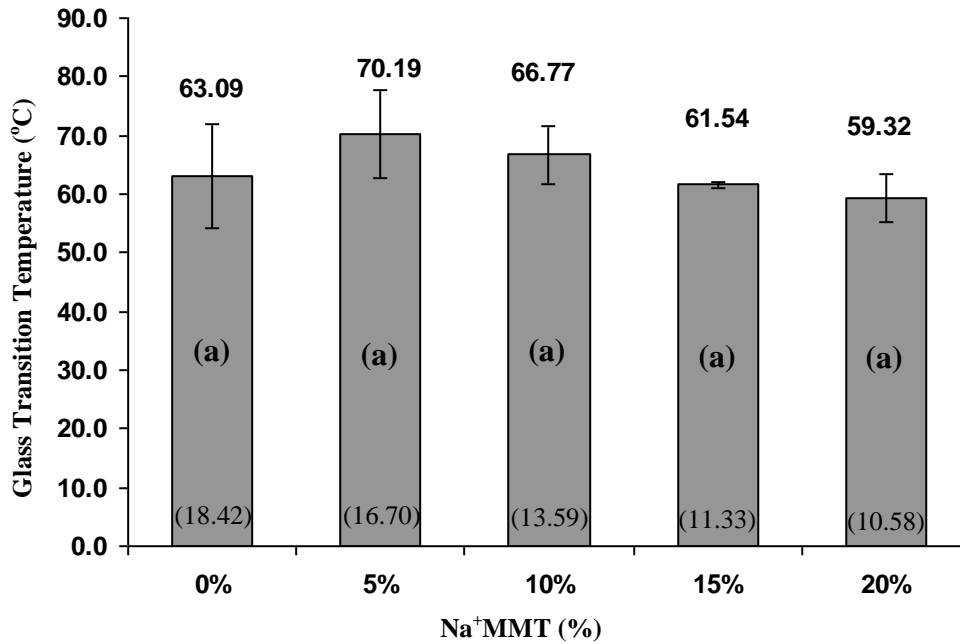


Figure 3-4 Glass Transition Temperature (T_g) at different Na⁺MMT levels. Results with same letters are statistically non-significant. Values at the bottom of the bars show moisture content of films. Error bars indicate standard deviation.

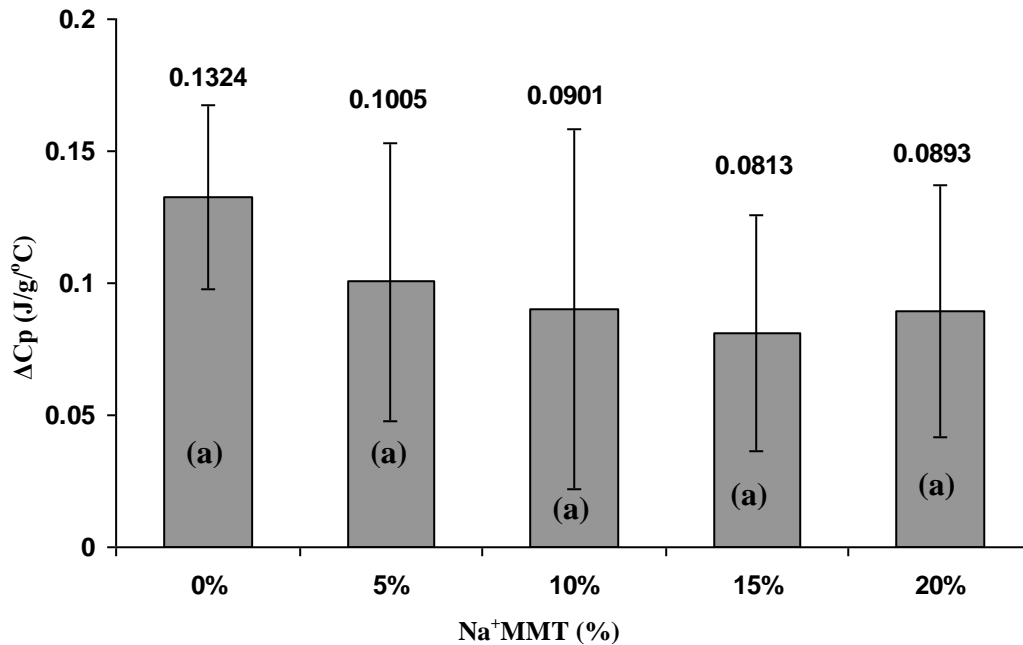


Figure 3-5 ΔC_p at T_g for nanocomposites with different levels of Na⁺MMT. Results with same letters are statistically non-significant. Error bars indicate standard deviation.

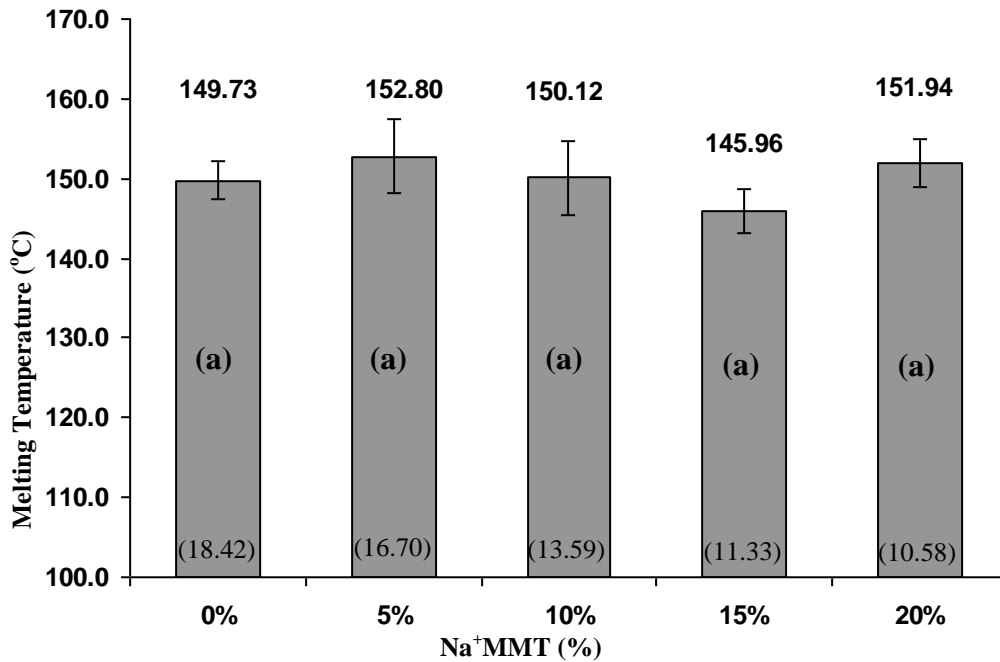


Figure 3-6 Melting Temperature (T_m) with different Na^+ MMT levels. Results with same letters are statistically non-significant. Values at bottom of the bars show moisture content (% wet basis) of films. Error bars indicate standard deviation.

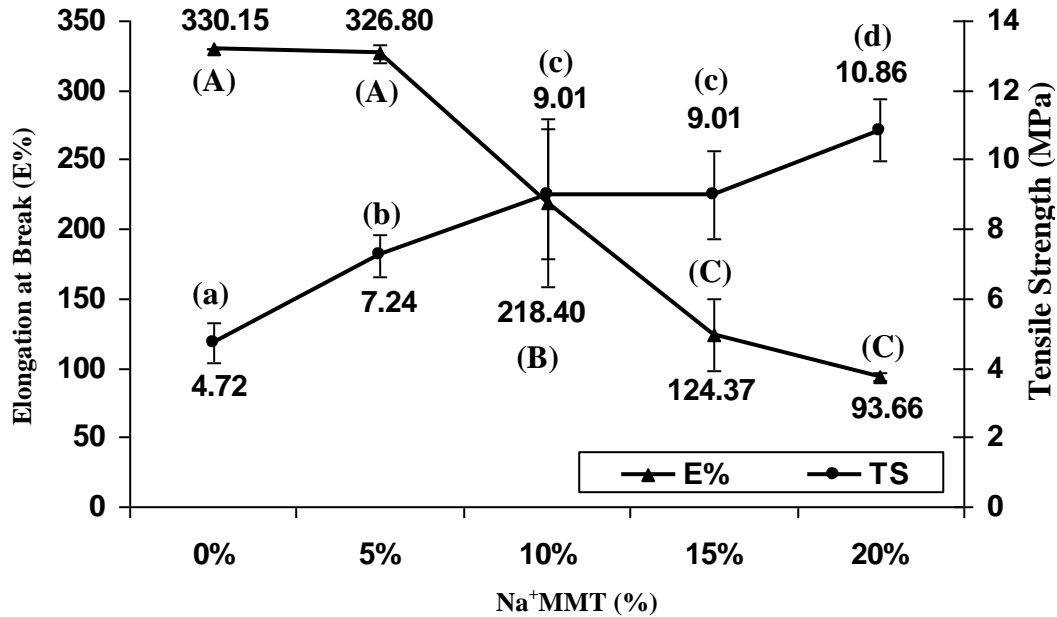


Figure 3-7 Tensile strength and elongation at break with different levels of Na^+ MMT. Results with similar letters are not significantly different. Error bars indicate standard deviation.

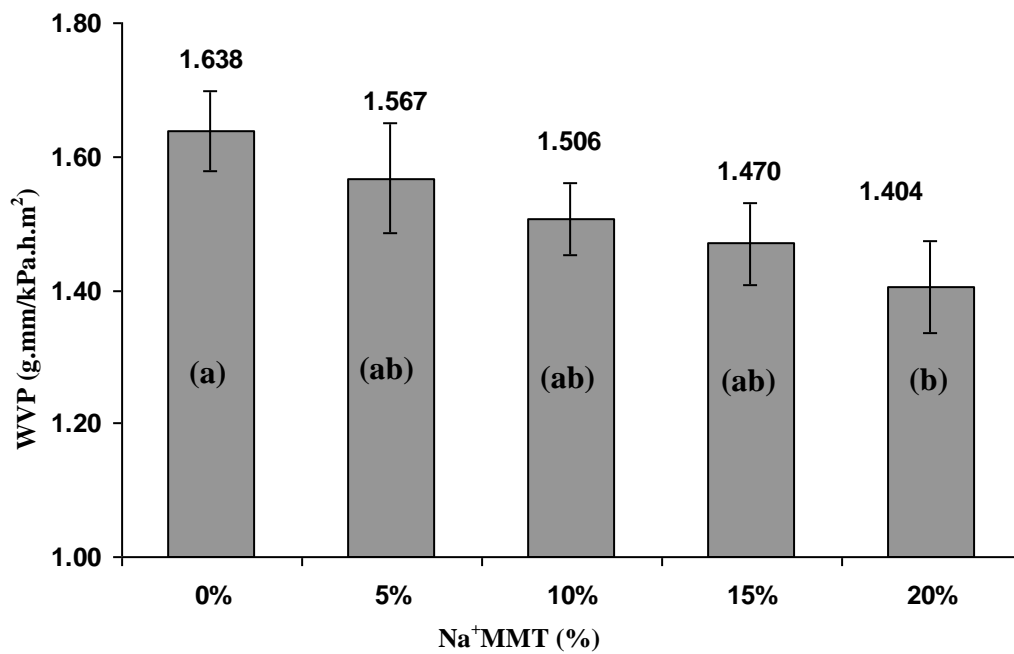


Figure 3-8 WVP for nanocomposite films with different levels of Na⁺MMT. Results with same letters are statistically non-significant. Error bars indicate standard deviation.

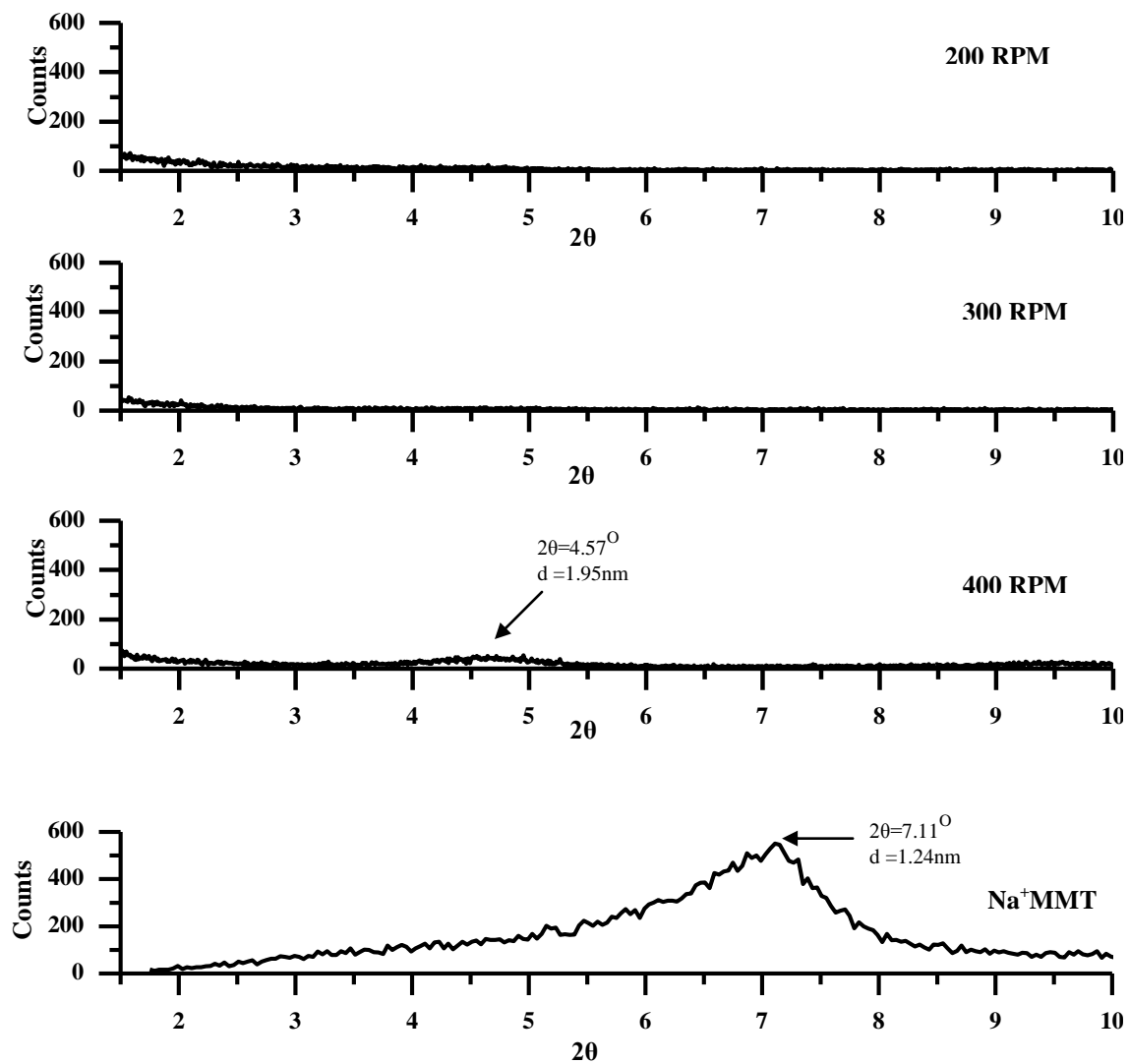


Figure 3-9 XRD patterns for nanocomposites with different screw speeds.

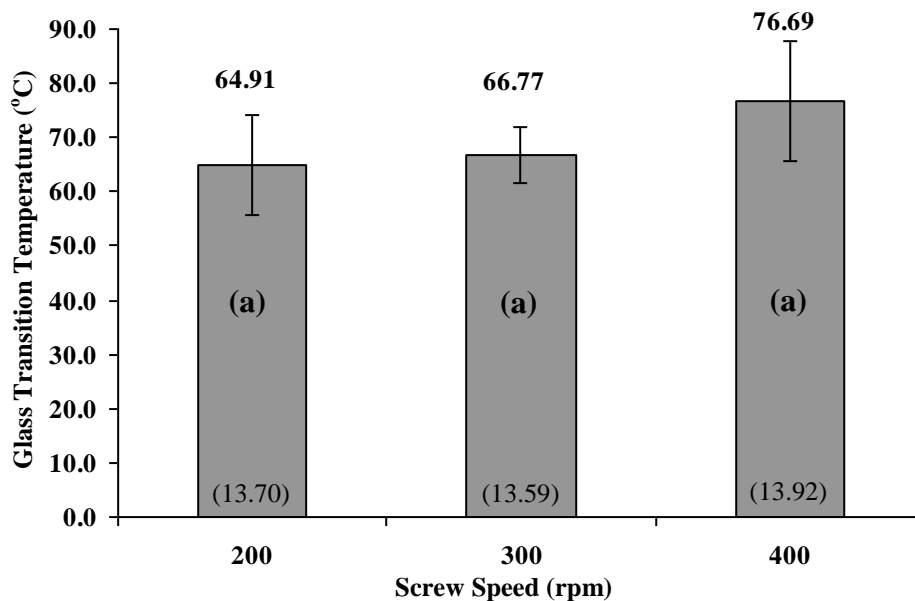


Figure 3-10 Glass transition temperature of nanocomposites at different screw speeds. Results with same letters are statistically non-significant. Values at the bottom of the bars show moisture content (% wet basis) of films. Error bars indicate standard deviation.

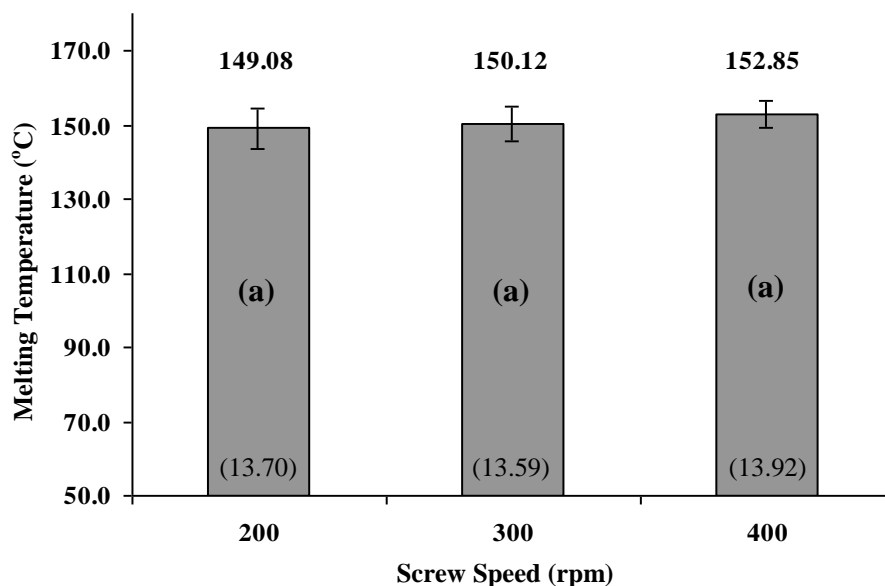


Figure 3-11 Melting temperature of nanocomposites at different screw speeds. Results with same letters are statistically non-significant. Values at the bottom of the bars show moisture content (% wet basis) of films. Error bars indicate standard deviation.

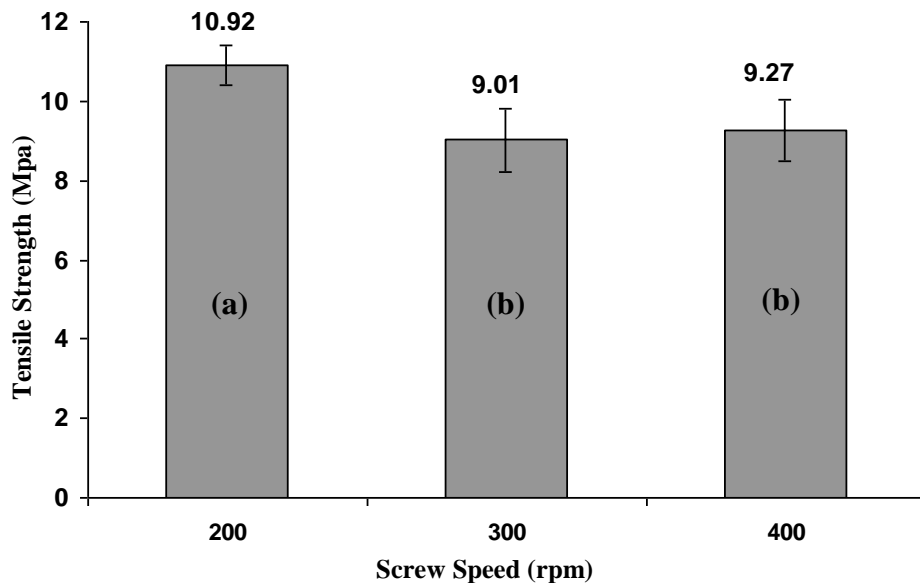


Figure 3-12 Tensile Strength of nanocomposites at different screw speeds. Results with same letters are statistically non-significant. Error bars indicate standard deviation.

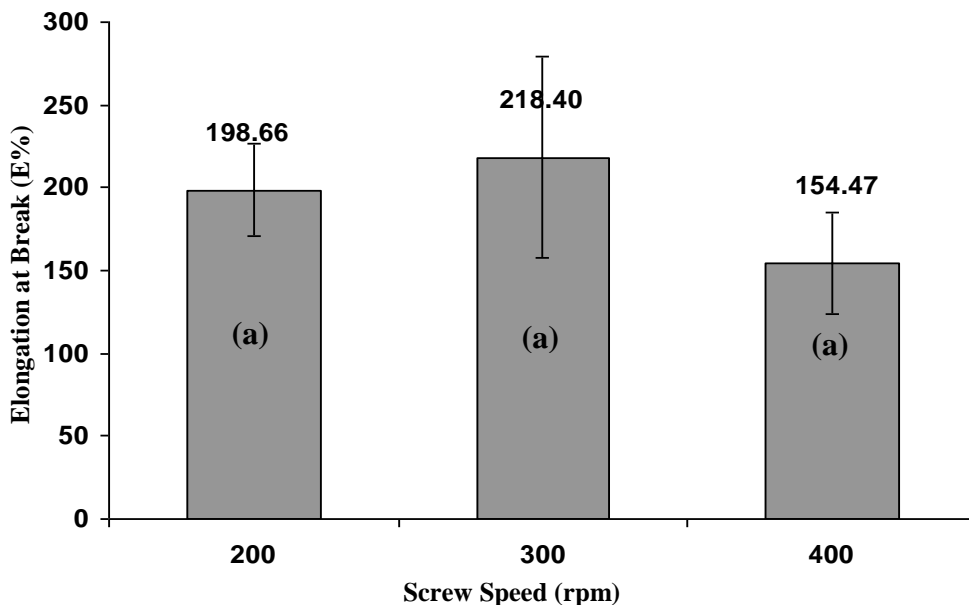


Figure 3-13 Elongation at break of nanocomposite films at different screw speeds. Results with same letters are statistically non-significant. Error bars indicate standard deviation.

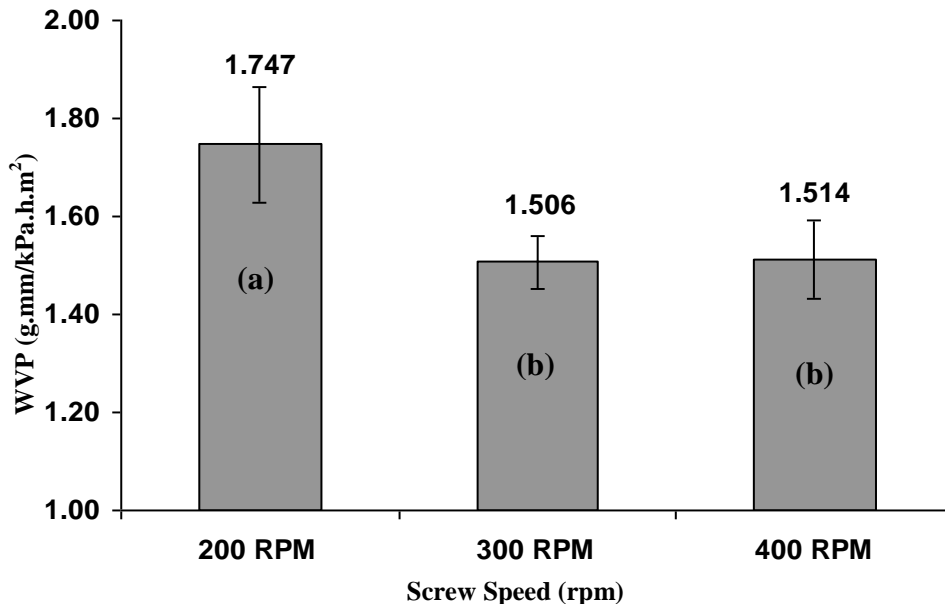


Figure 3-14 WVP for nanocomposite films at different screw speeds. Results with same letters are statistically non-significant. Error bars indicate standard deviation.

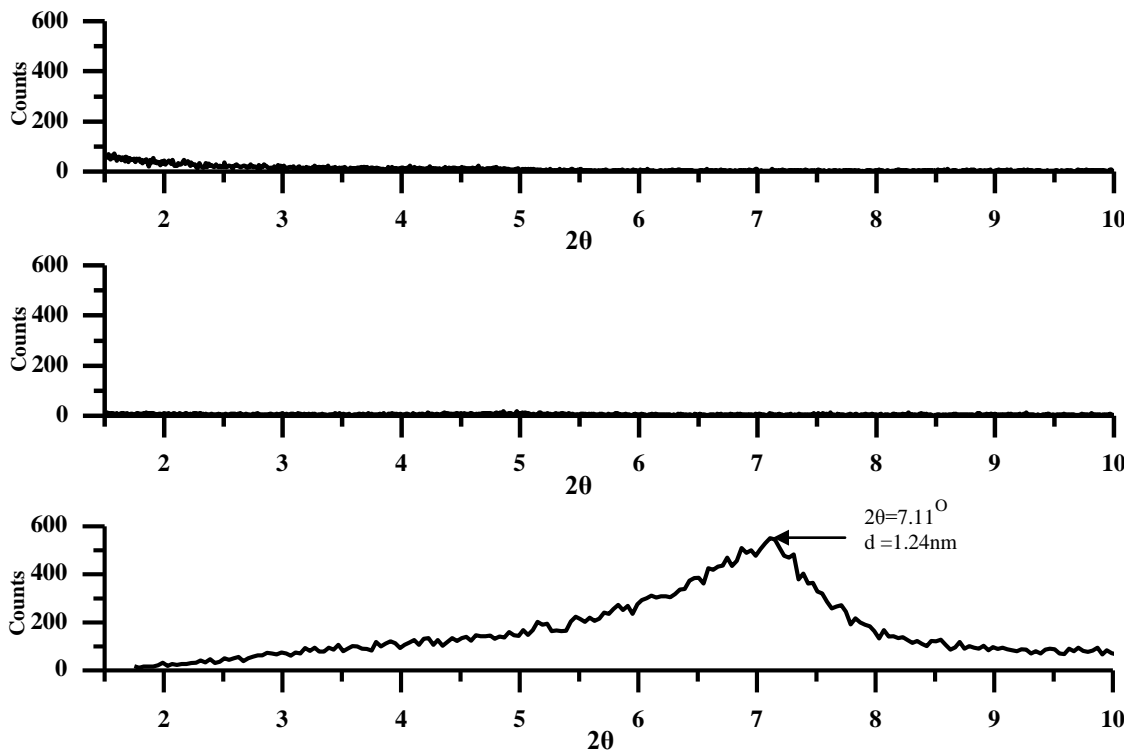


Figure 3-15 XRD patterns for nanocomposites with different barrel temperature profiles

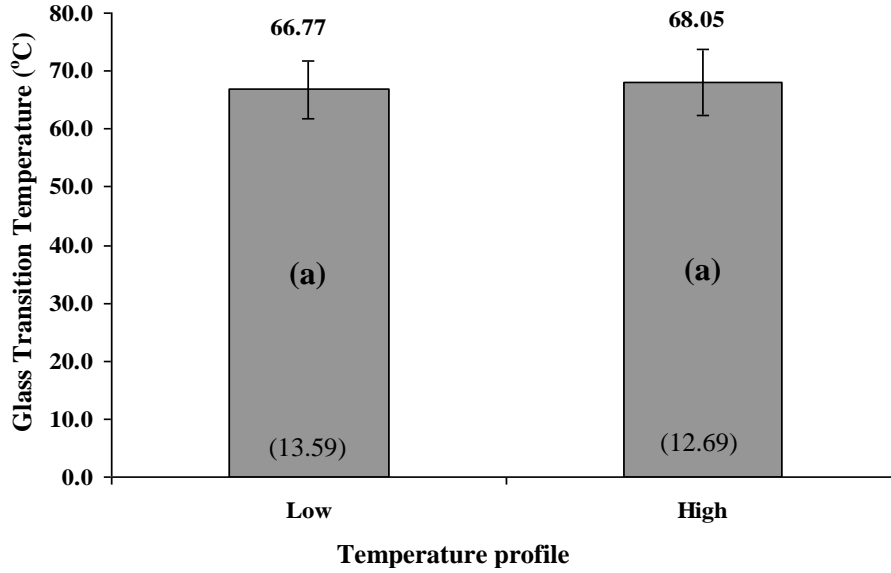


Figure 3-16 Tg for nanocomposite films with different temperature profiles. Results with same letters are statistically non-significant. Values at the bottom of the bars show moisture content (% wet basis) of films. Error bars indicate standard deviation.

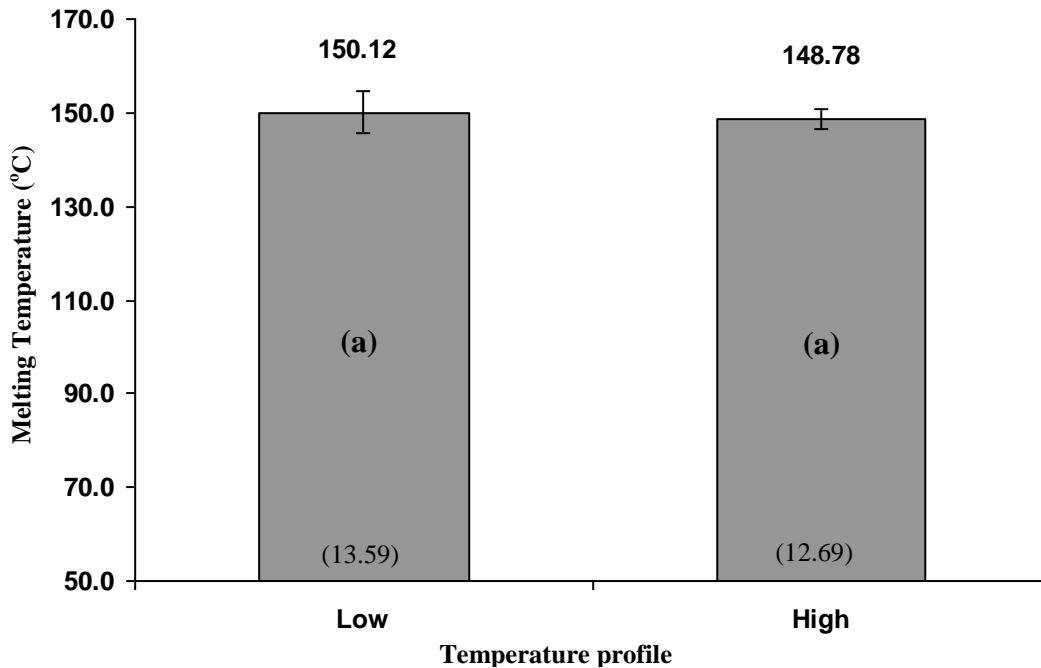


Figure 3-17 Melting temperature of nanocomposite films with different temperature profiles. Results with same letters are statistically non-significant. Values at the bottom of bars show moisture content (% wet basis) of films. Error bars indicate standard deviation.

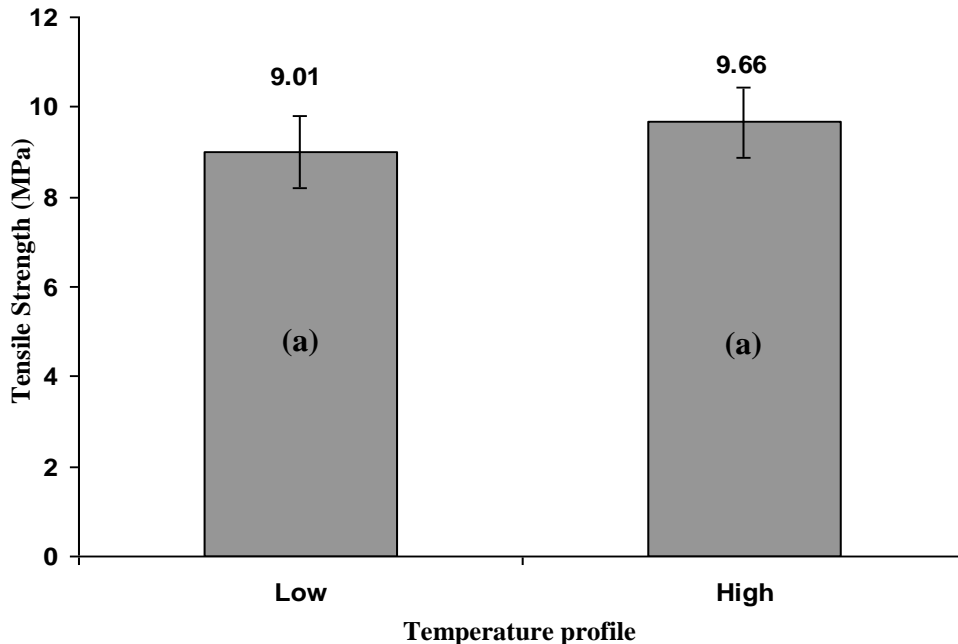


Figure 3-18 Tensile Strength for nanocomposite films with different temperature profiles of extruder. Results with same letters are statistically non-significant. Error bars indicate standard deviation.

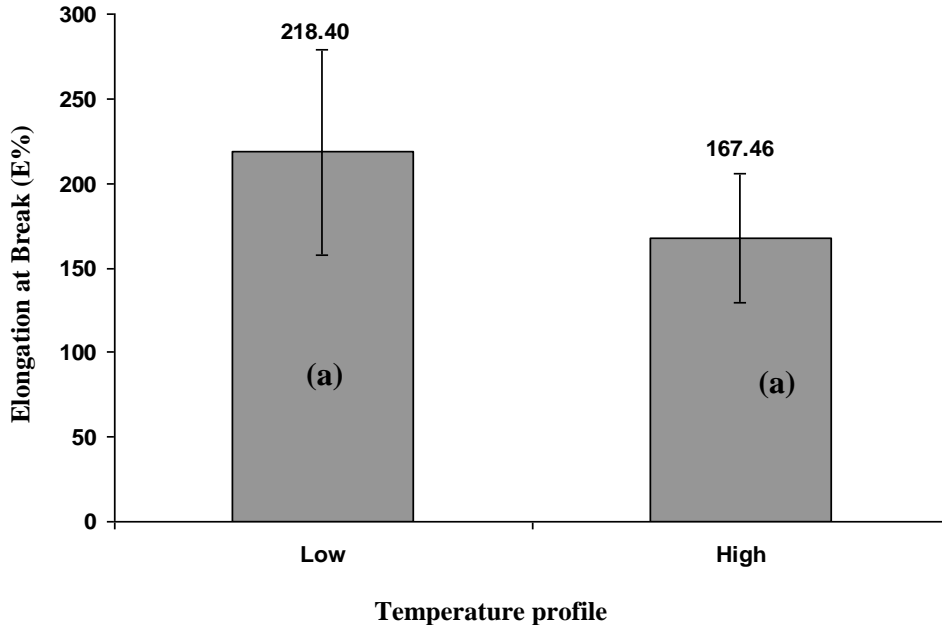


Figure 3-19 Elongation at break for nanocomposite films with different temperature profiles of extruder. Results with same letters are statistically non-significant. Error bars indicate standard deviation.

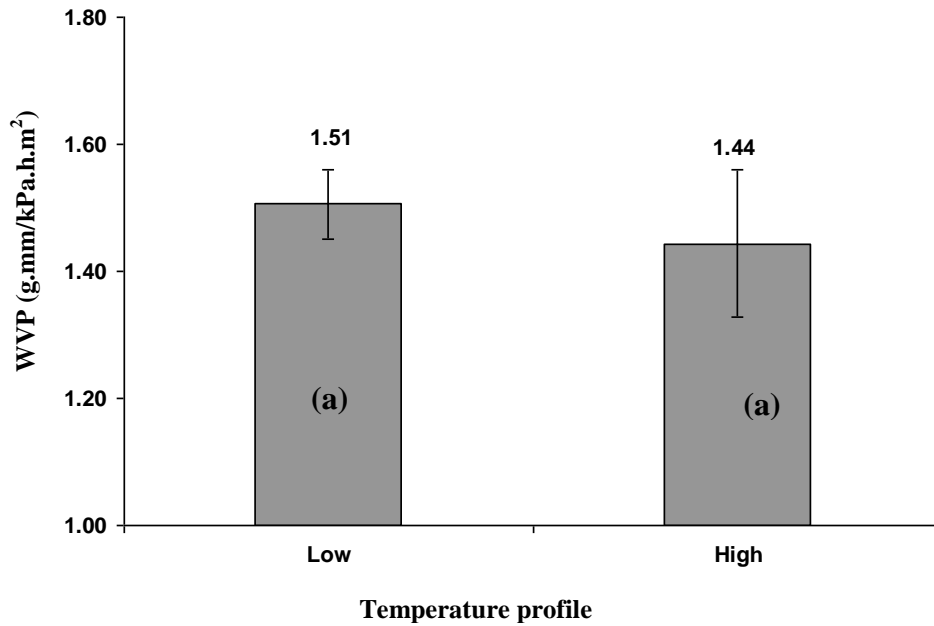


Figure 3-20 Water Vapor Permeability (WVP) for nanocomposite films at temperature profiles of extruder. Results with same letters are statistically non-significant. Error bars indicate standard deviation.

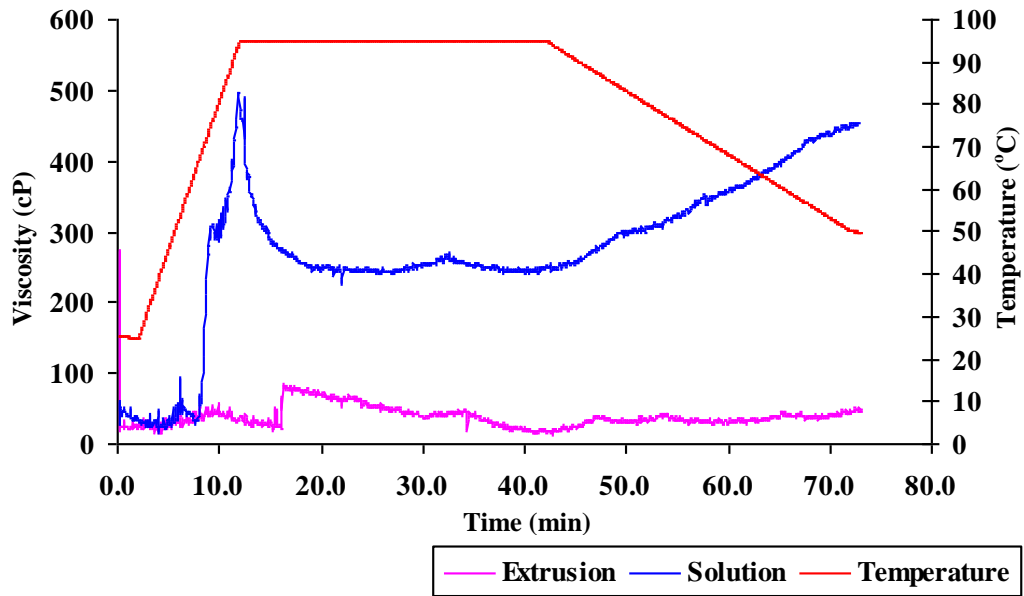


Figure 3-21 RVA profiles for nanocomposites through extrusion and solution method.

Table 3-1 Moisture content of nanocomposite films at different levels of Na⁺MMT

0%	5%	10%	15%	20%
18.42±1.40	16.70±0.99	13.59±1.22	11.33±1.07	10.58±0.89

Table 3-2 Specific mechanical energy (SME) for different treatments.

TREATMENT	SME (KJ/Kg)		TREATMENT	SME (KJ/Kg)
Temperature Profile			Na⁺MMT Content (%)	
Low	805.93		0	407.65
High	522.36		5	437.84
			10	805.93
Screw Speed			15	774.20
200	537.29		20	911.90
300	805.93			
400	795.98			

Table 3-3 Comparison of nanocomposit films through solution casting melt extrusion

Properties	Na ⁺ MMT Content (%)	Solution Casting	Melt Extrusion Processing
XRD	5	Exfoliated	Exfoliated
	10	Partially exfoliated	Exfoliated
	15	Intercalated	Partial exfoliation and
	20	Intercalated	Partial exfoliation and
Tg	0	70.28 ± 4.97 °C	63.79 ± 12.59 °C
	5	71.75 ± 10.28 °C	74.37 ± 3.03 °C
	10	68.45 ± 3.93 °C	69.31 ± 3.32 °C
	15	66.14 ± 8.11 °C	61.63 ± 0.67 °C
	20	61.22 ± 7.94 °C	58.21 ± 5.20 °C
TS	0	8.39 ± 0.5 MPa	4.72 ± 0.21 MPa
	5	11.60 ± 0.62 MPa	7.24 ± 0.29 MPa
	10	17.06 ± 1.87 MPa	9.01 ± 0.80MPa
	15	18.84 ± 1.27 MPa	9.01 ± 0.25MPa
	20	18.41 ± 0.91 MPa	10.86 ± 0.38MPa
E%	0	136.82±11.82	330.15 ± 0.37
	5	103.00±17.03	326.80 ± 6.33
	10	101.28±13.14	218.40 ± 60.40
	15	61.83± 6.99	124.37±26.12
	20	41.57± 3.78	93.66 ± 3.14
WVP	0	1.683± 0.057 g.mm/kPa.h.m ²	1.672± 0.017 g.mm/kPa.h.m ²
	5	1.235± 0.099 g.mm/kPa.h.m ²	1.614± 0.007g.mm/kPa.h.m ²
	10	1.054 ± 0.050 g.mm/kPa.h.m ²	1.562 ± 0.071g.mm/kPa.h.m ²
	15	0.726± 0.023 g.mm/kPa.h.m ²	1.525± 0.093 g.mm/kPa.h.m ²
	20	0.719 ±0.023 g.mm/kPa.h.m ²	1.485± 0.062 g.mm/kPa.h.m ²

References

- Ahmad, M. B., Shameli, K., Darroudi, M., Wan Yunus, W. M. Z., & Ibrahim, N. A. (2009). Synthesis and characterization of Silver/Clay/Chitosan Bionanocomposites by UV-Irradiation method. *American Journal of Applied Sciences*, 6(12), 2030-2035.
- Alberta Araújo, M., Cunha, A. M., & Mota, M. (2004). Enzymatic degradation of starch-based thermoplastic compounds used in protheses: identification of the degradation products in solution. *Biomaterials*, 25(13), 2687-2693.
- Alexandre, M., & Dubois, P. (2000). Polymer-layered silicate nanocomposites: preparation, properties and uses of a new class of materials. *Materials Science & Engineering R-Reports*, 28(1-2), 1-63.
- ASTM, & Standards (2000). Standard test methods for water vapor transmission of materials. *Annual book of ASTM standards* pp. 907–914). Philadelphia
- ASTM Standards. (2002). D882-02. Standard test method for tensile properties of thin plastic sheeting. Philadelphia.
- Avella, M., De Vlieger, J. J., Errico, M. E., Fischer, S., Vacca, P., & Volpe, M. G. (2005). Biodegradable starch/clay nanocomposite films for food packaging applications. *Food Chemistry*, 93(3), 467-474.
- Averous, L. (2004). Biodegradable multiphase systems based on plasticized starch: A review. *Journal of Macromolecular Science-Polymer Reviews*, C44(3), 231-274.
- BeMiller, J., & Whistler, R. (2009). *Starch: chemistry and technology*. Academic.
- Chen, B., Evans, J. R. G., Greenwell, H. C., Boulet, P., Coveney, P. V., Bowden, A. A., & Whiting, A. (2008). A critical appraisal of polymer-clay nanocomposites. *Chemical Society Reviews*, 37(3), 568-594.
- Chivrac, F., Pollett, E., Schmutz, M., & Averous, L. (2008). New approach to elaborate exfoliated starch-based nanobiocomposites. *Biomacromolecules*, 9(3), 896-900.
- Dean, K., Yu, L., & Wu, D. Y. (2007). Preparation and characterization of melt-extruded thermoplastic starch/clay nanocomposites. *Composites Science and Technology*, 67(3-4), 413-421.
- Dean, K. M., Do, M. D., Petinakis, E., & Yu, L. (2008). Key interactions in biodegradable thermoplastic starch/poly(vinyl alcohol)/montmorillonite micro- and nanocomposites. *Composites Science and Technology*, 68(6), 1453-1462.
- Dimonie, D., Constantin, R., Vasilievici, G., Popescu, M. C., & Garea, S. (2008). The Dependence of the XRD Morphology of Some Bionanocomposites on the Silicate Treatment. *Journal of Nanomaterials*.
- El-Kader, K., Hamied, S., Mansour, A., El-Lawindy, A., & El-Tantaway, F. (2002). Effect of the molecular weights on the optical and mechanical properties of poly(vinyl alcohol) films. *Polymer Testing*, 847-850.
- Elizondo, N. J., Sobral, P. J. A., & Menegalli, F. C. (2009). Development of films based on blends of *Amaranthus cruentus* flour and poly(vinyl alcohol). *Carbohydrate Polymers*, 75(4), 592-598.
- Follain, N., Joly, C., Dole, P., & Bliard, C. (2005). Properties of starch based blends. Part 2. Influence of poly vinyl alcohol addition and photocrosslinking on starch based materials mechanical properties. *Carbohydrate Polymers*, 185-192.
- Fornes, T. D., Yoon, P. J., Keskkula, H., & Paul, D. R. (2001). Nylon 6 nanocomposites: the effect of matrix molecular weight. *Polymer*, 42(25), 9929-9940.

- Gowariker, V., R, Viswanathan, N., V, & Sreedhar, J. (2003). *Polymer Science*. New Age International.
- Jang, W. Y., Shin, B. Y., Lee, T. X., & Narayan, R. (2007). Thermal properties and morphology of biodegradable PLA/starch compatibilized blends. *Journal of Industrial and Engineering Chemistry*, 13(3), 457-464.
- Jayasekara, R., Harding, I., Bowater, I., Christie, G. B. Y., & Lonergan, G. T. (2004). Preparation, surface modification and characterisation of solution cast starch PVA blended films. *Polymer Testing*, 23(1), 17-27.
- Jun, C. L. (2000). Reactive blending of biodegradable polymers: PLA and starch. *Journal of Polymers and the Environment*, 8(1), 33-37.
- Krevelen, D., & Nijenhuis, K. (2009). *Properties of Polymers: Their Correlation with Chemical Structure; Their Numerical Estimation and Prediction from Additive Group Contributions*. Elsevier.
- Kumar, P. (2009). Development of Bio-nanocomposite Films with Enhanced Mechanical and Barrier Properties Using Extrusion Processing. Raleigh, North Carolina: North Carolina State University.
- Lee, E. C., Mielewski, D. F., & Baird, R. J. (2004). Exfoliation and dispersion enhancement in polypropylene nanocomposites by in-situ melt phase ultrasonication. *Polymer Engineering and Science*, 44(9), 1773-1782.
- Leja, K., & Lewandowicz, G. (2010). Polymer Biodegradation and Biodegradable Polymers - a Review. *Polish Journal of Environmental Studies*, 19(2), 255-266.
- Lim, L. Y., & Wan, L. S. C. (1994). The effect of plasticizers on the properties of polyvinyl alcohol films. *Drug Development and Industrial Pharmacy*, 20(6), 1007-1020.
- Liu, H., Xie, F., Yu, L., Chen, L., & Li, L. (2009). Thermal processing of starch-based polymers. *Progress in Polymer Science*, 1348-1368.
- Lu, H. B., & Nutt, S. (2003). Restricted relaxation in polymer nanocomposites near the glass transition. *Macromolecules*, 36(11), 4010-4016.
- Mao, L. J., Imam, S., Gordon, S., Cinelli, P., & Chiellini, E. (2000). Extruded cornstarch-glycerol-polyvinyl alcohol blends: Mechanical properties, morphology, and biodegradability. *Journal of Polymers and the Environment*, 8(4), 205-211.
- Mark, J. E. (2004). *Physical properties of polymers*. Cambridge University Press.
- Marsh, K., & Bugusu, B. (2007). Food packaging - Roles, materials, and environmental issues. *Journal of Food Science*, 72(3), R39-R55.
- Massey, L. K. (2003). *Permeability properties of plastics and elastomers: a guide to packaging and barrier materials*. Elsevier.
- Mohee, R., & Unmar, G. (2007). Determining biodegradability of plastic materials under controlled and natural composting environments. *Waste Management*, 27(11), 1486-1493.
- Nair, L. S., & Laurencin, C. T. (2007). Biodegradable polymers as biomaterials. *Progress in Polymer Science*, 32(8-9), 762-798.
- Narayan, R. (1993). Biodegradable plastics. Opportunities For innovation in Biotechnology.
- Nielsen, L. E., & Landel, R. F. (1994). *Mechanical properties of polymers and composites*. CRC Press.
- Okada, A., & Usuki, A. (2006). Twenty years of polymer-clay nanocomposites. *Macromolecular Materials and Engineering*, 291(12), 1449-1476.
- Oriakhi, C. (1998). Nano sandwiches. *Chemistry in Britain*, 34(11), 59-62.

Parulekar, Y., & Mohanty, A. K. (2007). Extruded biodegradable cast films from polyhydroxyalkanoate and thermoplastic starch blends: Fabrication and characterization. *Macromolecular Materials and Engineering*, 292(12), 1218-1228.

Paul, D. R., & Robeson, L. M. (2008). Polymer nanotechnology: Nanocomposites. *Polymer*, 49(15), 3187-3204.

Ramaraj, B. (2007). Crosslinked poly(vinyl alcohol) and starch composite films: Study of their physicomechanical, thermal, and swelling properties. *Journal of Applied Polymer Science*, 103(2), 1127-1132.

Ray, S. S., & Okamoto, M. (2003). Polymer/layered silicate nanocomposites: a review from preparation to processing. *Progress in Polymer Science*, 28(11), 1539-1641.

Robertson, G. L. (2006). *Food packaging: principles and practice*. CRC press.

Roohani, M., Habibi, Y., Belgacem, N. M., Ebrahim, G., Karimi, A. N., & Dufresne, A. (2008). Cellulose whiskers reinforced polyvinyl alcohol copolymers nanocomposites. *European Polymer Journal*, 44(8), 2489-2498.

Russo, M., O'Sullivan, C., Rounsefell, B., Halley, P., Truss, R., & Clarke, W. (2009). The anaerobic degradability of thermoplastic starch: Polyvinyl alcohol blends: Potential biodegradable food packaging materials. *Bioresource Technology*, 1705-1710.

Sekisui Chemical Co., L.

Shen, Z. Q., Simon, G. P., & Cheng, Y. B. (2002). Effects of molecular weight and clay organo-ions on the melt intercalation of poly(ethylene oxide) into layered silicates. *Polymer Engineering and Science*, 42(12), 2369-2382.

Sorrentino, A., Tortora, M., & Vittoria, V. (2006). Diffusion behavior in polymer-clay nanocomposites. *Journal of Polymer Science, Part B: Polymer Physics*, 44(2), 265-274.

Spiridon, I., Popescu, M. C., Bodarlan, R., & Vasile, C. (2008). Enzymatic degradation of some nanocomposites of poly(vinyl alcohol) with starch. *Polymer Degradation and Stability*, 93(10), 1884-1890.

Strawhecker, K. E., & Manias, E. (2000). Structure and properties of poly(vinyl alcohol)/Na⁺ montmorillonite nanocomposites. *Chemistry of Materials*, 12(10), 2943-2949.

Tang, X. (2008). Use of extrusion for synthesis of starch-clay nanocomposites for biodegradable packaging films. *Food Science Institute*. Manhattan, Kansas: Kansas State University.

Tang, X., Alavi, S., & Herald, T. (2008a). Barrier and mechanical properties of starch-clay nanocomposite films. *Cereal Chemistry*, 433-439.

Tang, X., Alavi, S., & Herald, T. (2008b). Effects of plasticizers on the structure and properties of starch-clay nanocomposite films. *Carbohydrate Polymers*, 552-558.

Tran, T. A., Said, S., & Grohens, Y. (2005). Nanoscale characteristic length at the glass transition in confined syndiotactic poly(methyl methacrylate). *Macromolecules*, 38(9), 3867-3871.

Vaia, R. A., Jandt, K. D., Kramer, E. J., & Giannelis, E. P. (1995). KINETICS OF POLYMER MELT INTERCALATION. *Macromolecules*, 28(24), 8080-8085.

Vaia, R. A., Sauer, B. B., Tse, O. K., & Giannelis, E. P. (1997). Relaxations of confined chains in polymer nanocomposites: Glass transition properties of poly(ethylene oxide) intercalated in montmorillonite. *Journal of Polymer Science Part B-Polymer Physics*, 35(1), 59-67.

Vasile, C., Stoleriu, A., Popescu, M., Duncianu, C., Kelnar, I., & Dimonie, D. (2008a). Morphology and thermal properties of some green starch/poly(vinyl alcohol)/montmorillonite nanocomposites. *Cellulose Chemistry and Technology*, 549-568.

Vasile, C., Stoleriu, A., Popescu, M. C., Duncianu, C., Kelnar, I., & Dimonie, D. (2008b). Morphology and thermal properties of some green starch/poly(vinyl alcohol)/montmorillonite nanocomposites. *Cellulose Chemistry and Technology*, 42(9-10), 549-568.

Vyazovkin, S., & Dranca, I. (2004). A DSC study of alpha and beta-relaxations in a PS-clay system. *Journal of Physical Chemistry B*, 11981-11987.

Yang, S., & Huang, C. (2008). Plasma treatment for enhancing mechanical and thermal properties of biodegradable PVA/starch blends. *Journal of Applied Polymer Science*, 2452-2459.

Zax, D., Yang, D., Santos, R., Hegemann, H., Giannelis, E., & Manias, E. (2000). Dynamical heterogeneity in nanoconfined poly(styrene) chains. *Journal of Chemical Physics*, 2945-2951.

Zhang, J. F., & Sun, X. Z. (2004). Mechanical properties of poly(lactic acid)/starch composites compatibilized by maleic anhydride. *Biomacromolecules*, 5(4), 1446-1451.

Zhang, X., & Loo, L. (2009). Study of Glass Transition and Reinforcement Mechanism in Polymer/Layered Silicate Nanocomposites. *Macromolecules*, 5196-5207.

Zhong, Y., & De Kee, D. (2005). Morphology and properties of layered silicate-polyethylene nanocomposite blown films. *Polymer Engineering and Science*, 45(4), 469-477.

Zhou, X. Y., Cui, Y. F., Jia, D. M., & Xie, D. (2009). Effect of a Complex Plasticizer on the Structure and Properties of the Thermoplastic PVA/Starch Blends. *Polymer-Plastics Technology and Engineering*, 48(5), 489-495.

Zou, G. X., Ping-Qu, J., & Liang-Zou, X. (2008). Extruded Starch/PVA Composites: Water Resistance, Thermal Properties, and Morphology. *Journal of Elastomers and Plastics*, 40(4), 303-316.

Appendix A - Replicated figures and raw data tables for Chapter 2

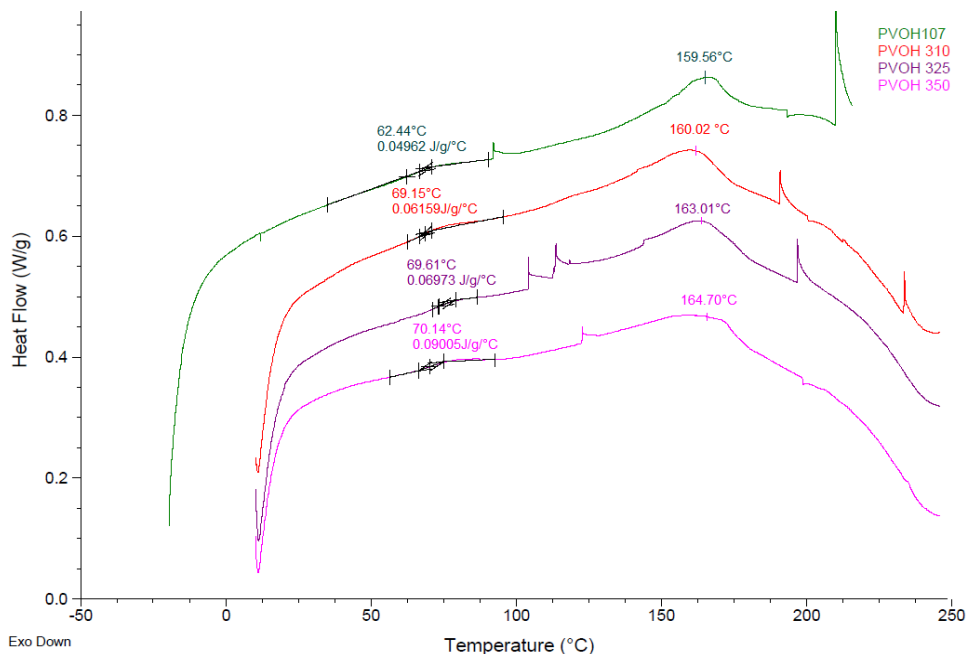


Figure A-1 DSC Curves of first replicate for nanocomposites with different molecular weights of PVOH

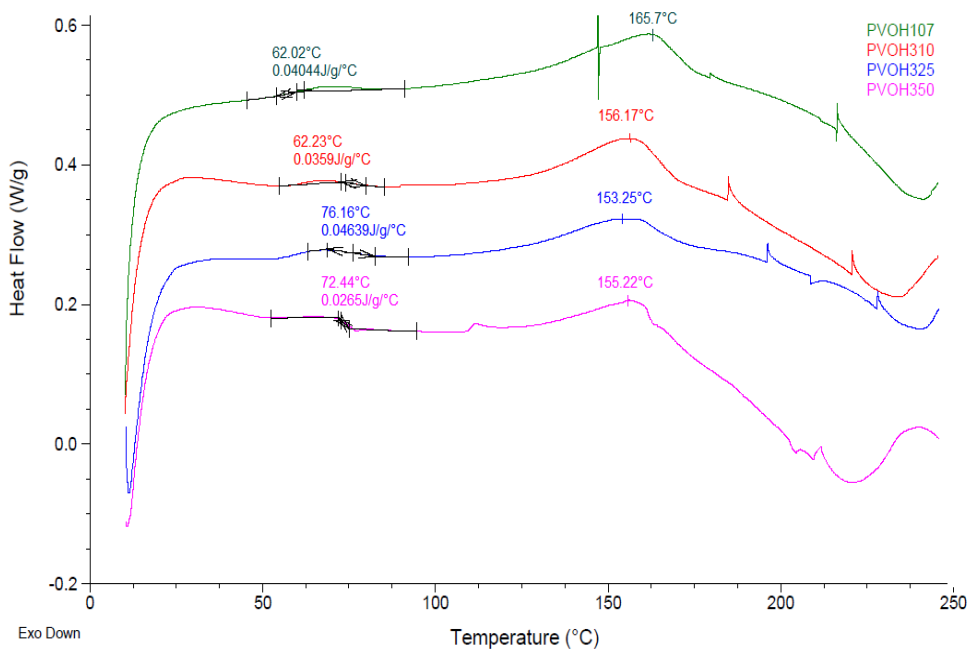


Figure A-2 DSC Curves of second replicate for nanocomposites with different molecular weights of PVOH

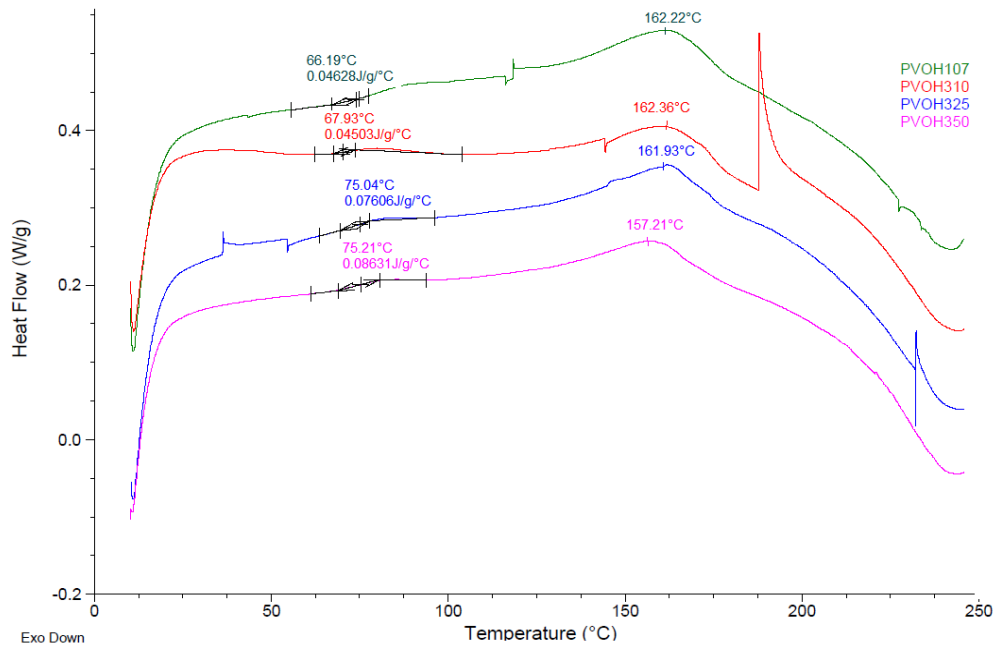


Figure A-3 DSC Curves of third replicate for nanocomposites with different molecular weights of PVOH

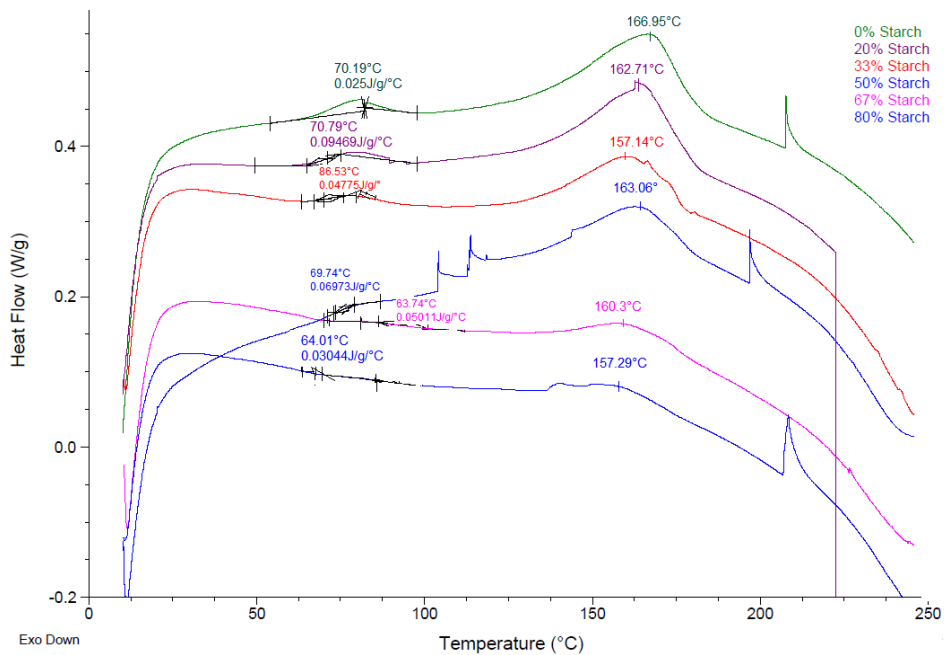


Figure A-4 DSC Curves of first replicate for nanocomposites with different starch levels

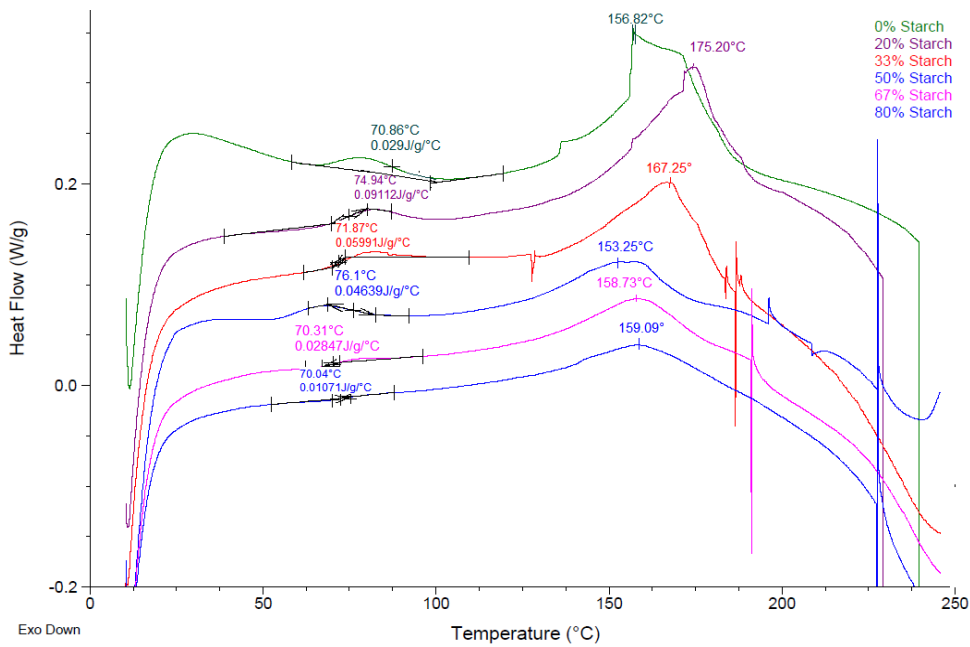


Figure A-5 DSC Curves of second replicate for nanocomposites with different starch levels

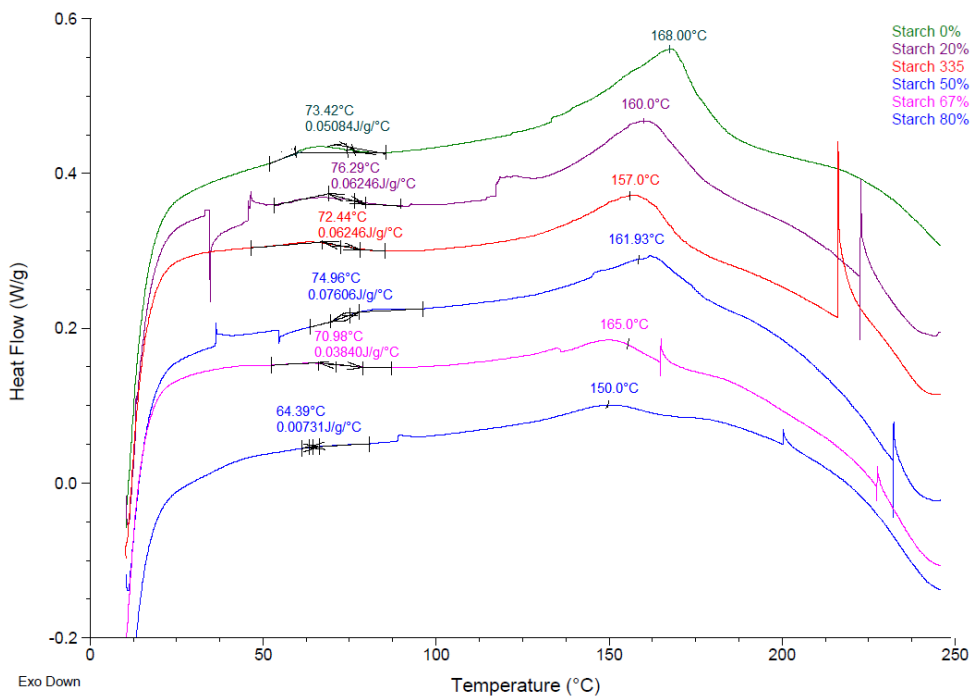


Figure A-6 DSC Curves of third replicate for nanocomposites with different starch levels

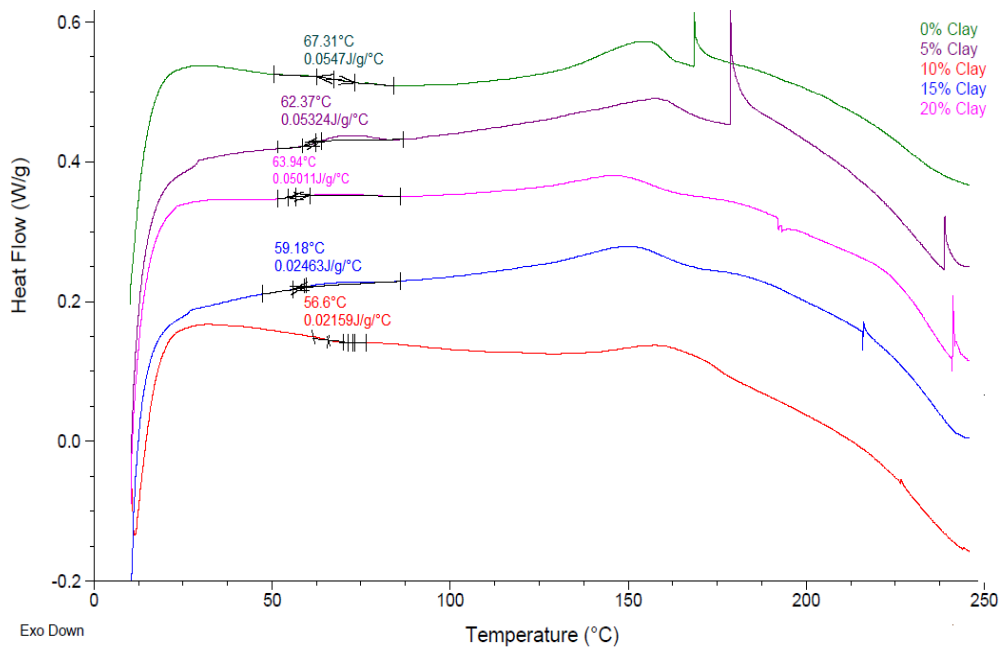


Figure A-7 DSC Curves of first replicate for nanocomposites with different Na⁺MMT content

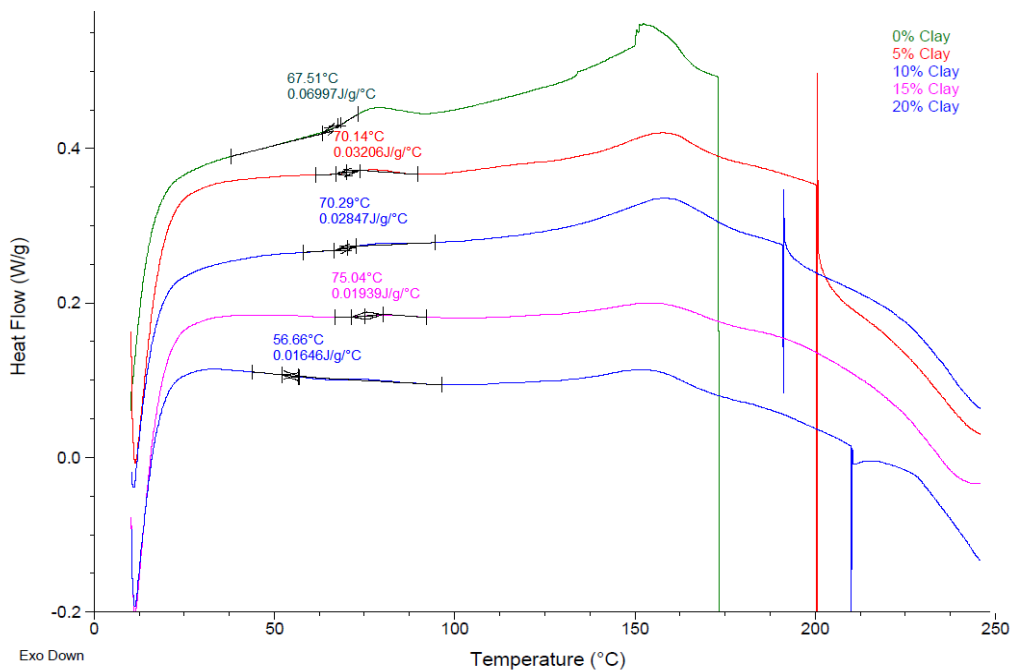


Figure A-8 DSC Curves of second replicate for nanocomposites with different Na⁺MMT content

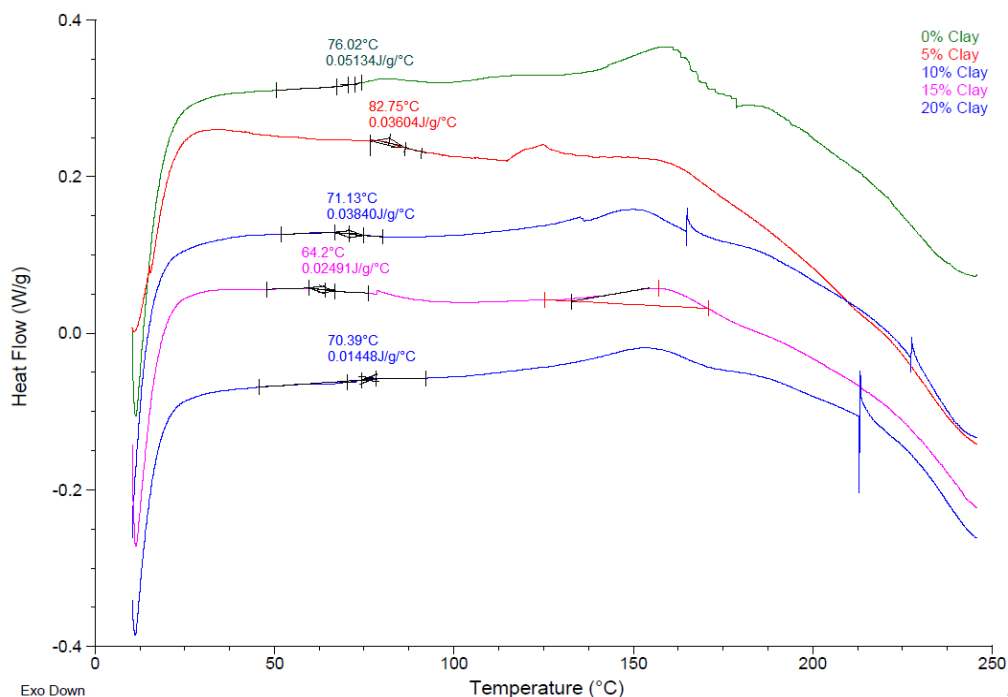


Figure A-9 DSC Curves of third replicate for nanocomposites with different Na⁺MMT content

Table A-1 Tensile strength for nanocomposite films with different molecular weight ranges of PVOH

Replicate No.	Celvol107	Celvol310	Celvol325	Celvol350
1	11.32	14.31	15.74	14.51
2	12.05	13.8	16.19	13.83
3	12.24	12.28	17.39	14.8
Average	11.87	13.46	16.44	14.38
Std. dev.	0.4857	1.0560	0.8529	0.4979

Table A-2 Elongation at break for nanocomposite films with different molecular weight ranges of PVOH

Replicate No.	Celvol107	Celvol310	Celvol325	Celvol350
1	79.4	95.96	152.02	150.53
2	53.11	73.11	169.68	143.05
3	67.67	72.67	163.84	193.02
Average	66.73	80.58	161.85	162.20
Std. Dev	13.17	13.32	9.00	26.95

Table A-3 Tensile strength for nanocomposite films with different starch levels

Replicate No.	0%	20%	33%	50%	66%	80%
1	22.00	24.41	19.08	15.74	14.95	18.02
2	22.02	22.07	18.79	16.19	18.51	17.67
3	25.00	20.58	16.75	17.39	17.71	18.54
Average	23.01	22.35	18.21	16.44	17.06	18.71
Std. Dev	1.30	1.93	3.06	0.85	0.87	0.86

Table A-4 Elongation at break for nanocomposite films with different starch levels

Replicate No.	0%	20%	33%	50%	66%	80%
1	324.59	205.71	182.70	152.02	112.85	23.78
2	324.17	186.24	200.62	169.68	104	22.76
3	225.07	242.26	179.14	163.84	87	40.25
Average	291.28	211.40	187.49	161.85	101.28	28.93
Std. Dev	57.34	28.44	11.52	8.99	13.14	9.82

Table A-5 Tensile strength for nanocomposite films with different Na⁺MMT content

Replicate No.	0%	5%	10%	15%	20%
1	7.93	10.90	14.95	17.73	17.93
2	8.18	12.05	18.51	20.22	17.83
3	9.05	11.86	17.71	18.56	19.46
Average	8.39	11.60	17.06	18.84	18.41
Std. Dev	0.59	0.61	1.87	1.27	0.91

Table A-6 Elongation at break for nanocomposite films with different Na⁺MMT content

Replicate No.	0%	5%	10%	15%	20%
1	146.23	90.52	112.85	54.63	37.36
2	123.55	122.40	104	68.58	42.68
3	140.69	96.07	87	62.27	44.66
Average	136.82	103.0	101.28	61.83	41.57
Std. Dev	11.82	17.03	13.14	6.98	3.77

Table A-7 WVP for nanocomposite films with different molecular weight ranges of PVOH

Replicate No.	Celvol107	Celvol310	Celvol325	Celvol350
1	1.5235	1.2254	1.2596	1.2715
2	1.3156	1.3026	1.1375	1.2880
3	1.3927	1.3572	1.0981	1.3185
Average	1.4106	1.2951	1.1651	1.2927
Std. Dev	0.105	0.066	0.084	0.024

Table A-8 WVP for nanocomposite films with different starch levels

Replicate No.	0%	20%	33%	50%	66%	80%
1	1.487	1.430	1.133	1.260	1.069	1.058
2	1.597	1.469	1.237	1.138	0.998	1.046
3	1.365	1.390	1.371	1.098	1.095	1.040
Average	1.483	1.430	1.247	1.165	1.054	1.048
Std. Dev	0.116	0.040	0.120	0.084	0.050	0.009

Table A-9 WVP for nanocomposite films with different Na⁺MMT content

Replicate No.	0%	5%	10%	15%	20%
1	1.687	1.207	1.069	0.752	0.744
2	1.737	1.154	0.998	0.714	0.709
3	1.63	1.345	1.095	0.711	0.702
Average	1.683	1.235	1.054	0.726	0.719
Std. Dev	0.06	0.099	0.050	0.023	0.023

Appendix B - Replicated figures and raw data tables for Chapter 3

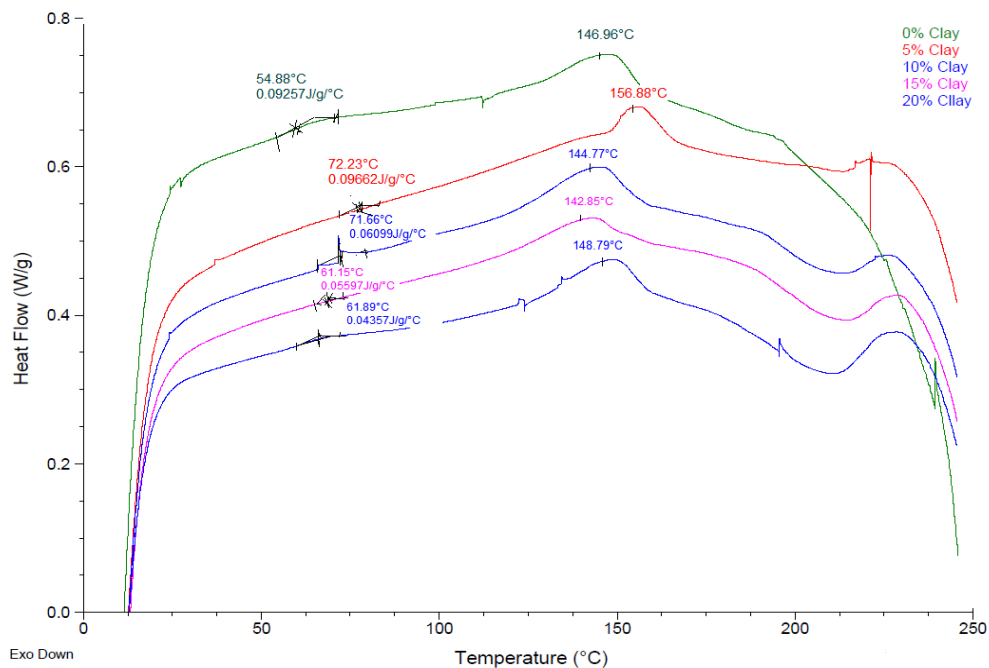


Figure B-1 DSC Curves of first replicate for nanocomposites with different Na⁺MMT content

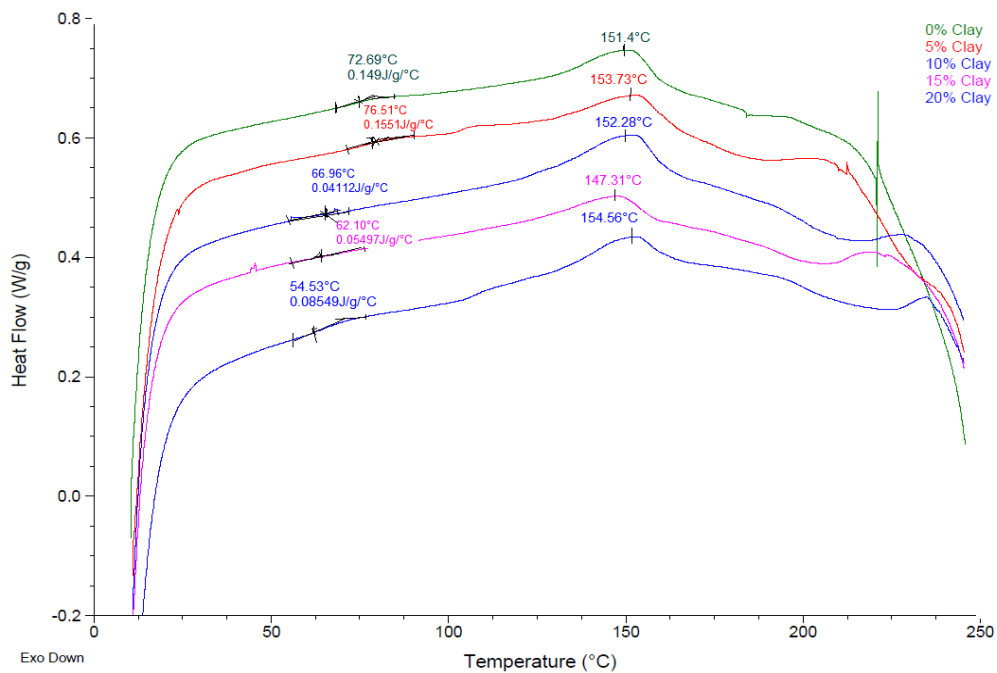


Figure B-2 DSC Curves of second replicate for nanocomposites with different Na⁺MMT content

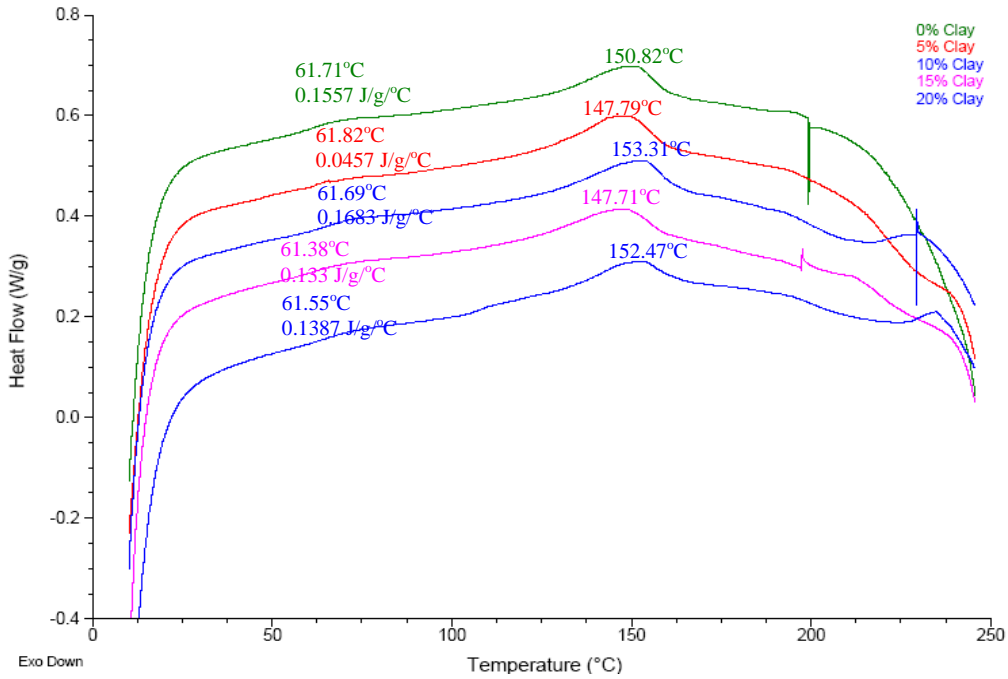


Figure B-3 DSC Curves of third replicate for nanocomposites with different Na⁺MMT content

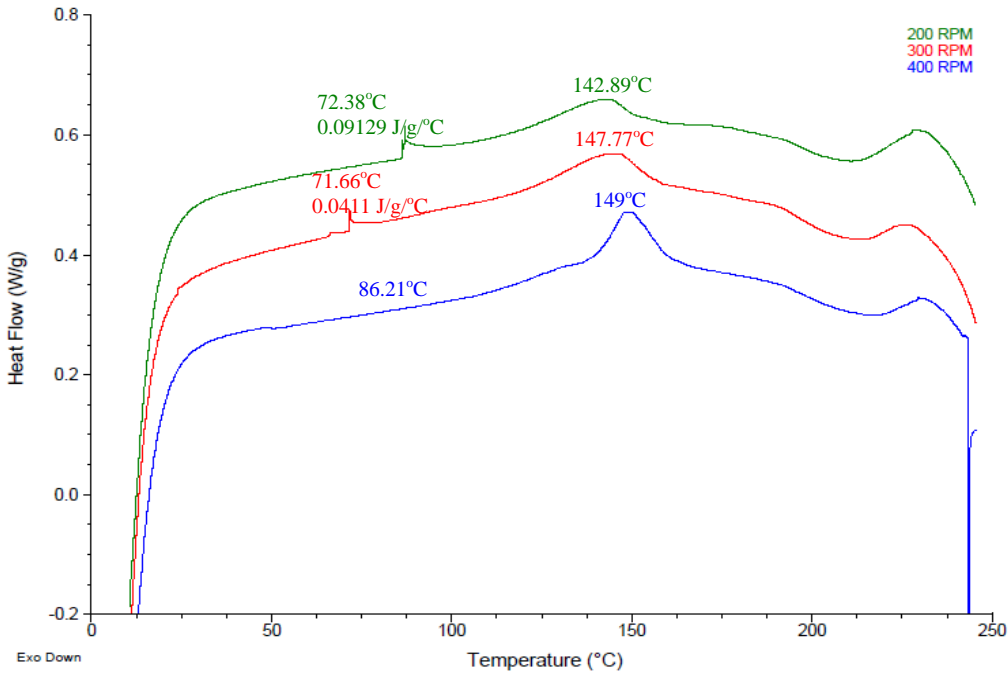


Figure B-4 DSC Curves of first replicate for nanocomposites produced with different screw speeds

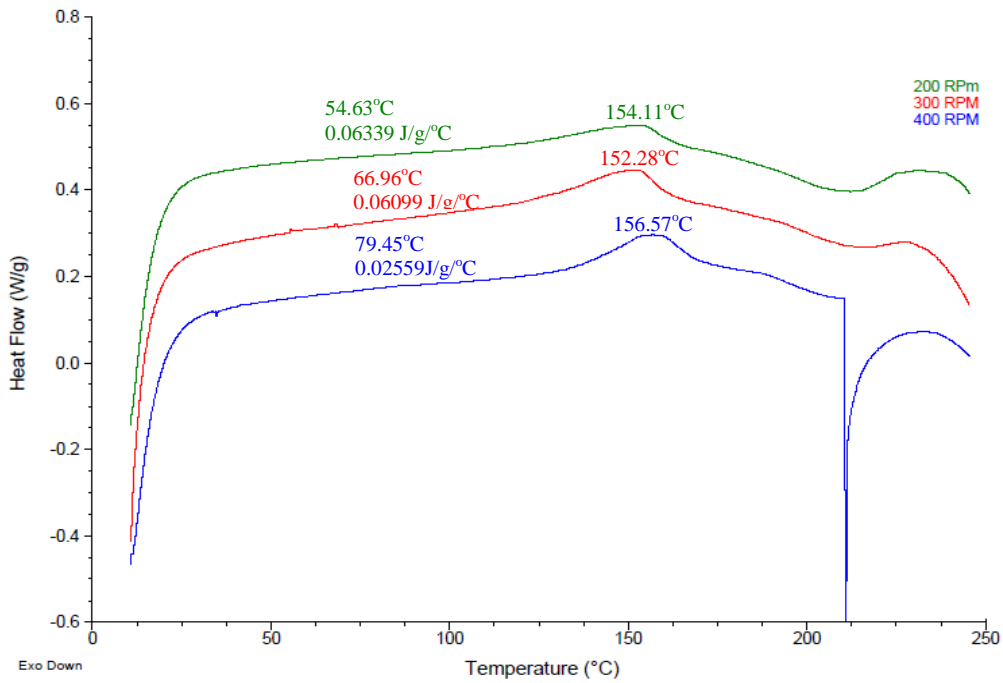


Figure B-5 DSC Curves of second replicate for nanocomposites produced with different screw speeds

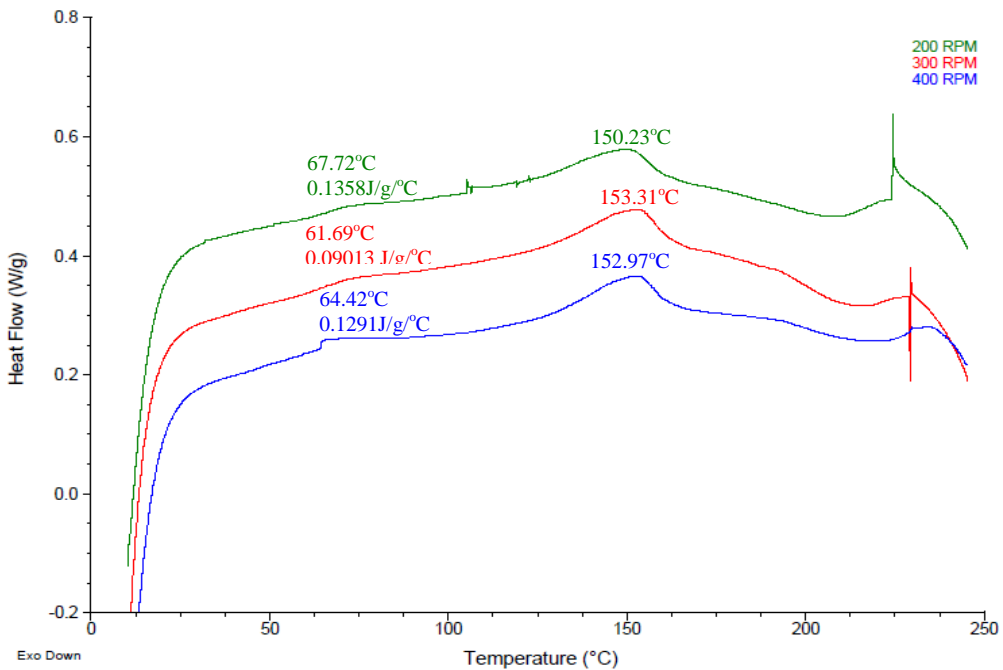


Figure B-6 DSC Curves of third replicate for nanocomposites produced with different screw speeds

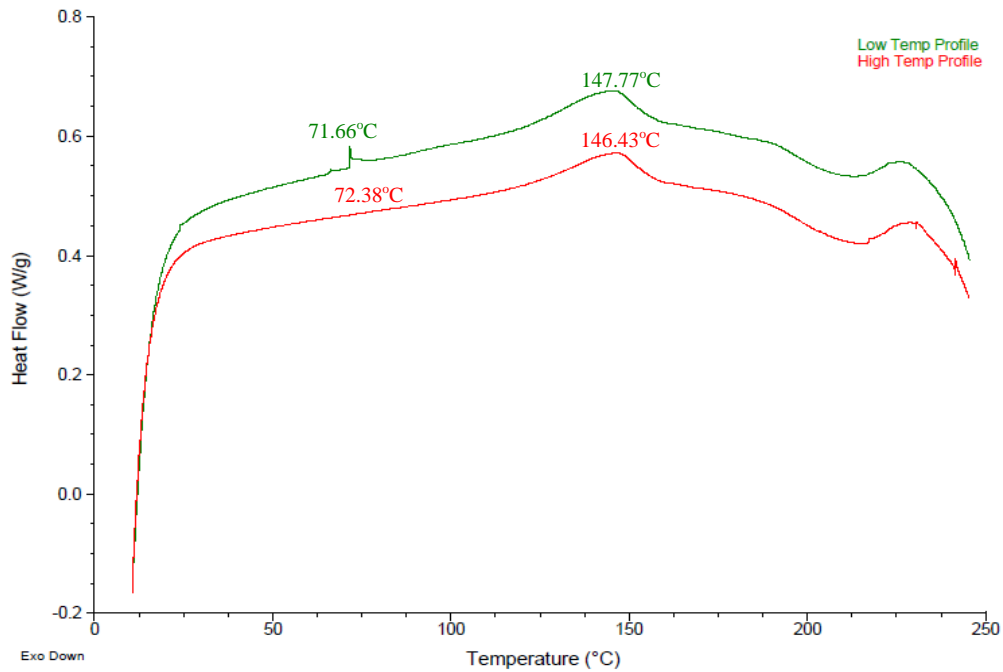


Figure B-7 DSC Curves of first replicate for nanocomposites produced at different temperature profiles of extruder

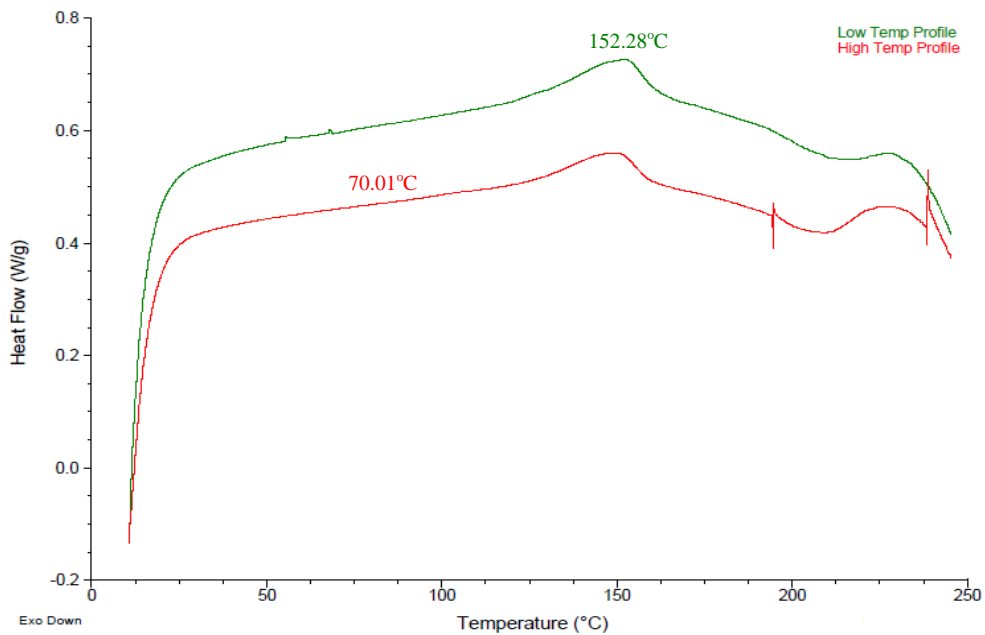


Figure B-8 DSC Curves of second replicate for nanocomposites produced at different temperature profiles of extruder

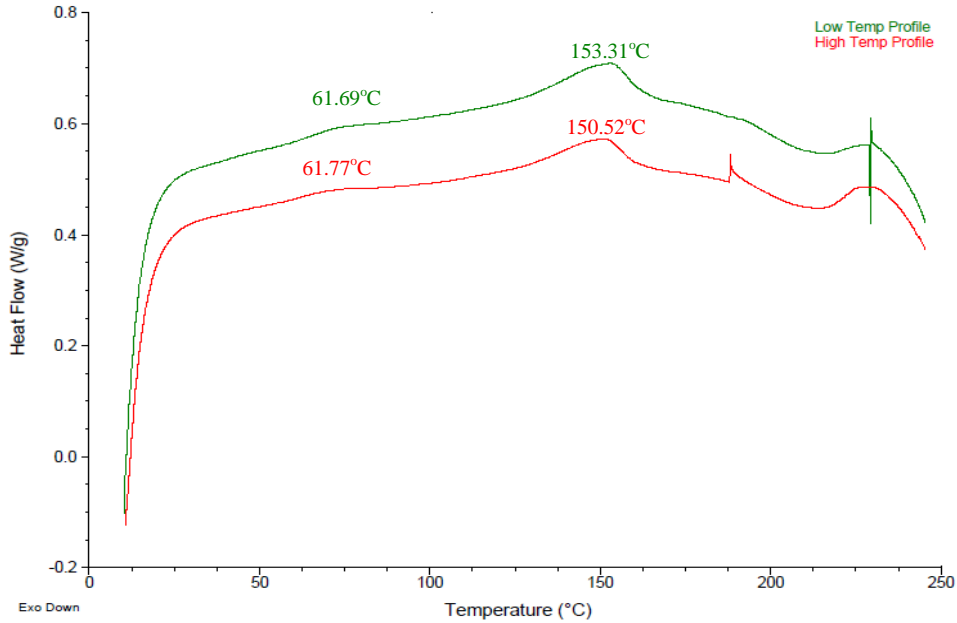


Figure B-9 DSC Curves of third replicate for nanocomposites produced at different temperature profiles of extruder

Table B-1 Tensile Strength for nanocomposite films with different Na⁺MMT content

Replicate No.	0%	5%	10%	15%	20%
1	8.21	8.92	11.66	5.62	11.95
2	6.06	9.52	11.88	9.86	13.93
3	5.38	7.88	12.08	5.84	12.04
Average	6.55	8.77	11.87	7.11	12.64
Std. Dev	1.48	0.83	0.21	2.39	1.12

Table B-2 Elongation at break for nanocomposite films with different Na⁺MMT content

Replicate No.	0%	5%	10%	15%	20%
1	304.27	282.09	222.43	156.63	138.79
2	307.49	276.23	220.18	197.25	150.62
3	301.14	295.39	218.33	131.72	117.43
Average	304.30	284.57	220.31	161.87	135.61
Std. Dev	3.17	9.81	2.05	33.08	16.82

Table B-3 WVP for nanocomposite films with different Na⁺MMT content

Replicate No.	0%	5%	10%	15%	20%
1	1.660	1.620	1.549	1.536	1.441
2	1.684	1.609	1.525	1.459	1.446
3	1.570	1.471	1.44	1.414	1.324
Average	1.638	1.567	1.506	1.470	1.404
Std. Dev	0.06	0.08	0.06	0.06	0.07

Table B-4 Tensile Strength for nanocomposite films produced with different screw speeds

Replicate No.	200 RPM	300 RPM	400 RPM
1	9.25	11.66	13.56
2	8.53	11.88	12.27
3	8.55	12.08	14.11
Average	8.78	11.87	13.31
Std. Dev	0.41	0.21	0.94

Table B-5 Elongation at break for nanocomposite films produced with different screw speeds

Replicate No.	200 RPM	300 RPM	400 RPM
1	136.45	222.	199.96
2	135.68	220.	148.16
3	110.38	218.	210.33
Average	127.50	220.	186.15
Std. Dev	14.83	2.05	33.30

Table B-6 WVP for nanocomposite films produced with different screw speeds

Replicate No.	200 RPM	300 RPM	400 RPM
1	1.784	1.54	1.560
2	1.842	1.52	1.559
3	1.616	1.44	1.421
Average	1.747	1.50	1.514
Std. Dev	0.12	0.05	0.08

Table B-7 Tensile Strength for nanocomposite films produced with different temperature profiles of extruder

Replicate No.	Temp 145	Temp 165
1	11.66	7.72
2	11.88	7.68
3	12.08	7.87
Average	11.87	7.76
Std. Dev	0.21	0.10

Table B-8 Elongation at break for nanocomposite films produced with different temperature profiles of extruder

Replicate No.	Temp 145	Temp 165
1	222.43	69.37
2	220.18	61.36
3	218.33	59.19
Average	220.31	63.31
Std. Dev	2.05	5.36

Table B-9 WVP for nanocomposite films produced with different temperature profiles of extruder

Replicate No.	Low	High
1	1.549	1.481
2	1.525	1.536
3	1.444	1.315
Average	1.506	1.444
Std. Dev	0.06	0.12